

Metallic-semiconducting separation of single wall carbon nanotubes and their application to electronic devices

Feng Ye

February 2011

Metallic-semiconducting separation of single wall carbon
nanotubes and their application to electronic devices

Feng Ye
(Doctoral Program in *Materials Science*)

Submitted to the Graduate School of
Pure and Applied Sciences
in Partial Fulfillment of the Requirements
for the Degree of Doctor of Philosophy in
Engineering

at the
University of Tsukuba

Content

INTRODUCTION.....	3
1.1 THE HISTORY OF CARBON NANOTUBES	3
1.2 THE STRUCTURE AND OPTICAL PROPERTIES OF SWCNTS	5
1.3 THE SYNTHESIS METHODS OF SWCNTS.....	10
1.4 THE SORTING METHODS OF SWCNTS ELECTRONIC TYPE.....	12
1.5 THE APPLICATIONS OF SWCNTS TO ELECTRONIC DEVICES.....	15
1.5.1 <i>Thin film transistors (TFTs)</i>	15
1.5.2 <i>Organic Photovoltaic devices</i>	18
1.6 PURPOSE OF THIS STUDY.....	21
2. SEPARATION OF SWCNTS BY DENSITY GRADIENT ULTRACENTRIFUGATION ...	22
2.1 EXPERIMENTAL	22
2.2 FIRST SEPARATION	24
2.2.1 <i>Optimization of separation condition</i>	24
2.2.2 <i>Dispersion of SWCNTs</i>	27
2.2.3 <i>Uniform DGU</i>	28
2.2.4 <i>Comparison of linear/step and uniform DGU</i>	34
2.3 SECOND SEPARATION	36
2.3.1 <i>Optimization of separation condition</i>	37
2.3.2 <i>Raman spectra of 1st/2nd separation</i>	41
2.4 I-V CHARACTERISTIC.....	43
2.4.1 <i>Experimental</i>	43
2.4.2 <i>The I-V characteristic of TFT</i>	46
2.5 CONCLUSION.....	50
3. THE APPLICATION TO ORGANIC SOLAR CELL.....	51
3.1 INTRODUCTION	51
3.2 THE OPTICAL PROPERTIES OF SWCNT-POLYMER COMPOSITES	52
3.2.1 <i>Experimental</i>	52

3.2.2	<i>Properties of SWCNT-polymer composites</i>	53
3.2.3	<i>Energy transfer</i>	58
3.2.4	<i>Energy transfer efficiency</i>	59
3.3	THE P3HT:PCBM SOLAR CELL WITH THE ADDITION OF SWCNTs	62
3.3.1	<i>Experimental</i>	62
3.3.2	<i>The solar cell with the addition of semiconducting SWCNTs</i>	64
3.3.3	<i>The solar cell with the addition of pristine and metallic SWCNTs</i>	66
3.3.4	<i>The mechanism of the solar cell of P3HT:PCBM:SWCNTs</i>	67
3.4	CONCLUSION	69
4.	SUMMARY	70
	REFERENCE	71
	ABBREVIATION	78
	APPENDIX	80
	ACKNOWLEDGEMENT	88

Introduction

1.1 The history of Carbon nanotubes

The interest of carbon nanotubes has been aroused since the very small diameter (less than 10nm) carbon filaments were observed in the 1970's and 1980's during the synthesis of carbon fiber with metal catalyst particles of < 10nm diameter.^{1,2} However, no detailed systematic studies of these very thin carbon filaments were reported in these early years, and it was not until the observation of multi-wall carbon nanotubes (MWCNT) was reported in 1991 by Iijima³ using High-Resolution Transmission Electron Microscopy (HRTEM) that the carbon nanotube field was seriously launched.

A direct stimulus to the systematic study of carbon filaments of very small diameters came from the discovery of fullerenes by *Kroto, Smalley, Curl*, and coworkers⁴. In fact, Smalley and others speculated publically in these early years that a single wall carbon nanotube might be a limiting case of a fullerene molecule. The connection between carbon nanotubes and fullerenes was further promoted by the observation that the termination s of the carbon nanotubes were fullerene-like caps or hemispheres. It is curious that the smallest reported diameter for a carbon nanotube is the same as the diameter of the C₆₀ molecule, which is the smallest fullerene to follow the isolated pentagon rule. This rule requires that no two pentagons be adjacent to one another, thereby lowering the strain energy of the fullerene cage. While there is not, as yet, a definite conclusion to identify carbon fibers with very small diameters as carbon nanotubes, the one-dimensional limit of a fullerene molecule. A recent report of a carbon nanotube which a diameter of 0.4 nm and a C₂₀ end cap may help to understand it.^{133, 134}

It was the Iijima's observation of the multiwall carbon nanotubes in Figure 1.1 that heralded the entry of many scientists into the field of carbon nanotubes, stimulated at first by the remarkable 1D dimensional quantum effects predicted for their electronic properties, and subsequently by the promise that the remarkable structure and properties of carbon nanotubes might give rise to some unique applications. Whereas the initial experimental observation of Iijima was for Multi-Wall carbon Nanotubes (MWCNTs), it was less than two years before Single-Wall carbon nanotubes (SWCNTs) were discovered experimentally by Iijima and his group at NEC laboratory⁵ and by Bethune and coworkers at the IBM Almaden laboratory⁶.

These findings were especially important because the single wall nanotubes are more fundamental, and had been the basis for a large body of theoretical studies and predictions that preceded the experimental observation of single wall carbon nanotubes. The most striking of these theoretical developments was the prediction that carbon nanotubes could be either semiconducting or metallic depending on their geometrical characteristics,^{7,8,9} namely their diameter and the orientation of their hexagons with respect to the nanotube axis (chiral angle). Though predicted in 1992, it was not until 1998 that these predictions regarding their remarkable electronic properties were corroborated experimentally.^{10,11}

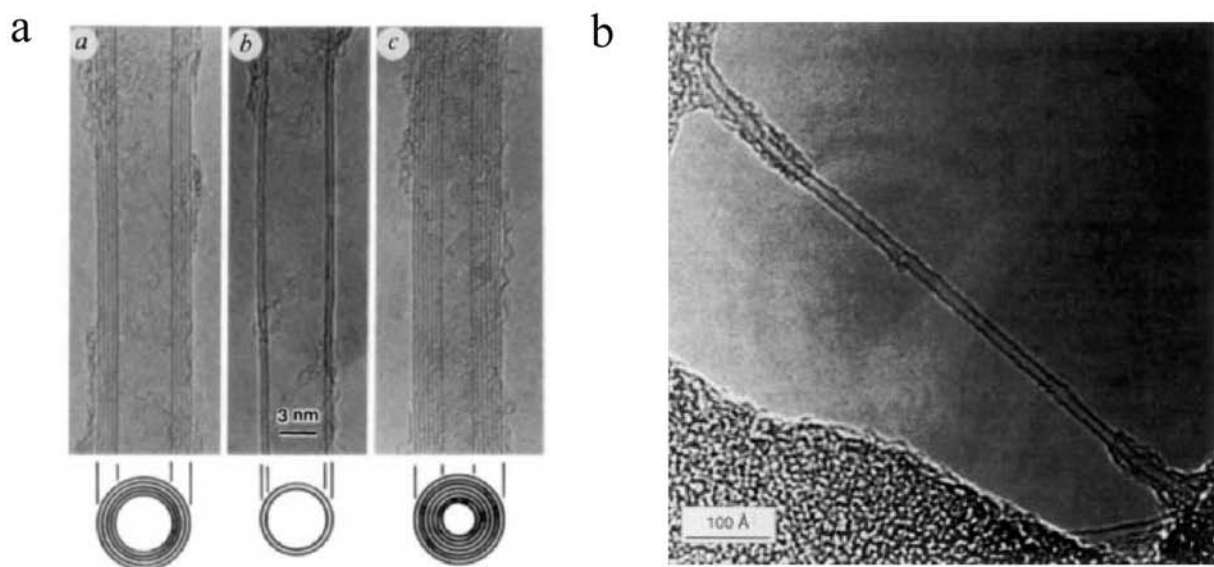


Figure 1.1. (a) The observation by TEM of multi-wall coaxial nanotubes with various inner and outer diameters.³ (b) TEM image of a bare section of a single-walled nanotube.⁶

A major breakthrough occurred in 1996 when Smalley and coworkers at Rice university successfully synthesized bundles of aligned single wall carbon nanotubes, with a small diameter distribution, thereby making it possible to carry out many sensitive experiments relevant to 1D quantum physics, which could not previously be undertaken.¹² Of course, actual carbon nanotubes have finite length, contain defects, and interact with other nanotubes or with the substrate and these factors often complicate their behavior.

To date, a great deal of progress has been made in characterizing carbon nanotubes and in understanding their unique properties. However, there are still many problems remaining unknown which need to be understood in future before carbon nanotubes can be widely applied to our lives.

1.2 The structure and optical properties of SWCNTs

Conceptually, a SWCNT is constructed by rolling a single atom-thick sheet of graphite into a seamless cylinder. The structure of a single-wall carbon nanotube is conveniently explained in terms of its 1D unit cell, defined by the vector \mathbf{C}_h and \mathbf{T} in Figure 1.2a. The circumference of any carbon nanotube is expressed in terms of the chiral vector $\mathbf{C}_h = n\hat{\mathbf{a}}_1 + m\hat{\mathbf{a}}_2$ which connects two crystallographically equivalent sites on a 2D grapheme sheet⁷. The construction in Figure 1.2a depends uniquely on the pair of integers (n, m) which specify the chiral vector¹³. Figure 1.2a shows the chiral angle θ between the chiral vector \mathbf{C}_h and the “zigzag” direction ($\theta=0$) and the unit vector $\hat{\mathbf{a}}_1$ and $\hat{\mathbf{a}}_2$ of the hexagonal honeycomb lattice of the graphene sheet. Three distinct types of nanotube structures can be generated by rolling up the grapheme sheet into a cylinder as described below and shown in Figure 1.2b. The zigzag and armchair nanotubes, respectively, correspond to chiral angles of $\theta=0$ and 30° , and chiral nanotubes correspond to $0 < \theta < 30^\circ$. The intersection of the vector \mathbf{OB} (which is normal to \mathbf{C}_h) with the first lattice point determines the fundamental one-dimensional (1D) translation vector \mathbf{T} . The unit cell of the 1D lattice is the rectangle defined by the vector \mathbf{C}_h and \mathbf{T} . In the (n, m) notation for $\mathbf{C}_h = n\hat{\mathbf{a}}_1 + m\hat{\mathbf{a}}_2$, the vectors $(n, 0)$ or $(0, m)$ denote zigzag nanotubes and the vectors (n, n) denote armchair nanotubes. All other vectors (n, m) correspond to chiral nanotubes. The nanotube diameter d_t is given by

$$d_t = \sqrt{3}a_{c-c}(m^2 + mn + n^2)^{1/2} / \pi = C_h / \pi, \quad (1)$$

Where C_h is the length of \mathbf{C}_h , a_{c-c} is the C—C bond length (1.42 Å). The chiral angle θ is given by

$$\theta = \tan^{-1} \left[\sqrt{3}n / (2m + n) \right] \quad (2)$$

From (2) it follows that $\theta = 30^\circ$ for the (n, n) armchair nanotube and that the $(n, 0)$ zigzag nanotube would have $\theta = 60^\circ$. From Figure 1.2a it follows that if we limit θ to be between $0 \leq \theta \leq 30^\circ$, then by symmetry $\theta = 0^\circ$ for a zigzag nanotube. Both armchair and zigzag nanotubes have a mirror plane and thus are considered as achiral. Difference in the nanotube diameter d_t and chiral angle θ , namely (n, m) , give rise to differences in the properties of the various carbon nanotubes.

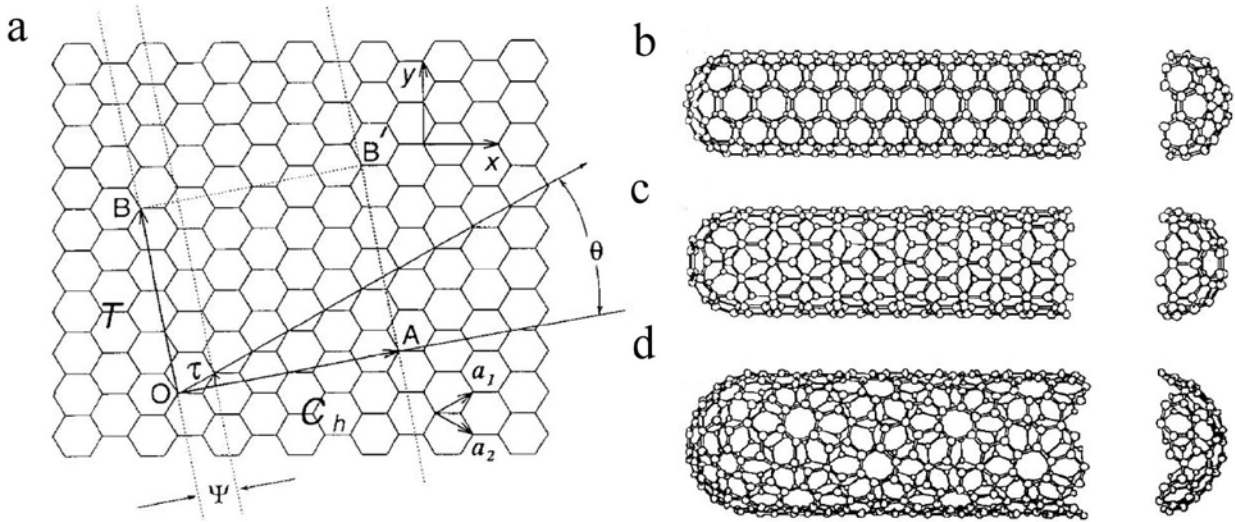


Figure 1.2 (a) The 2D grapheme sheet is shown along with the vector which specifies the chiral nanotube. (b) the $\theta = 30^\circ$ direction (an “armchair” tubule), (c) the $\theta = 0^\circ$ direction (a “zigzag” tubule), and (d) a general direction with $0 < |\theta| < 30^\circ$ (a “chiral” tubule). The actual tubules shown in the figure correspond to (n, m) values of: (b) (5,5), (c) (9,0), and (d) (10,5).

Using the simple tight-binding method and pair-wise atomic force constant models, we can derive the electronic and phonon structure, respectively. The 1D electronic Density of States (DOS) is given by the energy dispersion of carbon nanotubes which is obtained by zone folding of the 2D energy dispersion relations of graphite¹⁴. It is known that the (n, m) indices are crucial to the nanotube electronic structure. Specifically, SWCNT for which $|n - m| = 3q$ are metallic and those for which $|n - m| = 3q \pm 1$ are semiconducting, where q is an integer. A typical feature of one-dimensional nanomaterials is that their DOS is not a continuous function of energy, but it descends gradually and then increases in a discontinuous spike. In contrast, three-dimensional materials have continuous DOS, as shown in Figure 1.3a. The sharp peaks found in one-dimensional materials are called van Hove singularities (vHS). The interband energy E_{ii} with different singularities i was calculated¹⁵ and plotted versus the diameter in Figure 1.3b, as known as “Kataura plot”. The optical properties of SWCNTs can usually be identified with three methods: optical absorption, photoluminescence and resonance Raman.

Optical absorption in carbon nanotubes differs from absorption in conventional 3D materials by presence of sharp peaks (1D nanotubes) instead of an absorption threshold followed by an absorption increase (most 3D solids). Absorption in nanotubes originates from electronic transitions from the v_2 to c_2 (energy E_{22}) or v_1 to c_1 (E_{11}) levels, etc¹⁵. The transitions are relatively sharp and can be used to identify nanotube types. Note that the sharpness

deteriorates with increasing energy, and that many nanotubes have very similar E22 or E11 energies, and thus significant overlap occurs in absorption spectra. This overlap is avoided in photoluminescence mapping measurements (see below), which instead of a combination of overlapped transitions identifies individual (E_{22} , E_{11}) pairs. Interactions between nanotubes, such as bundling, broaden optical lines¹⁶. While bundling strongly affects photoluminescence due to the quench of metallic SWCNTs, it has much weaker effect on optical absorption and Raman scattering. Optical absorption is routinely used to quantify quality of the carbon nanotube. The spectrum is analyzed in terms of intensities of nanotube-related peaks, background and pi-carbon peak; the latter two mostly originate from non-nanotube carbon.

Photoluminescence (PL) is one of the important tools for nanotube characterization. The

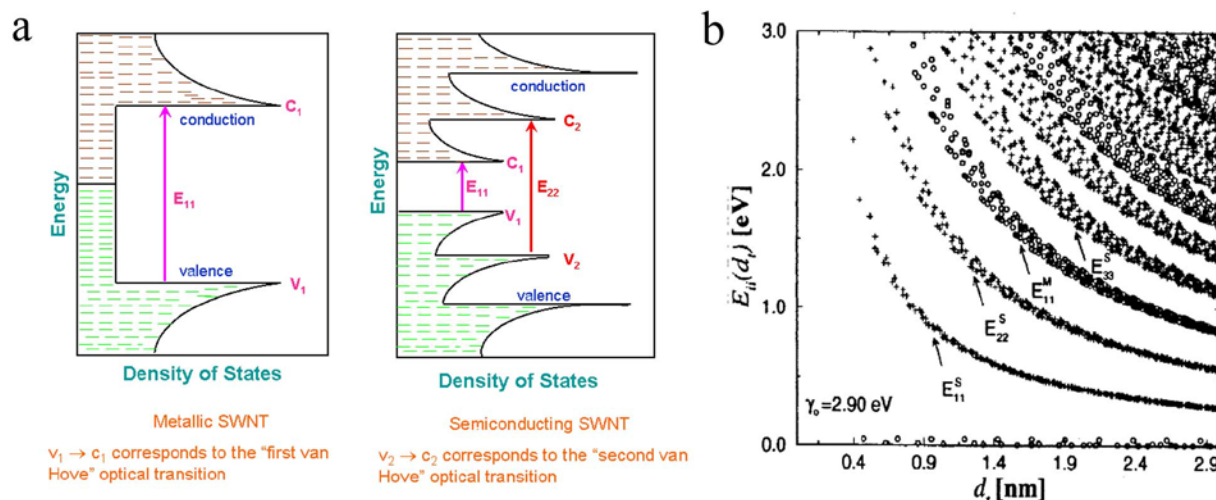


Figure 1.3 (a) Density of states of metallic and semiconducting SWCNTs. (b) Calculation of the energy separations $E_{pp}(d_i)$ for all (n,m) values as a function of the nanotube diameter.¹⁸

excitation of PL usually occurs as follows: an electron in a nanotube absorbs excitation light via S22 transition, creating an electron-hole pair (exciton). Both electron and hole rapidly relax (via phonon-assisted processes) from c2 to c1 and from v2 to v1 states, respectively. Then they recombine through a c1 – v1 transition resulting in light emission. No excitonic luminescence can be produced in metallic tubes. Electron can be excited, thus resulting in optical absorption, but the hole is immediately filled by another electron out of many available in metal. Therefore no exciton is produced.

Raman spectroscopy is a spectroscopic technique used to study vibrational, rotational, and other low-frequency modes in a system. For carbon nanotubes, phonons provide a sensitive probe of the electronic structure through the coupling between electrons and phonons in this

one-dimensional system. Furthermore, this coupling gives rise to highly unusual Raman spectra, when the phonon involved in the Raman process is in resonance with an electronic state in this highly one-dimensional material. Since the electronic states are highly sensitive to the diameter of the nanotube, the resonance Raman effect is likewise highly sensitive of the nanotube diameter¹⁷. In some cases, chirality-dependent behavior is also observed.

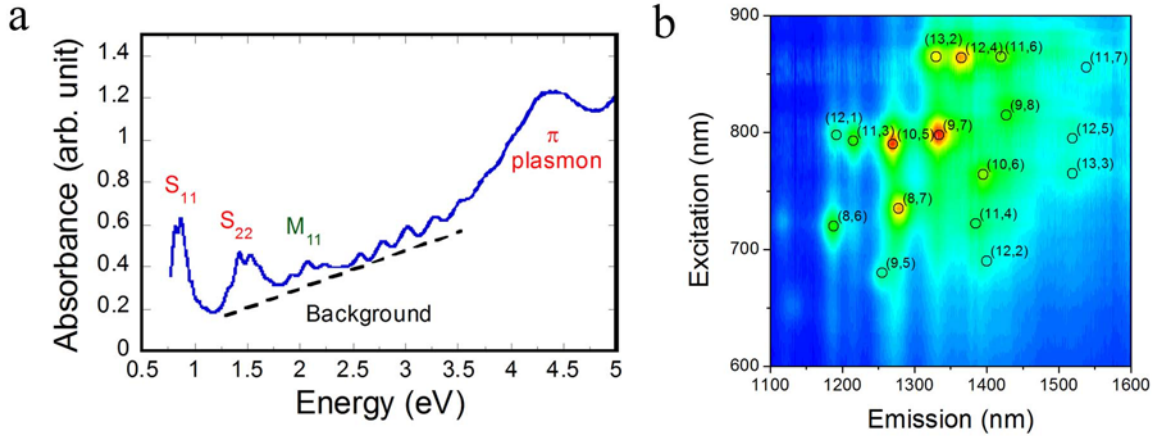


Figure 1.4 (a) Absorption of SWCNTs D₂O dispersion produced by laser ablation with a average diameter of 1.2 nm. (b) The photoluminescence mapping the solution with the excitation in S₂₂ range and emission in S₁₁ range.

Figure 1.5 shows a typical Raman spectra of SWCNTs which includes the most important features in the nanotubes: the radial breathing mode (RBM), the tangential G-band (derived from the graphite-like in-plane mode), the disorder-induced D-band, and its second-order harmonic (the G'-band). Each Raman feature will be explained in detail in the followings.

RBM corresponds to radial expansion-contraction of the nanotube. Since the RBM frequency, ω_{RBM} , depends linearly on the reciprocal nanotube diameter d_t ,¹⁷ each (n, m) nanotube in a sample with a wide diameter distribution, such as in Figure 1.5, will have a different RBM spectrum. The frequency of the RBM varies as α/d_t , and for the Si/SiO₂ substrate α is experimentally found to be 248 cm⁻¹ nm for isolated SWCNTs. This frequency is usually used to determine (n, m) indices. it depends primarily on the determination of E_{ii} using the unique relation between E_{ii} and (n, m) shown in Figure 1.3b, since d_t can be induced directly from $\omega_{RBM} = 248/d_t$.

The G-band in carbon nanotubes occurring in the 1500-1605 cm⁻¹ range is basically derived from the Raman allowed optical mode E_{2g} of 2D graphite by two zone folding the 2D grapheme

Brillouin zone into the 1D nanotube Brillouin zone, noting that only modes with A , E_1 , and E_2 symmetry are Raman active for SWCNTs.¹⁷ The most dramatic features of the G-band spectra are the characteristic differences between the G-band spectra for metallic and semiconducting nanotubes.^{18, 19} Isolated semiconducting nanotubes characteristically show two dominant Lorentzian features with 6-15 cm^{-1} (FWHM) linewidth at room temperature, the lower frequency component associated with vibrations along the circumferential direction (ω_G^-), and the higher frequency component (ω_G^+) attributed to vibrations along the direction of the nanotube axis. In contrast, the Raman spectra for metallic nanotubes also have two dominant components with similar origins, but in this case the upper frequency component ω_G^+ has a Lorentzian lineshape that is almost as narrow as that for the semiconducting nanotubes, but the lower frequency component ω_G^- is a very broad Breit-Wigner-Fano line, with a strong coupling to a continuum identified with surface plasmons.²⁰ ω_G^+ shows diameter dependence, while ω_G^- has a strong d_t^{-2} dependence, that differs according to whether the nanotubes are semiconducting or metallic.

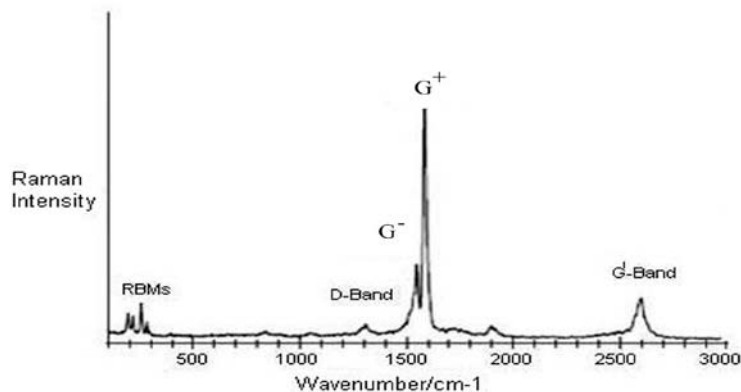


Figure 1.5. A typical Raman spectrum of SWCNTs bundles.

The D-band and G'-band features are both observed in the Raman spectra of semiconducting and metallic SWCNTs at the single nanotube level. They are induced by disorder of C-C interaction and exhibit a strongly dispersive behavior as a function of laser excitation energy,^{21, 22} which is similar to those in other sp^2 carbons.^{23, 24} But some distinct characteristic behaviors are also observed for SWCNTs, such as a step or oscillatory effect observation of Raman spectra of SWCNTs bundles²¹, which is not presented in other sp^2 carbons. The name of G' mode is

misleading: it is given because in graphite, this mode is usually the second strongest after the G mode. However, it is actually the second overtone of the defect-induced D mode (and thus should logically be named D').

Other overtones, such as a combination of RBM+G mode at $\sim 1750\text{ cm}^{-1}$, are frequently seen in CNT Raman spectra. However, they are less important and are not considered for characterization.

1.3 The synthesis methods of SWCNTs

The past decade witnessed significant research efforts in efficient and high-yield nanotube growth methods. The main methods include arc-discharge^{25, 26}, laser ablation²⁷ and chemical vapor deposition^{28–32}, by which the produced SWCNTs have different diameter distribution and characteristics that are used for experiments with different motivations. In this study, we used all the SWCNTs made by three methods. Thus in this section, we simply introduced these methods.

Arc discharge: Nanotubes observed in 1991 by Iijima were produced by arc discharge that intensified to produce fullerenes. In arc-discharge, carbon atoms are evaporated by plasma of helium gas ignited by high currents passed through opposing carbon anode and cathode (Figure 1.6a). For the growth of SWCNTs, a metal catalyst is needed in the arc-discharge system. The SWCNTs produced by arc-discharge are straight and few defects. The yield for this method is up to 30 percent by weight and it produces both single- and multi-wall nanotubes.

Laser ablation: In this process, a pulsed laser is utilized to ablate a carbon target containing catalysts of nickel and cobalt. The target was placed in a high-temperature actor while an inert gas is bled into the chamber to carry the grown nanotubes downstream to be collected on a cold finger. The produced SWCNTs are mostly in the form of ropes consisting of tens of individual nanotubes close-packed into hexagonal crystals via van der Waals interaction. The laser ablation method yields around 70% and produces primarily SWCNTs with a controllable diameter determined by the reaction temperature. However, it is more expensive than either arc discharge or chemical vapor deposition.

Chemical Vapor Deposition (CVD): The growth process involves heating a catalyst material to high temperatures in a tube furnace (Figure 1.6c) and flowing a hydrocarbon gas through the

tube reactor for a period of time. Materials grown over the catalyst are collected upon cooling the system to room temperature. The key parameters in nanotube CVD growth are the hydrocarbons, catalysts and growth temperature. The diameters of the nanotubes that are to be grown are related to the size of the metal particles. High temperature is necessary to form SWCNTs that have small diameters and allow for nearly-defect free crystalline nanotube structures. Among all hydrocarbon molecules, methane is the most stable at high temperatures against self-decomposition. CVD methods are promising for producing high quality nanotube materials at large scales and recently are found to grow with aligned and ordered nanotube with control^{34–36} that is not possible with arc-discharge or laser ablation techniques.

Although the synthesis methods had much developed to date, the synthesis of a SWCNT

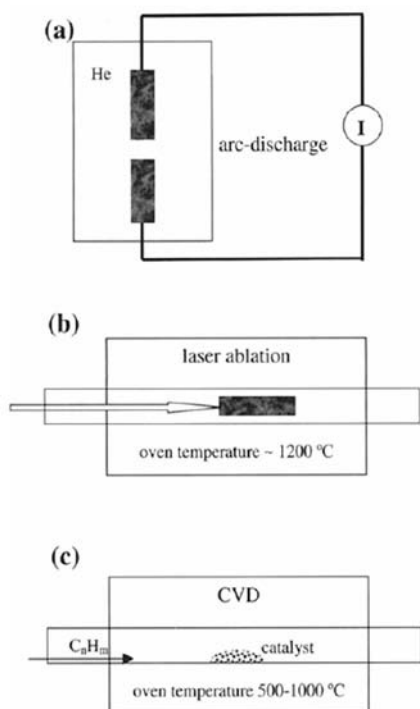


Figure 1.6. Schematic experimental setups for nanotube growth methods.

sample with a single chirality is an ultimate objective for carbon nanotube researchers. Indeed, significant progress has been made in this area: CVD methods with and without plasma enhancement have been used for preferential production of SWNTs, with a high percentage of semiconducting nanotubes (~90%)³⁷ or even SWNTs with a specific chirality distribution.^{38–42} However, there is still not enough for high purity single chirality SWCNTs which can only be obtained by some post-synthetic sorting methods so far.

1.4 The sorting methods of SWCNTs electronic type

As described above, synthetic methods have lacked sufficient control over SWCNT structure, leading to inhomogeneity in the resulting properties, mainly in the electronic type. These issues have hindered efforts to move carbon nanotubes from the research laboratory to the marketplace, especially for electronic and optoelectronic applications where reliable and reproducible performance is a requirement. Many separation techniques have been developed to separate SWCNTs of different electronic type, such as electrophoresis,^{43,44} gel chromatography,⁴⁵⁻⁴⁷ and DNA wrapping,⁴⁸⁻⁵⁵ density-gradient ultracentrifugation (DGU).⁵⁶⁻⁶⁹

Due to its ability to efficiently disperse SWCNTs in aqueous solution, DNA has been widely used in SWCNT sorting techniques, including ultracentrifugation⁴⁸⁻⁴⁹ and chromatography.⁵⁰⁻⁵³ Although these early efforts identified some dependence on SWCNT sorting effectiveness on the DNA sequence, a systematic search for DNA sequences that yield single-chirality sensitivity has been reported only recently.^{54,55} In particular, using a sequences-pattern expansion scheme, Zheng et al. have identified more than 20 DNA sequences that each select for a specific SWCNT chirality.⁵⁵ However, the yield of this method is very low and it is hard to remove the DNA wrapped around SWCNTs. Recently, the similar selective sorting of SWCNTs has been realized with gel chromatography method (unpublished), which can proceed with continuous and large scale separation.

Gels are commonly used in bioseparation techniques, which were focused on the use of agarose gels for SWCNT sorting recently.⁴⁵ This method can be used both for electronic type and diameter sorting.⁷⁰ While the initial paper assigned the sorting mechanism to preferential affinity of semiconducting SWCNTs to the agarose gel,⁴⁶ subsequent work concluded that Sodium Dodecyl Sulphate (SDS) more effectively disperse metallic SWCNTs, thus enabling them to move more easily through the agarose gel, while the semiconducting ones were held by the gels.⁴⁷ Then with a high concentration of SDS or other surfactants solution with stronger affinity to them, the semiconducting SWCNTs with different diameters can be washed out with control of the concentration.⁷⁰ The resulting semiconducting SWCNTs have been successfully employed in thin-film FETs.⁷¹ But so far gel chromatography does not work well on the SWCNTs with larger diameters and still needs more researches on it.

DGU is also a bioinspired sorting technique that allows SWCNTs to be separated by their

buoyant density.⁵⁶ In this method, SWCNTs are loaded into a density gradient that is intentionally formed in a centrifuge tube. In the presence of a centrifugal field, the SWCNTs are driven to move toward their isopycnic points where the buoyant density matches the local density of the gradient. Once the SWCNTs have layered in the gradient according to their buoyant density, established fractionation schemes are employed to extract the density-sorted SWCNTs. Traditionally, DGU has been performed in aqueous solution, thus necessitating the use of surfactant chemistry to disperse the hydrophobic SWCNTs in water. Since the buoyant density of SWCNTs in aqueous solution depends on the details of the surfactant encapsulation and affiliated hydration,^{58,59} the choice of surfactant chemistry enables significant sorting tenability. For example, the chiral nature of sodium cholate (SC) implies different adsorption as a function of SWCNT chiral handedness, resulting diameter sorting only with SC.^{57,60} Furthermore, co-surfactant mixtures of SC and SDS allow electronic type separation with purities exceeding 99%.⁶¹ And with controlled addition of deoxycholate sodium salts (DOC) as another co-surfactant, metal-semiconductor sorting of different diameter average was realized as well as the separation capability was improved.⁷² By operating in the transient regime, DGU has further been employed for length fractionation of SWCNTs.⁶⁷ Ultimately, the flexibility of DGU has been exemplified by its recent application to a variety of other nanomaterials, including double-walled carbon nanotubes,^{68,69} MWNT,⁷³ ultrashort SWCNT capsules,⁷⁴ single-walled carbon nanohorns,⁷⁵ gold nanocrystals,⁷⁶ and graphene.⁷⁷

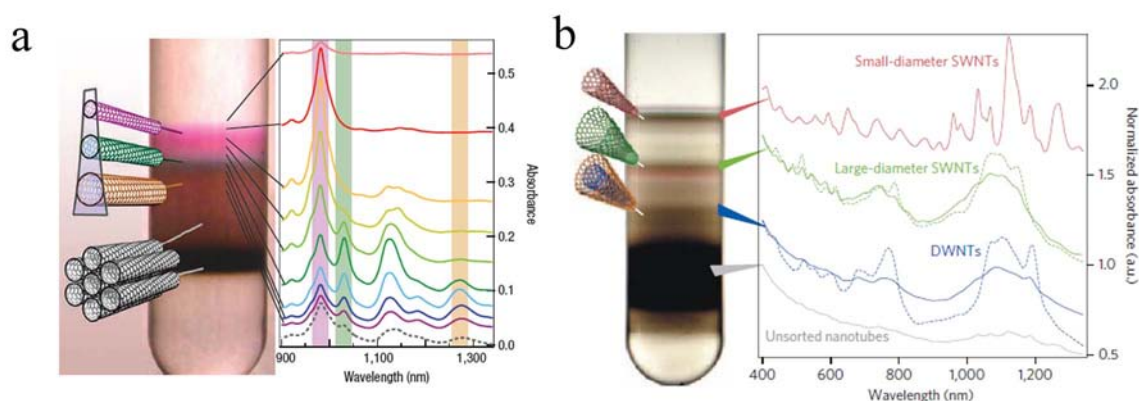


Figure 1.7. (a) Observation of diameter sorting for SC-encapsulated SWCNT.⁵⁷ (b) Monodispersed SWCNTs and DWCNTs are isolated using DGU.⁶⁸

As the sorting of SWCNT depends on the final buoyant density in the centrifugal tube, formation of a suitable density gradient in the centrifugation tube is important in separation. Typically, an initial linear⁷⁸ or step-like⁷⁹ density gradient is formed by mixing with iodixanol,

surfactants, and water to achieve the appropriate density, as shown in Figure 1.9. Nonlinear density gradients have also been used for improved separation.⁸⁰ In these methods, the SWCNTs are loaded into a narrow region with a small volume at the midpoint of the final positions of the metallic and semiconducting SWCNTs, in order to shorten the travelling distance. However, this procedure is limited in that the amount of SWCNTs injected into the centrifugation tube is only a small fraction of the total tube volume.

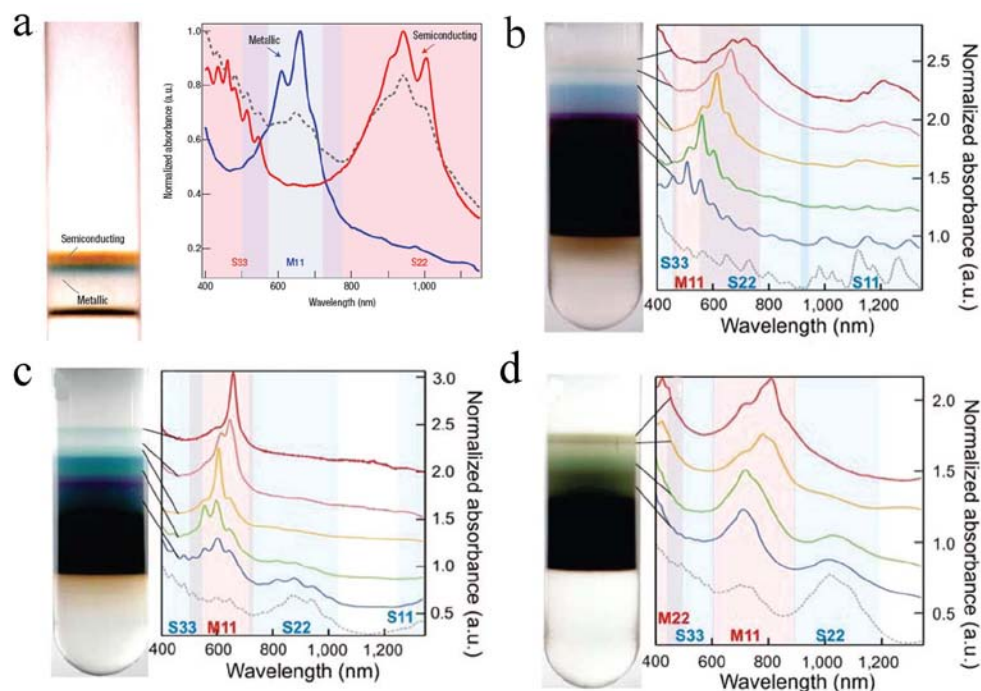


Figure 1.8 (a) Metal-semiconducting separation with co-surfactants of SC and SDS.⁵⁷ (b-d) High purity monodispersed metallic SWCNTs are isolated using DGU.⁶⁰

Iodixanol generates a spontaneous density gradient under ultracentrifugation.⁸¹ In this study, we attempted to start from a uniform density of iodixanol and use a self-generated density gradient for the separation. Uniform mixtures of SWCNTs, surfactants, water, and appropriate amount of iodixanol were prepared and filled in the whole centrifugation tube. In this case, the entire capacity of the centrifugation tube could be utilized for SWCNT dispersion. Interestingly, the separation ability was also improved. As a result, the amount of SWCNTs that could be separated at one time was successfully increased without degrading the separation purity. The large scale sorting of metallic and semiconducting SWCNTs are important for the practical application and some new scientific researches, such as neutron scattering.

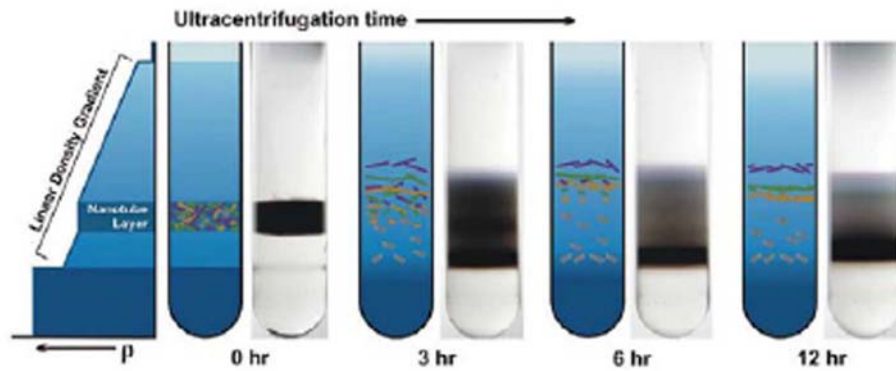


Figure 1.9 Schematics and photography of the SWCNT separation with a linear DGU process.⁸²

1.5 The applications of SWCNTs to electronic devices

1.5.1 Thin film transistors (TFTs)

The unique atomic and electronic structures of a CNT provide a number of unique advantages for making a FET channel. First, its small diameter (0.8 ~ 2 nm) allows optimum coupling between the gate and the channel. Second, because the surface of CNTs is atomically smooth and all carbon bonds are satisfied (i.e., no dangling bonds), scattering by surface states or roughness that plague conventional FETs are absent in CNT-FETs. Last, the reduced phase space for scattering along with the energy and momentum conservation requirements imply that the CNT channel is an exceptional medium for carrier transport. Since the first CNT-FET was reported in 1998,^{83,84} tremendous progress have been achieved. Despite their outstanding performance, the practical implementation of single CNT-FET faces a number of hurdles. The principal one is the heterogeneity of the as-produced CNT mixtures. This is an important problem, since the reliable and reproducible devices are basic requirement for large-scale integration. A nanotube-based electronic technology that has, to some extent, by passed the heterogeneity problem is that of CNT thin-film transistors (CNT-TFTs).⁸⁵ In such a TFT, a film of typically randomly oriented, as-prepared CNTs is deposited on an insulator. The electrodes then are patterned on top of it. The result is a channel having properties that are an ensemble average over all CNT species present in the layer. Multiple CNTs having multiple tube-tube junctions form the switching channel, and transport involves percolation across CNTs having random orientation, chirality, and diameter.

For applications, the presence of metallic CNTs in the mixture obviously poses problems, since they tend to short-circuit the FET channels. To avoid this, the device has generally longer

source-drain separation compared to the average length of the CNTs. This approach ensures that metallic tubes do not directly bridge the gap between source and drain contacts, and the transport is dominated by percolation through semiconducting CNTs.⁸⁶ One can optimize the current throughput of the CNT-TFT by controlling the CNT coverage. The challenge is to achieve the largest coverage of semiconducting CNTs, while staying below the threshold for metallic percolation. For example, Fujii et al. reported 100% yield of TFTs with on/off ratios higher than 10^4 using 95% semiconducting SWCNTs obtained by gel chromatography.⁷¹ But the current was lower because it had to keep a low density of SWCNTs to reduce the influence of metallic SWCNTs. The performance optimization in this case is a compromise between the on-current and the on/off ratio.

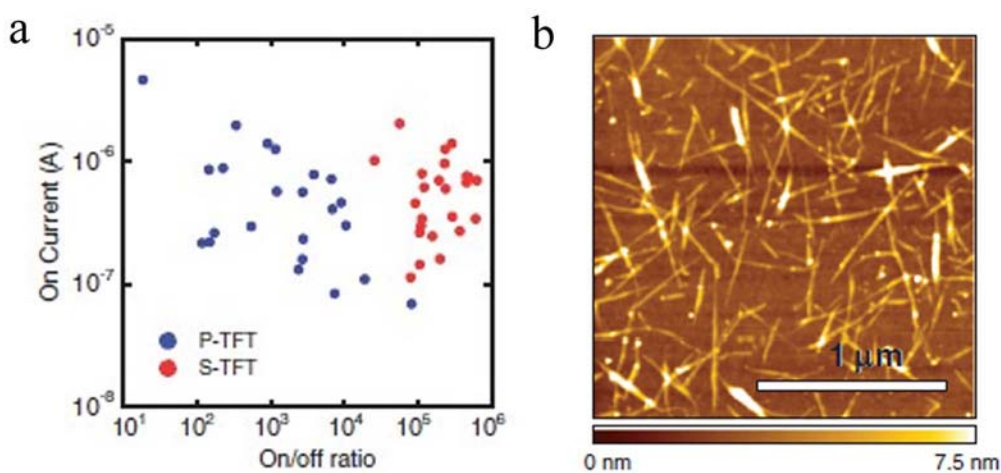


Figure 1.10. (a) On-state current plotted against on/off ratio of devices with 95% semiconducting SWCNTs obtained by gel chromatography. (b) AFM image of SWCNT bundles on substrate between source/drain electrodes.⁷¹

Two main methods have been employed to fabricate TFTs on flexible substrates using SWCNTs as a channel: solution processing^{87,88} and transfer printing.^{89,90} Producing SWCNT TFTs by solution processing has several advantages over producing them by transfer printing, including facile processability at room temperature, mass production at low cost and large-area fabrication. Recently, selectively adsorbed semiconducting SWCNTs⁹¹ and semiconductor-enriched SWCNTs⁹²⁻⁹⁴ have been used to fabricate solution-processed TFTs because electrical breakdown treatment⁹⁵ is not required to eliminate metallic SWCNTs. High-performance TFTs have been fabricated using selectively adsorbed semiconducting SWCNTs during spin coating.⁹¹ High-performance TFTs with high on/off ratios of up to 10^6 have also been obtained by using s-SWCNTs extracted by density-gradient

ultracentrifugation⁵⁷ and subjected to additional interfacial purification.⁹² However, for both these methods, the on/off ratios of about 20–30% of the fabricated TFTs were too low (i.e., below 10³) probably because the influence of metallic SWCNTs was not completely removed. However, there is still plenty of space for improving the performance of TFTs so that more of the excellent intrinsic electrical characteristic of SWCNT devices can be recovered. One is to minimize the resistance of CNT-CNT junctions by sorting CNTs in a way that minimized the diameter distributions and maximize their alignment. In a recent study using self-assembled and aligned 99% pure semiconducting CNT,⁹³ such improvements have been applied to produce TFTs with high on-currents and on/off ratio. In these experiments, a self-assembly technique was devised for the production of the highly aligned nanotube network, as seen in Figure 1.11a,b. The properties of the TFTs were much improved in terms of current drive, and reasonably on/off ratios about 10⁴ were obtained. Another way is to use high pure semiconducting CNTs so that the problems with the metallic CNTs are eliminated, which is one

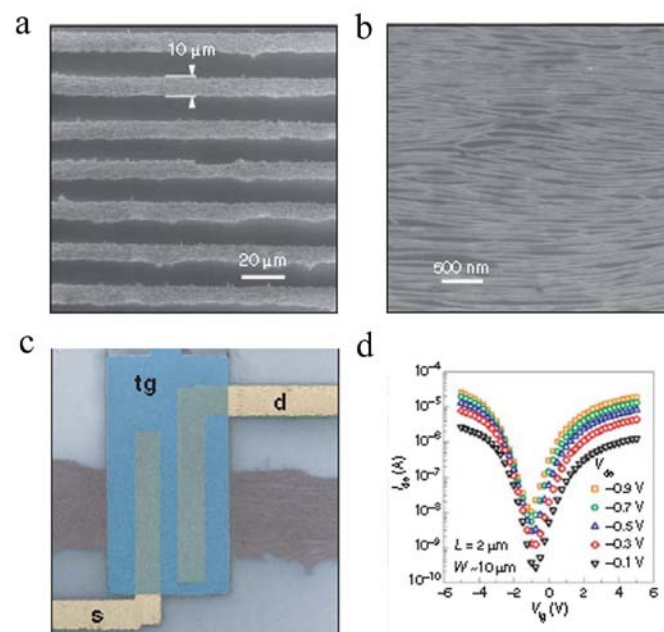


Figure 1.11.⁹³ Carbon nanotube thin-film transistor (CNT-TFTs). (a) Optical micrograph of large-scale self-assembled, aligned arrays of 99% pure semiconducting CNTs. (b) SEM micrograph of nanotubes within a strip. (c) Optical image of an individual CNT-TFT fabricated from one of the arrays showing the source (s), drain (d), and top-gate (tg) structures. (d) Transfer characteristics of the CNT-TFT having a 2 μm long channel and a 10 μm width. The characteristics are ambipolar.

objective of this study.

1.5.2 Organic Photovoltaic devices

Photovoltaic effects have long been observed in inorganic semiconductors. Early work was inspired by photosynthesis in which light is absorbed by chlorophyll, a member of the porphyrin family. The earliest OPVs were Schottky-type (Figure 1.12a) devices in which a rectifying contact is formed at one of the organic-electrode interfaces in a metal-organic-metal sandwich. Such devices are intrinsically inefficient as charge photogeneration takes place only in a thin layer near the metal-organic interface,^{96,97} limiting the quantum yield of charge photogeneration. Exciton quenching at metal-organic interfaces⁹⁸ can also reduce photocurrent yields.

The most successful organic solar cells are based on charge generation at an interface between two different organic semiconductors, also known as an organic heterojunction (Figure 1.12b). It is the key to the properties of organic solar cell. In a conventional *pin* photocell, photocarriers are directly created by absorption of light within the bulk of the undoped, intrinsic layer and are swept to the electrode by a built-in electric field due to the difference in the Fermi energy relative to the band edges of the p-type and n-type layers. However, light absorption in an organic semiconductor generates a neutral excited state akin to a tightly bound, Frenkel exciton. The built-in electric field arising from the different work functions of cathode and anode is insufficient to ionize such a state. In such solar cells, exciton dissociation occurs almost exclusively at the interface between two materials of different electron affinities (and/or ionization potentials): the electron donor and the electron acceptor. To generate an

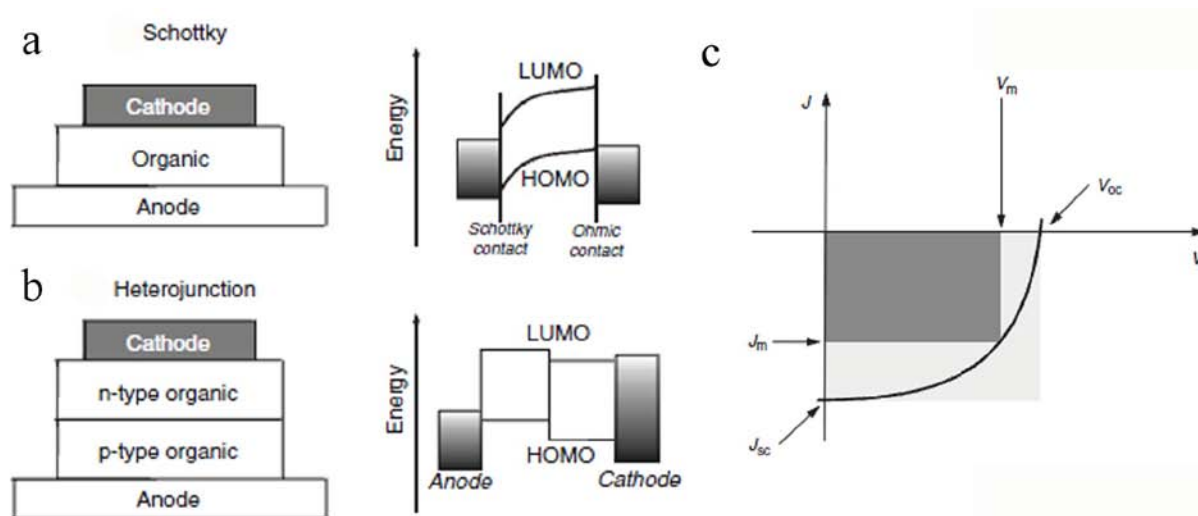


Figure 1.12. Schematic diagram of (a) Schottky-type and (b) heterojunction OPVs. (c) Current-voltage response of photovoltaic device under illumination. The open-circuit voltage (V_{oc}), short-circuit current (J_{sc}), and the current and voltage at maximum power output (V_m and J_m , respectively) are defined.⁹⁹

effective photocurrent in these organic solar cells, an appropriate donor-acceptor pair and device architecture must be selected.

The parameters used to characterize the performance of photovoltaic devices were briefly described here. Figure 1.12c shows a schematic diagram of the current-voltage curve of a photodiode under illumination. Devices are generally characterized by the short-circuit current (J_{sc}), the open-circuit voltage (V_{oc}), and the Fill Factor (FF). The fill factor of a device is defined as the ratio between the maximum power delivered to an external circuit and the potential power:

$$FF = \frac{P_m}{I_{sc} V_{oc}} = \frac{I_m V_m}{I_{sc} V_{oc}} \quad (3)$$

The Fill Factor is the ratio of the darkly shaded to lightly shaded regions in Figure 1.12c. The power conversion efficiency of a device is defined as the ratio between the maximum electrical power generated (P_m) and the incident optical power P_0 :

$$\eta = \frac{I_m V_m}{P_0} \quad (4)$$

In the more than 20 years since the seminal work of Tang,¹⁰⁰ organic solar cells have undergone a gradual evolution that has led to energy conversion efficiencies of about 5%,¹⁰¹⁻¹⁰⁶ basing on the heterojunction structure of Poly(3-hexylthiophene) and [6,6]-phenyl C₆₁ butyric acid methyl ester (PCBM). Two main approaches have been explored in the effort to develop viable devices: the donor-acceptor bilayer,¹⁰⁷⁻¹⁰⁸ commonly achieved by vacuum deposition of molecular components, and the so-called bulk heterojunction (BHJ),¹⁰⁹⁻¹¹⁰ which is represented in the ideal case as a bicontinuous composite of donor and acceptor phased, thereby maximizing the all-important interfacial area between the donors and acceptors. Polymer-based photovoltaic systems which can be processed in solution, and which generally take the form of BHJ devices, most closely conform to the ultimate vision of organic solar cells as low-cost, lightweight, and flexible devices. The real advantage of these BHJ devices, which can be processed in solution, over vacuum deposition is the ability to process the composite active layer from solution in a single step, by using a variety of techniques that range from inkjet printing to spin coating and roller casting. However, regardless of the method of preparation, one feature that extends across all classes of organic solar cells is the almost

ubiquitous use of fullerenes as the electron accepting component. The high electron affinity and superior ability to transport charge make fullerenes the best acceptor component currently available for these devices.

Recently, CNTs were considered as a substitute of PCBM with additional advantages due to their larger surface area which was supposed to provide more exciton dissociation centers and higher carrier mobilities which transfer the free charges to electrodes faster.¹¹¹ Previous researchers have used SWCNTs as electron acceptors in polymeric photovoltaics and shown an increase photoresponse compared to the pristine polymer devices.^{112,113} However, their efficiency is so far not possible to approach that of other composites, such as those using PCBM for example.

Several factors are thought to contribute to the limited efficiency. Firstly, the presence of charge recombination pathways must be taken into account, since CNTs are, in contrast to PCBM, only randomly dispersed within the P3HT matrix. Secondly, an incomplete exciton dissociation, especially at low nanotube concentration, about 1.0 wt% for SWCNT¹¹¹ and 5 wt% for MWCNT,¹¹⁴ is another factor. Dissolving, on the other hand, higher percentages of CNT within the polymer matrix decrease the efficiency. It is rationalized on the basis of short circuits, since the CNT length is comparable to the overall thickness of the photoactive layer. Finally, the presence of CNT ropes/bundles and moreover, appreciable amounts of metallic entities should be considered. All these rationales decrease the carrier selectivity in the device and favor the recombination process.

Another direction to integrate CNT into OPVs is to blend CNTs to the existing structure of P3HT:PCBM, solely acting as conductors for the collected charge carriers. The devices blended with MWCNTs fabricated by Berson et al. showed a power conversion efficiency of 2.0%.¹¹⁵ And a power conversion of 4.9% was obtained in a modified ITO/PEDOT:PSS /P3HT:PCBM/Al solar cell,¹¹⁶ after depositing a SWCNT layer between the ITO and the PEDOT:PSS or between the PEDOT:PSS and the photoactive blend. These results also raised the consideration if CNTs are actually suitable to act as the electron acceptor in OPVs.

In this study, the pure SWCNT-polymer composites were prepared and the optical properties were investigated to understand the photoconversion process between them. Different electronic types were mixed into organic photovoltaic devices in various

concentrations, and their photovoltaic characteristics were investigated.

1.6 Purpose of this study

In summary, the purpose of my study can be classified into the following three parts:

- (1) Separation of high-purity metallic and semiconducting SWCNTs with density gradient ultracentrifugation.
- (2) Fabrication of high-performance thin film transistor with high-purity semiconducting SWCNTs.
- (3) Understand the role of different electronic type SWCNT in the photovoltaic devices and utilization of them for better performance.

2. Separation of SWCNTs by Density Gradient Ultracentrifugation

2.1 Experimental

SWCNT Preparation

In this research, we focused on the separation of SWCNTs with large diameter. We used many types of SWCNTs provide by different companies, such as Honjo Chemical Corp and Meijo nano carbon. These SWCNTs are both synthesized by arc discharge and have similar diameter distribution with the range of 1.3~1.5 nm, which can be estimated from the breathing mode Raman spectrum. Although the sources of SWCNTs are different, they showed consistent separation ability in our experiment. It implies that our method is compatible with SWCNTs from different sources. If not specified, the SWCNTs used in the following parts should be Meijo SO type.

Dispersion preparation

At first, 25 mg of SWCNTs was dispersed in 100 ml of a 2 wt% sodium cholate hydrate (SC) because SC has better dispersibility than sodium dodecyl sulfate (SDS). The aqueous solution was sonicated using a 1/2 inch tip type ultrasonic homogenizer (Branson, Sonifier 450D, 20% output power) for 24 h. With the increase of sonication time, the isolated SWCNTs increased. Figure 2.1a shows a comparison among the absorption spectra of supernatant after different sonication time. The spectra show similar shape and peak positions. The resolved peaks mean the SWCNTs have been greatly dispersed. The optical density in case of 10h is about 2 times than that of 1h. It means more SWCNTs are isolated with long time sonication. However, the long time sonication will cut the SWCNTs and increase the defects. This will influence the performance of electronic devices made with SWCNTs. During sonication, the bottle containing the SWCNT solution was immersed in cold water (15 °C) to prevent heating.

The solution was then ultracentrifuged (Hitachi Koki, CS100GX II, Appendix D) at 289,000 g for 15 min to remove impurities and large bundles using an angle rotor (Hitachi Koki, S58A). The upper 80% of the supernatant was collected and used for separation. With the increase of ultracentrifugation time, more SWCNTs will be deposited and the concentration will decrease. In order to get high concentration for large amount separation, we performed shorter time

(15min) purification. Thus, some small bundles will remain in the supernatant and decrease the purity of separated SWCNTs. If longer time, such as 1h, was used, the supernatant will be enriched of isolated SWCNTs.

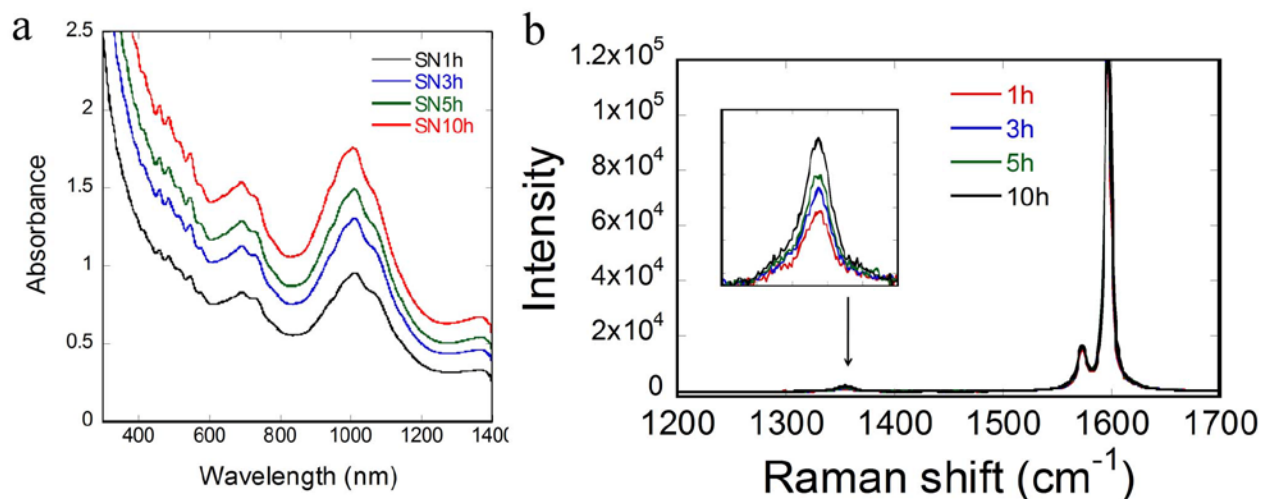


Figure 2.1. (a) Absorption spectra of SWCNT dispersion sonicated by different time. (b) Raman spectra of the dispersions. Inset is the amplification the D-band.

Step Density Gradient Ultracentrifugation (S-DGU)

SDS was added to the SWCNTs solution as a co-surfactant for the separation. At the same time, the SWCNT solution density was adjusted with iodixanol (Daiichi Pure Chemicals, Optiprep). Another medium, such as sucrose, had also been used in the DGU separation, but worse capability was observed. For the S-DGU, four density steps were prepared from the top to the bottom, using 30, 33, 40, and 60% (v/v) iodixanol, with a volume ratio of 2:1:1.5:0.5. SWCNTs were mixed in the 33% (v/v) layer. All layers contained 0.6 wt% of SC and 2.4 wt% of SDS. Separation was carried out using a swing rotor (Hitachi Koki, S52ST, 276,000 g, Appendix I). After ultracentrifugation for 24 h, the colored solution was collected using a fraction collector (Hitachi Koki, DGU-U).

Uniform Density Gradient Ultracentrifugation (U-DGU)

For the U-DGU, the preparation process is greatly simplified. The SWCNT solution was prepared as 0.6 wt% SC, 2.4 wt% SDS, and 33% (v/v) of iodixanol, and then injected into the centrifugation tube. The rest of procedure is as same as S-DGU.

Absorption spectra

The optical absorption spectrum of each fraction was recorded from 390 to 1000 nm using a plate reader (Corona Electric, SH-1000, Appendix II). The absorption spectra of selected portions were also measured from 200 to 1400 nm using a UV-Vis-NIR spectrophotometer (Shimadzu, SolidSpec-3700DUV, Appendix III).

Raman spectra

Raman spectra were measured using a single monochromator (Bunko Keiki, M331-TP, Appendix IV) with an edge filter for an excitation wavelength of 488 nm.

2.2 First separation

2.2.1 Optimization of separation condition

In DGU, aqueous dispersions of surfactant-encapsulated tubes are ultracentrifuged in a performed density gradient medium (DGM). During the process, they move along an ultracentrifuge cell, dragged by the centrifugal force, until they reach the corresponding isopycnic points. Such process depends only on the buoyant density of the particles. Thus, it is important to optimize the condition to make a density difference between different SWCNTs. As the surfactants have different affinities to SWCNTs according to their structures, the SWCNTs are structure-dependent encapsulated in the dispersion. Usually, the co-surfactants, such as SC and SDS are used to improve the electronic type separation. Further introduction of another surfactant, DOC, can achieve in a separation of high purity metallic SWCNTs. Recently, electronic type separation is also realized only by one surfactant, SDS, with change of the NaCl concentration in the solution. However, SDS has a weaker dispersivity of SWCNTs than SC, which results in a worse purity in the separated SWCNTs. Therefore, we dispersed the SWCNTs SC and separate them by adding the SDS.

The result of separation only with SC was shown in the Figure 2.2. All the conditions are same except for the SC concentration. The concentration varied from 3% to 0.6%. From Figure 2.2a, it was seen that in the high concentration of SC, such as 3% and 2%, the SWCNTs were not nearly separated. They stayed in the upper position of the tubes and moved down to the lower position with the decrease of the concentration. The trend of density of the SWCNTs was

shown in Figure 2.2b. It showed that with the decrease of SC concentration, the density of SWCNTs increased. It should be noted that some SWCNTs were separated in the case of low concentration. But it does not show the ability of electronic type separation. As SC is usually used for chirality separation, the separated SWCNTs ought to show chirality difference from the SWCNTs in the lower dark layer. However, the SWCNTs used in this study have a narrow diameter distribution and the chirality separation is not as obvious as that for SWCNTs made with CVD.

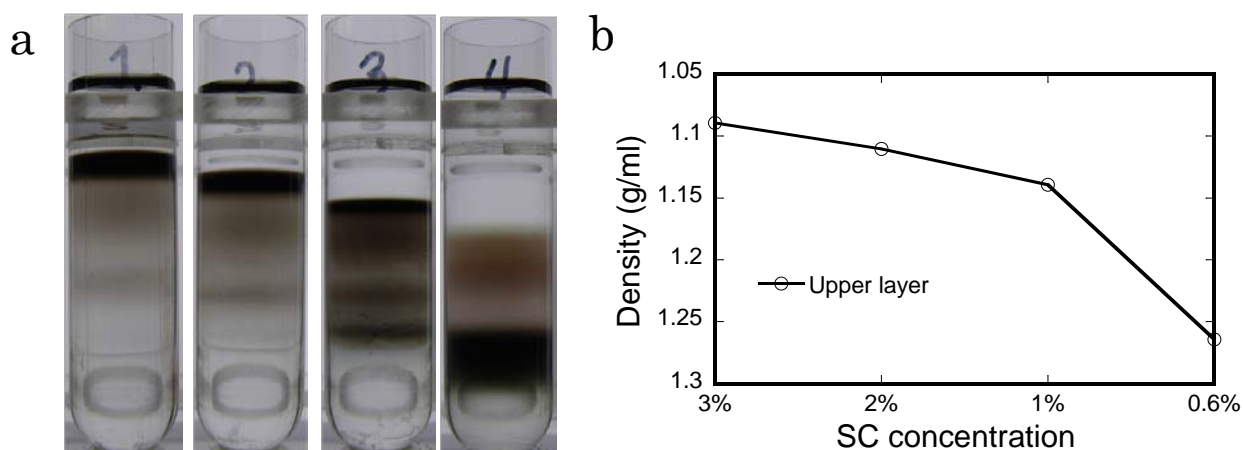


Figure 2.2. (a) Separation result with different SC concentration (from left to right: 3%, 2%, 1%, 0.6%).
(b) The density of SWCNTs layer.

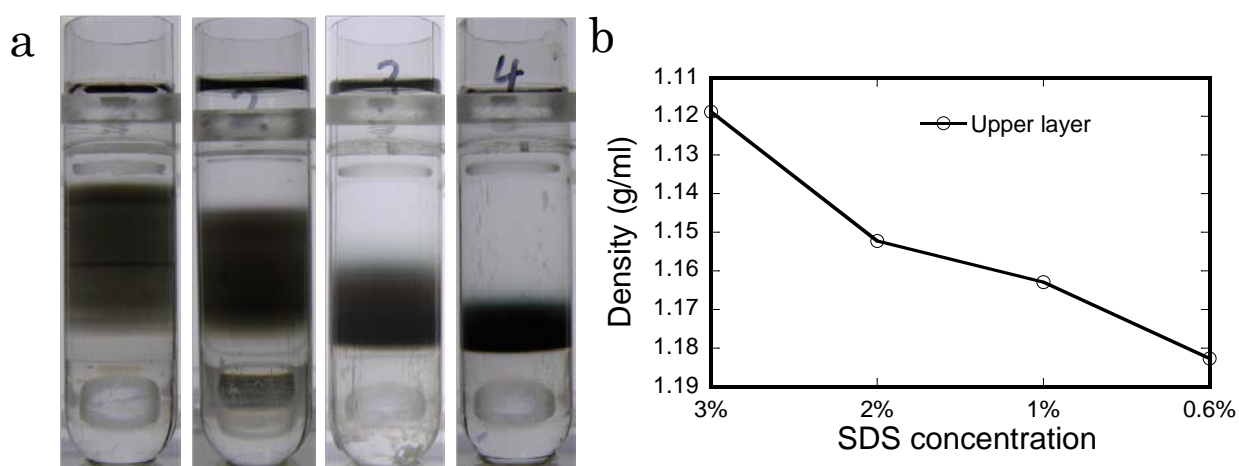


Figure 2.3. (a) Separation result with different SDS concentration (from left to right: 3%, 2%, 1%, 0.6%).
(b) The density of SWCNTs layer.

The separation only with SDS is also carried out and the result is shown in Figure 2.3. We can see that SWCNTs almost stayed in the lower position of the tube in the case of lower concentration (0.6%). With the increase of SDS concentration, the SWCNTs layer expanded and

some SWCNTs moved up. The higher the concentration is, the wider the layer expanded. It means that the density of some species of SWCNTs decreased with the increase of concentration, but the others have less change. From the above results, it is known that the difference of densities of SWCNTs depends on not only the kind of surfactants but also their concentrations. Thus, with the optimization of the absolute and relative concentration of two surfactants, the SWCNTs can be separated into different electronic type.

We optimized the ratio of surfactants to get the best ability. The total concentration of surfactant is set as 3%. Different SC:SDS ratios were performed and the result was shown in Figure 2.4. For the sample 1 and 2, three similar layers were observed: the upper metallic, the middle mixing and the lower semiconducting SWCNTs. If the SC percentage increased, the density of SWCNTs in the middle and lower layer increased so that they moved down and get narrower and closer in the ratio of 1:2. With a further increased SC, The mixing layer and the semiconducting layer got mixed, while the metallic layer expanded and some SWCNTs began

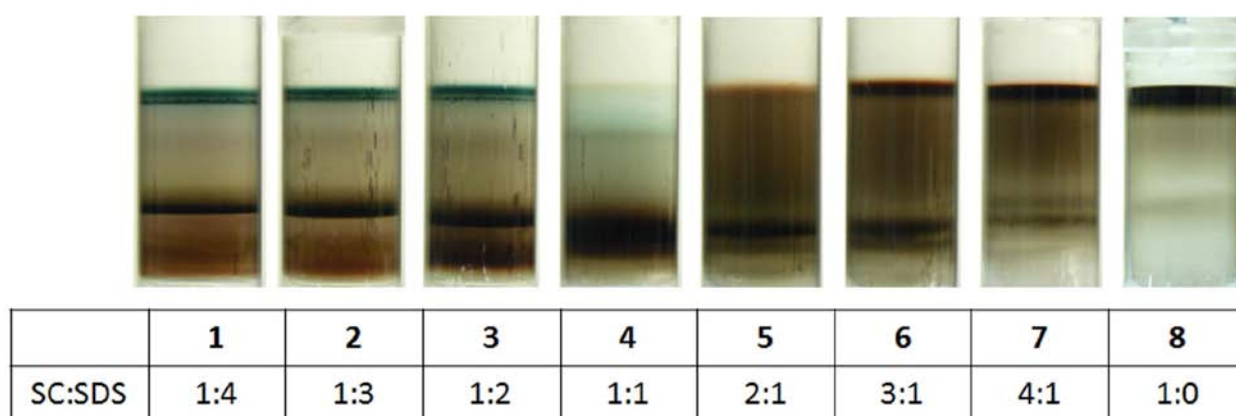


Figure 2.4. Photograph after separation with different SC:SDS ratios.

to move down, as seen for sample 4. In a higher SC concentration, the SWCNTs were almost wrapped by SC and showed little difference for different electronic type. Therefore, in sample 5 and 6, the color in the whole tube was almost same. For the sample 7 and 8, the SWCNTs concentrated in the upper position in the tube, as same as seen in the Figure 2.2. Considering the purity and the convenience of recovery, we used the ratio of 1:4 as the optimized condition. It should be noted that other parameter, such as temperature and pH value are same for all the samples.

2.2.2 Dispersion of SWCNTs

As seen in the sample 1 of Figure 2.4, a black layer was observed between metallic and semiconducting layer. It consisted of large amount of bundles. Depending on the size of bundles and the surrounding condition, the position of this layer changed and influenced the purity of separated SWCNTs, as seen in sample 3 and 4 of Figure 2.4. Therefore, it is important to isolate SWCNTs well. The increased sonication time can help to isolate the SWCNT, but induce more defects, as shown in Figure 2.1.

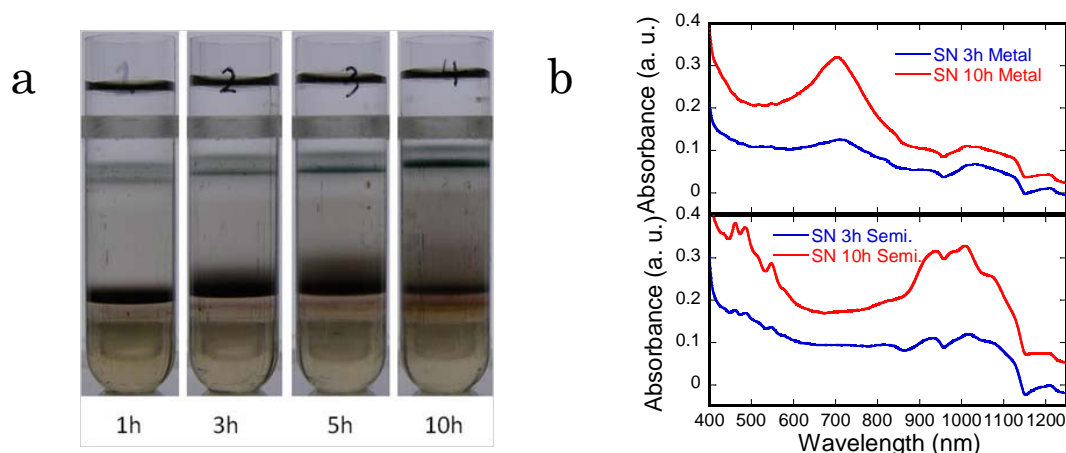


Figure 2.5. (a) Separation of SWCNTs sonicated with different times. (b) Absorption spectra of metallic and semiconducting layer of separation with 3h and 10h sonication.

Figure 2.5 shows the result of separation of SWCNTs dispersed with different sonication time. The concentrations of all samples are adjusted to the same before separation. In all the case, SWCNTs have been separated into three color zones: the upper green zone, the middle black zone and the lower brown zone. For the sample with 1h sonication time, the upper and lower layers were thin and can hardly be observed, while the black layer is thick. It means that few SWCNTs had been isolated within 1h sonication and most of them were bundles. With the increase of sonication time, the upper and lower layer got thick, which can be observed from either the color or the optical density, as shown in Figure 2.5b. The black zone expanded and became thinner. Some bundles were isolated by longer sonication and moved to metallic or semiconducting layer, respectively. Some others were still bundles but smaller. Therefore, they stayed in the center of the tube and formed a wide mixing zone. From the Figure 2.5b, we can see the purity of separated SWCNTs did not change, although the concentration increased. Therefore, a longer sonication time is necessary for mass separation of high purity metallic and

semiconducting SWCNTs. The influence of the defects induced by sonication will be discussed in later sections.

Even with long time sonication, the SWCNTs can't be completely isolated into individual ones. Therefore, we used ultracentrifugation to remove bundles. In our study, in order to get high concentration of SWCNTs, a short time (15min) ultracentrifugation was performed. Some small bundles will remain in the solution and can hardly be separated. If a longer time ultracentrifugation, such as one hour, the bundles will greatly decrease and the purity will be improved. In exchange, the concentration will decrease and the yield will be low.

2.2.3 Uniform DGU

In DGU process, typically, an initial linear⁷⁸ or step-like⁷⁹ density gradient is formed by mixing with iodixanol, surfactants, and water to achieve the appropriate density. Nonlinear density gradients have also been used for improved separation.⁸⁰ In these methods, the SWCNTs are loaded into a narrow region with a small volume at the midpoint of the final positions of the metallic and semiconducting SWCNTs, in order to shorten the travelling distance. However, this procedure is limited in that the amount of SWCNTs injected into the centrifugation tube is only a small fraction of the total tube volume.

Iodixanol generates a spontaneous density gradient under ultracentrifugation.⁸¹ In this study, we attempted to start from a uniform density of iodixanol and use a self-generated density gradient for the separation. Uniform mixtures of SWCNTs, surfactants, water, and appropriate amount of iodixanol were prepared and filled in the whole centrifugation tube. In this case, the entire capacity of the centrifugation tube could be utilized for SWCNT dispersion. Interestingly, the separation ability was also improved. As a result, the amount of SWCNTs that could be separated at one time was successfully increased without degrading the separation purity.

Figures 2.6a and 2.6b show before and after photographs of the centrifugation tubes for the S-DGU and U-DGU separations, respectively. In both cases, the same amount of SWCNTs (~53 μg) was used and the colors of the metallic (dark green) and semiconducting (brown) SWCNTs were clearly observed for similar conditions. The optical absorption spectra of the 20 fractionated colored solutions are shown in Figures 5c and 5d. The labels S₂₂ (800-1000 nm)

and S_{33} (390-550 nm) in the figures indicate the second and third optical absorption bands of semiconducting SWCNTs due to the second and third one-dimensional van Hove singularities (vHS). The label M_{11} (550-750 nm) corresponds to the first absorption band of the metallic SWCNTs.³ In the case of S-DGU, only the M_{11} band is observed in the uppermost fraction,

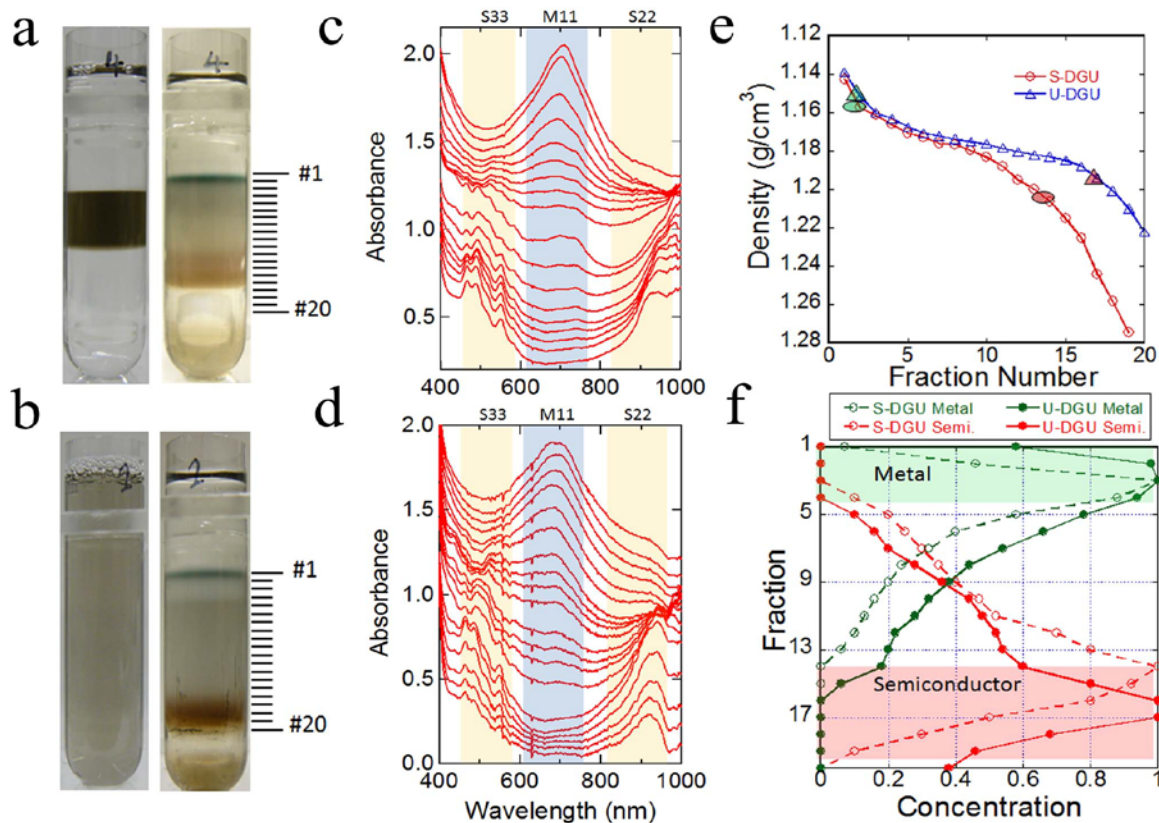


Figure 2.6. Photograph of centrifuge tubes before (left) and after (right) separation with (a) graded density and (b) uniform density. (c, d) Respective optical absorption spectra for fractions 1-20. (e) Variation in density as a function of fraction number. (f) Relative concentration of metallic (green circles) and semiconducting (red circles) SWCNTs as a function of fraction number.

which indicates high-purity metallic SWCNTs. With increasing depth, the intensity of the M_{11} peak decreases and the S_{22} and S_{33} peaks then appears. Finally, in a few of the bottom layers, the M_{11} peak almost disappears and only the S_{22} and S_{33} peaks are observed, which indicates high-purity semiconducting SWCNTs. A similar trend is also observed for the U-DGU fractions, as shown in Figure 2.6f. These spectra clearly show that metallic and semiconducting SWCNTs can be separated by both S-DGU and U-DGU. However, in the case of U-DGU, there were some interesting features. The distance between the metallic and semiconducting layers was larger than that for S-DGU, which makes collection of the sorted SWCNTs much easier. For U-DGU,

the highest purity metallic and semiconducting SWCNTs yields were 17.6 and 27.2%, respectively, of all the SWCNTs used for separation, while they were 12.4% and 23.6% for S-DGU. The purity of the metallic and semiconducting SWCNTs was evaluated from the optical absorption spectra (200 to 1400 nm).¹¹⁷ The purity of semiconducting SWCNTs was 98% and the purity of metallic SWCNTs was 95% for both U-DGU and S-DGU.

Figure 2.6e shows the density gradients for both methods after ultracentrifugation. The density of the most pure and concentrated fraction was selected as representative of the entire separated layer. The densities of the metallic and semiconducting layers for S-DGU were 1.14 and 1.21 g/ml, respectively. These values agree well with the values of 1.14 and 1.20 g/ml obtained for U-DGU, respectively. Because the ratio of surfactants was the same for both S-DGU and U-DGU, the densities of the metallic and semiconducting SWCNTs should be identical in both methods. The larger distance between the metallic and semiconductor layers in U-DGU resulted from the gentle slope of the final density gradient compared with that of S-DGU due to its uniform initial density.

The uniform initial density is an advantage of U-DGU, because the SWCNTs can be dispersed within the entire centrifuge tube, so that much more SWCNTs can be separated at one time. U-DGU separation was carried out for a larger amount of SWCNTs, up to 7 times larger than the amount shown in Figure 2.6. The result of separation with an amount 5 times larger is shown in Figure 2.7a, and the spectrum for each fraction is shown in Figure 2.7b. The high concentration makes it difficult to see the color of the layers in the centrifugation tube, as shown in Figure 2.7a. However, from the optical absorption spectra shown in Figure 2.7b, separation ability similar to that for the low concentration case is observed. In Figure 6c, the separation purity of the most concentrated metallic and semiconducting SWCNTs section is shown as a function of the SWCNT amount. The semiconducting SWCNTs maintain a purity higher than 98% even at 7 times higher concentration. The metallic SWCNTs maintain a purity above 90% up to 5 times higher concentration, but the purity is reduced at 7 times concentration. The difference in purity between metallic and semiconducting SWCNTs is probably caused by the difference in centrifugal force; in the upper part of the centrifugation tube, the centrifugal force is always less than that in the lower part, due to the smaller rotation radius. Since the metallic SWCNTs at the bottom are subjected to a higher centrifugal force,

they move more quickly to their equilibrium position. However, the semiconducting SWCNTs at the top part of the tube can require 24 h to achieve equilibrium, especially at high SWCNT concentration. In the case of 5 times concentration, approximately 260 μg of SWCNTs can be separated per tube. Because the S52ST swing rotor has 4 tubes, approximately 1 mg of SWCNTs can be separated into 176 μg of metallic SWCNTs and 272 μg of semiconducting SWCNTs in one separation.

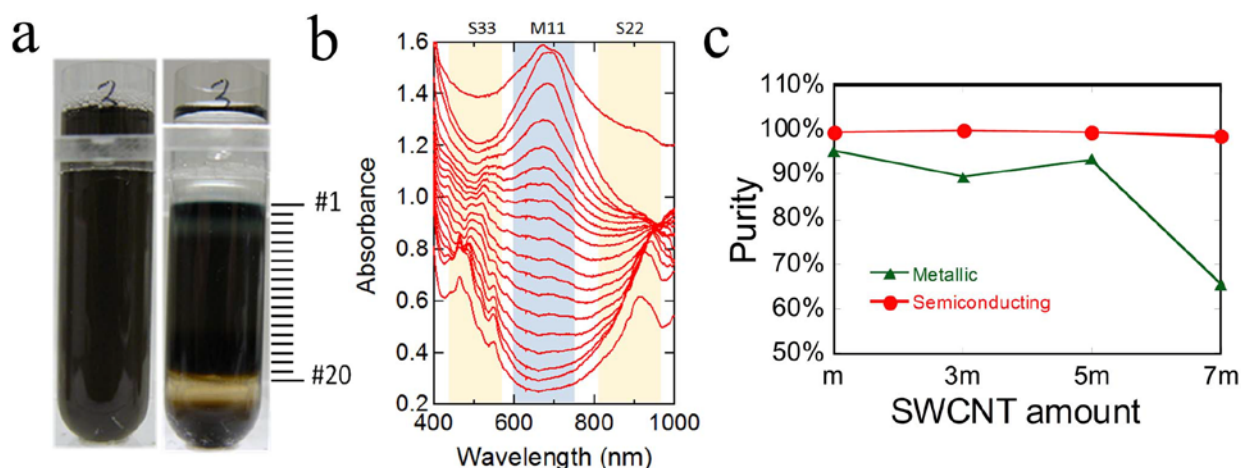


Figure 2.7. (a) Photograph of centrifuge tube before (left) and after (right) separation by U-DGU with 5 times the amount of SWCNTs. (b) Optical absorption spectra for each fraction. (c) Purity of metallic and semiconducting SWCNTs vs. the amount of pristine SWCNTs (where m is the amount used in Figure 1).

Some uncertainties may be present in the purities determined from the optical absorption spectra due to the large background absorption; therefore, the purities of the separated SWCNTs were also evaluated using resonance Raman spectroscopy. Figure 2.8 presents radial breathing mode (RBM) Raman spectra of the pristine and separated SWCNTs in a solution phase. The samples were excited at 488 nm, which corresponds to the S_{33} excitation of the SWCNTs used in this work. Thus, only the resonance peak due to the semiconducting SWCNTs can be observed. The Raman intensity is proportional to the concentration of SWCNTs,¹¹⁸ namely the concentration of semiconductors in the sample in this case. Here, the samples were prepared to have the same absorbance at 488 nm and each measurement was carefully performed under the same conditions. A sharp peak at 169 cm^{-1} is observed for both the pristine and semiconducting SWCNT samples. In the case of U-DGU, the intensity of the RBM peaks is 1462 and 2130 (arbitrary unit), respectively. If the semiconducting concentration in pristine SWCNTs was assumed as 67%, which is the theoretical concentration in as-grown SWCNTs,

then the purity of the semiconducting SWCNT obtained by U-DGU can be estimated to be 98% by multiplying by the RBM intensity ratio. This value corresponds to the purity estimated from the optical absorption spectrum, which is also comparable to that reported previously.¹¹⁷

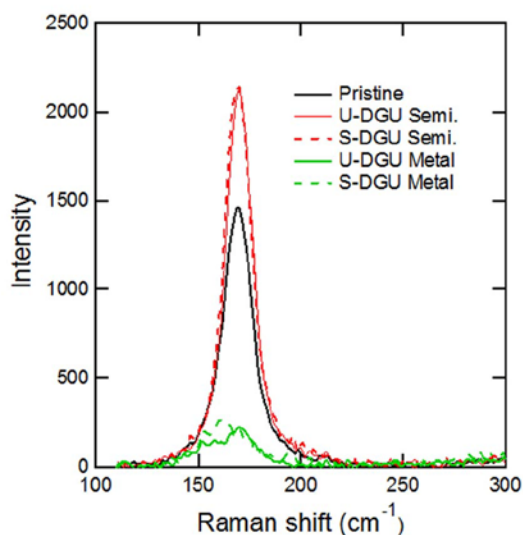


Figure 2.8. Raman spectra of the radial breathing mode (RBM) of pristine, metallic and semiconducting SWCNTs separated by the S-DGU (dash) and U-DGU (solid) methods.

For S-DGU, the same value was obtained for the purity of the semiconducting SWCNTs. This means that U-DGU can be used for the separation of high purity semiconducting SWCNTs as same as S-DGU. On the other hand, the purity of metallic SWCNT is estimated to be 90% for U-DGU and 89% for S-DGU from the Raman spectra of metallic SWCNTs, which is slightly lower than the value obtained from the optical absorption spectra. In Figure 2.8, not only the peak around 169 cm^{-1} , but also a small shoulder at 155 cm^{-1} is observed. The diameters of the SWCNTs are known to be inversely proportional to the RBM frequency.¹¹⁹ Therefore, the peak at 155 cm^{-1} corresponds to SWCNTs with larger diameters. This result indicates that some larger diameter semiconducting SWCNTs tend to stay in the upper layer, probably due to their lower density.⁷⁸

The difference in peak positions of S22 absorption band can also be observed from the absorption spectra of metallic/mixed/ semiconducting SWCNTs sections, as shown in Figure 2.9. The S22 absorption band clearly exhibits a blue shift from the upper to the lower layer in the centrifugation tube, while the M11 band does not exhibit any significant variation. The weak S22 absorption band in the metallic SWCNTs layer appears around 1029 nm. For the middle layer, this band shifts to 1000 nm, and finally moves to around 980 nm for the semiconducting SWCNTs layer. The surfactant concentration in all solutions was adjusted to be same prior to

the measurement. Therefore, the peak shift is not due to difference in the surfactant. This means that the lower layer contains smaller diameter semiconducting SWCNTs.¹⁵

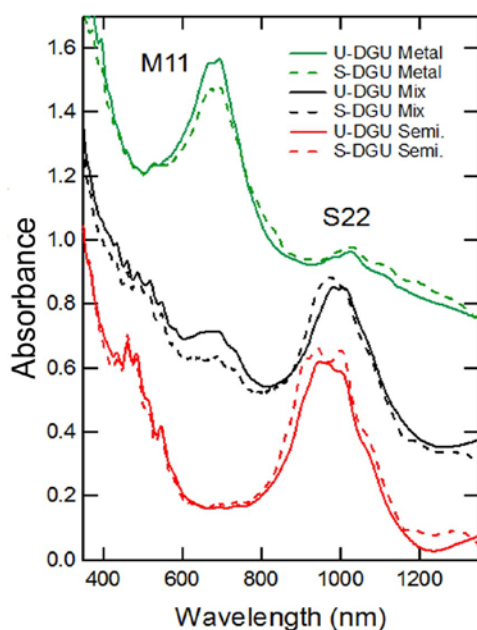


Figure 2.9. Optical absorption spectra of the metallic, mixed and semiconducting section in S-DGU (dash) and U-DGU (solid) separation.

Present results have shown that U-DGU can separate SWCNTs into metallic and semiconducting ones as well as S-DGU. For DGU separation of SWCNTs, sucrose can also be used as density gradient medium.¹²⁰ However, sucrose doesn't change its density gradient under ultracentrifugation process. It means U-DGU method is available only when we use the iodixanol as density gradient medium. In the usual DGU process, the linear/step density was formed and SWCNTs were injected in the midpoint of gradient to minimize the moving distance of both metallic and semiconducting SWCNTs. However, nobody confirmed to date whether it is really important or not. In this work, we demonstrated that even starting with uniform density, SWCNTs could be separated with high-purity. This result suggests that the movement of SWCNT is much faster than the velocity we expected. By considering the lower separation purity of sucrose-DGU method, the iodixanol molecule acts important role for the high-purity separation of SWCNTs. The self-generation of density gradient means that considerable amount of iodixanol molecules moved for long distance in the DGU process. This molecular flow probably accelerated the SWCNT movement and realized the high-purity separation.

If the SWCNTs could move quickly, the final density gradient turns more important for the high efficiency separation. To get larger separation distance between metallic and

semiconducting layers at the centrifugation tube, lower slope of the final density gradient is better. In this meaning, U-DGU is better than S-DGU and linear DGU method, because additional self-generated density gradient was always applied to the initial density gradient. The comparison of separation with different initial density was shown in the next section.

2.2.4 Comparison of linear/step and uniform DGU

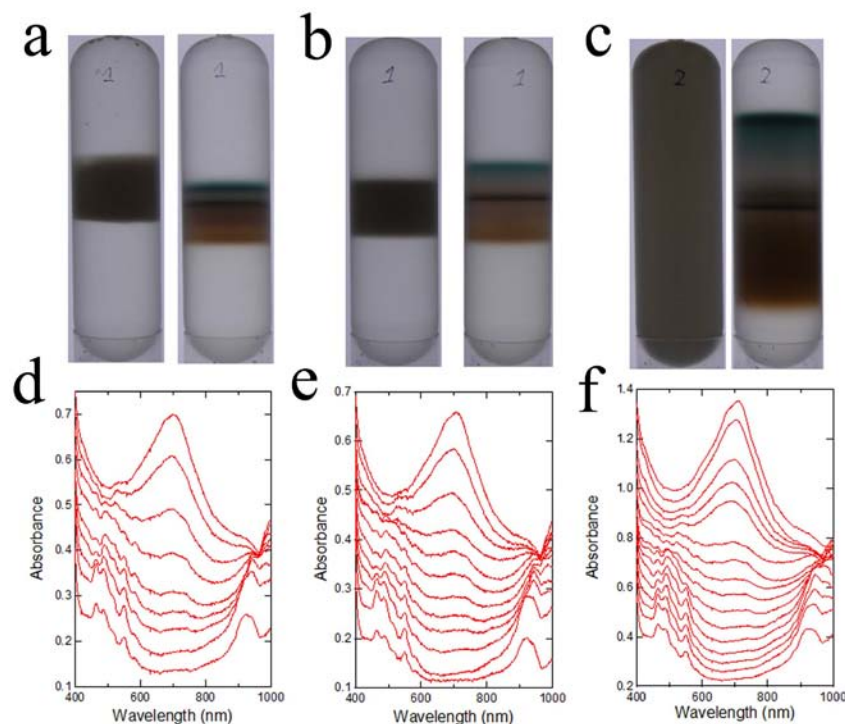


Figure 2.10. The photograph before and after separation with linear (a), step (b) and uniform (c) initial density. The absorption spectra of the fractions of separated SWCNTs in linear (d), step (e) and uniform (f) DGU.

The separation with linear, step and uniform initial density were performed and the results were shown in Figure 2.10. The linear density varied from 1.125 g/ml in the top to the 1.3 g/ml in the bottom, which was similar as the final density gradient in the U-DGU. The S-DGU and U-DGU were prepared as the methods described in section 2.1. The photographs before and after separation for Linear, Step and Uniform DGU were shown in Figure 2.10a,b,c. The L-DGU showed a narrow color zone after separation, while the zone in S-DGU is wider. In the case of U-DGU, the zone expanded much wider to about two times than that of S-DGU. It is because the initial density of U-DGU is flat and results in a gentle slope in the centrifuge tube after ultracentrifugation by the moving of iodixanol self. For the L and S DGU, as an original density gradient already exists before ultracentrifugation, the slope will be sharper with the

plus of self-generated density gradient. As the separation parameters, such as surfactants ratio, temperature and pH value, were all same for three cases, the density of each species of SWCNTs should be same due to the identical surrounding conditions. Therefore, the distance between different species will be extended due to the flatter gradient, as seen in the Figure 9. However, the distribution of these species will not change. It can be confirmed from the absorption spectra trend of the fractions of the separated SWCNTs, as shown in Figure 9d,e,f.

The comparison of absorption spectra of metallic and semiconducting layer in linear, step and uniform DGU was shown in Figure 2.11. It was seen that the spectra of semiconducting SWCNT (Figure 2.11b) were similar for each case. It means that high purity semiconducting SWCNTs can be obtained by any method, without affect of initial density. However, the metallic layer in L-DGU showed a stronger absorption band in S22 than in U-DGU, as seen in Figure 10a. Because the separated SWCNTs were compressed in a narrow layer in a narrow zone, the upper metallic layer got closer to the lower semiconducting layer. The closer distance made it difficult to recover the metallic layer accurately with the present fraction machine in the lab, especially in the high concentration. But it should be noted the actual purity of the metallic SWCNT should be same for any methods because of the same experiment conditions. In spite of that, from the view of the large-scale production and the simplification of industry procedure, the separation with uniform initial density is the best choice for the mass production of high purity metallic and semiconducting SWCNTs.

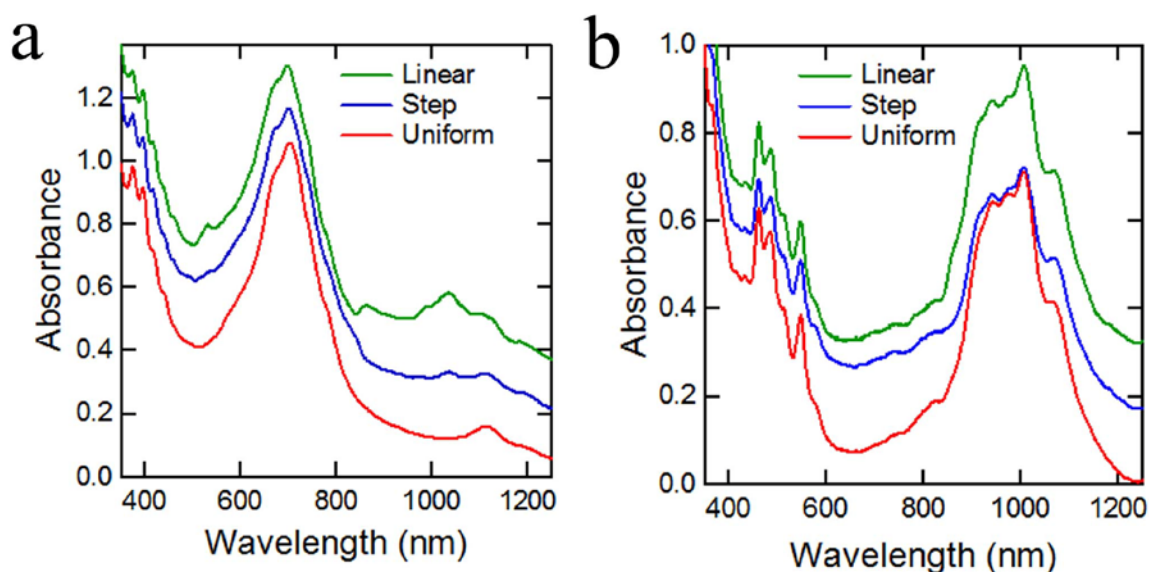


Figure 10. The absorption spectra of metallic SWCNTs layers (a) and semiconducting SWCNTs layers (b) in linear, step and uniform DGU.

The density gradient profiles before and after separation for the linear, step and uniform density were shown in Figure 2.12. As the iodixanol moves by itself under the ultracentrifugation, a extra density gradient will be applied to the initial density and sharps the gradient in the centrifuge tube. Furthermore, with the movement of iodixanol, the boundary of each density gradient will become indistinct and the gradient turns to a continuous one. Because the SWCNTs were not sorted into an absolutely single species, which were mixed with similar species with slightly different density, the layers of the separated SWCNTs always had a wild distribution and had a intersection with others. It will induce the decrease of purity of each species. Using the uniform density, the gradient after separation became flatter and resulted in a wilder layer of separated SWCNTs. It will decrease the intersection of different species and distinguish them more clearly.

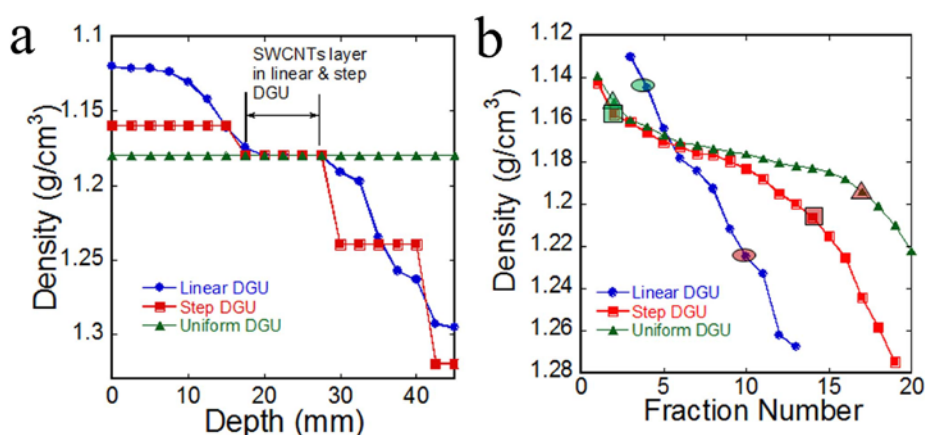


Figure 2.12. The density gradient before (a) and after (b) ultracentrifugation in Linear, step and uniform DGU

2.3 Second separation

The SWCNTs used in this study has a relatively narrow distributed diameter. The difference between densities of different species is small. Although the semiconducting SWCNTs were widely distributed in the tube, there was no clear boundary between different species. Because of the intersection with metallic and mixing layer, the purity of the semiconducting SWCNTs is different according to the position. Usually the lower the position is, the higher the purity is. From the spectra shown in Figure 11, the blue zone had a lower purity than red zone. As there is no clear boundary between SWCNTs with different purity, it is hard to recover them respectively and simply and resulted in a lower purity in whole. Therefore, a second separation is necessary to further purify the SWCNTs.

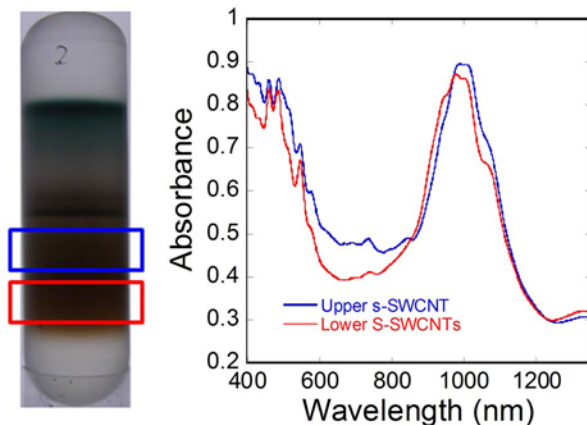


Figure 2.13. The absorption spectra of semiconducting SWCNTs in different positions.

2.3.1 Optimization of separation condition

We recovered both blue and red zone in the 1st separation for further purification. As the semiconducting layer stays in the lower of centrifuge tube, they contain a high concentration of iodixanol that makes them high density. The high density is inconvenient for setting the position of SWCNTs in the DGU method so that the iodixanol needs to be removed. And after 1st separation, the morphology of surfactants wrapped on the surface of SWCNTs changed and became unclearly. The dielectric environment is also needed to be re-adjusted.

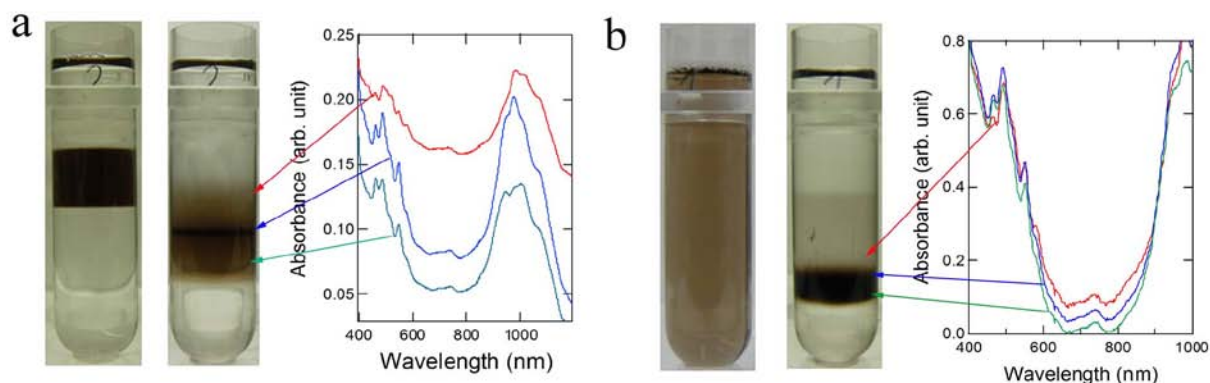


Figure 2.14. The photograph and absorption spectra of 2nd separation of 1st separated semiconducting SWCNTs with step (a) and uniform (b) DGU method

We collected the semiconducting SWCNTs separated in the first step and removed the iodixanol by flowing them through a column filled with suphcral-300 gel. The detail was described in section 3.1. Then the solution was concentrated at 289,000 g for 2h using an angle rotor. The deposition was collected and re-dispersed with a 2 wt% SC solution. At first, we tried the same parameter as the 1st separation. The detail procedure can refer to the description in

section 2.1. Both step and uniform DGU were performed but no good result was observed, as shown in Figure 2.14. Because the contents in the 1st separated semiconducting SWCNTs were different from that in the pristine ones, especially the metallic parts. Most of the metallic parts in the pristine solution exist in isolated way, while they exist in small bundles with semiconducting SWCNTs in the 1st separated semiconducting SWCNT solution. As the affinities to the surfactant are different for two kinds of metallic parts, the ratio of surfactant must be optimized again to make a difference between the densities of metallic bundles and the pure semiconducting SWCNTs.

At first, 4 ml solution was filled in the centrifuge tube, which was optimized as 3 wt% SDS, x wt% SC and 40% (v/v) iodixanol. The concentration of SC, namely x , changed from 0% to 0.75%. Then 1ml 2 wt% semiconducting SWCNTs was injected on the top of it, followed by ultracentrifugation for 24 h by a swing rotor (Hitachi Koki, S52ST, 276,000 g). The detail parameters were listed in Table 2.1 and the result was shown in Figure 2.15.

Table 2.1. The surfactant concentration in 2nd separation

SC% (x %)	0%	0.1%	0.25%	0.5	0.75%
SC:SDS in lower Layer	0:1	1:30	1:12	1:6	1:4
SC:SDS in whole tube	1:6	1:5	1:4	1:3	1:2.4

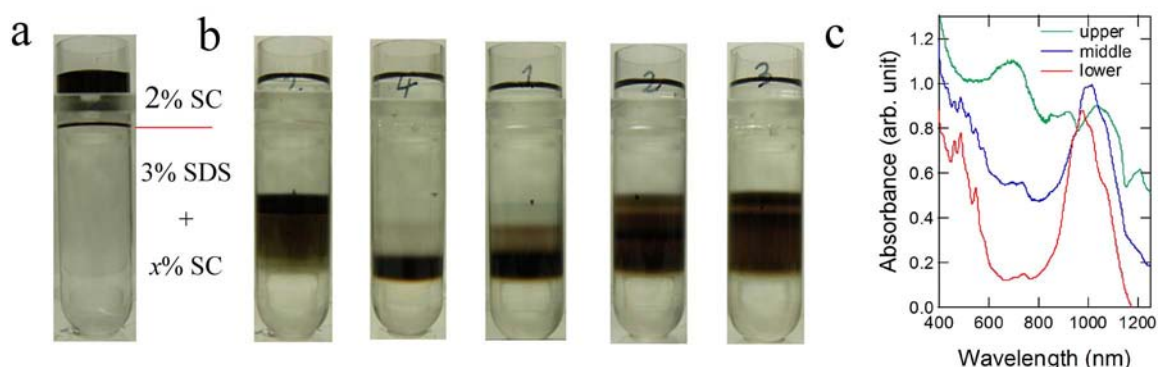


Figure 2.15. (a) Photograph before ultracentrifugation. (b) Photograph after separation with different concentration of SC (from left to right: 0%, 0.1%, 0.25%, 0.5% and 0.75%). (c) The absorption spectra of separated SWCNT with 0.25% SC.

From Figure 2.15, we could see that the SWCNTs after ultracentrifugation stayed in the lower position in the centrifuge tube, in which was away from the position before ultracentrifugation. It means that the SWCNTs were always in identical dielectric environment when they moved from start point to the final point. Therefore the dielectric

environment in the lower position decided the interaction between surfactants and SWCNTs, as well as the density of SWCNTs. When the lower solution was totally SDS solution, the SWCNTs were concentrated in the upper layer showing no selectivity to different electronic type. With the addition of SC, even as low as 0.1%, the SWCNTs suddenly moved down and concentrated in the lower layer. It indicates that the density of SWCNTs increased. One explanation is that the SDS wrapped on the surface of SWCNTs were mostly replaced by SC, which induced the increase of density, as seen in the separation with low concentration of SC shown in Figure 2.2. But we noticed the pH value is 5 when the surfactant is only SDS, while turns to 7 when the SC is added. When we adjusted the pH to 7 with NaOH, the SWCNTs in totally SDS solution also moved down to the lower layer. It suggested an affect of pH value on the density of SWCNTs, which was reported by *Aronld* et al. It also might be induced by the change of the concentration of sodium ion, which resulted in a vertical morphology of SDS on the surface of SWCNTs, as reported by Niyogi.⁶²

With the increase of SC concentration, some green SWCNTs were separated from the lower brown ones at the concentration of 0.25%. From the spectra in Figure 13c, it is known this portion was enriched of metallic SWCNTs. However, the spectrum was different from the metallic ones in the 1st separation because of its stronger semiconducting absorption band around 1000 nm. It indicates that this portion were bundles enriched of metallic SWCNTs, which can't be separated as well as isolated metallic ones in the 1st separation. When the SC concentration became higher, some SWCNTs in the lower layer moved up and mixed with the green ones. At the SC concentration as high as 0.75%, most of them moved up and concentrated at the upper layer. Although we could recover some pure semiconducting SWCNTs stays in the lower layer, the yield became low.

Although the bundles enriched of metallic SWCNTs had been separated from the semiconducting SWCNTs, we can still observe weak metallic absorption peak around 750 nm in the absorption spectrum of the lower SWCNTs. It is because some bundles not enriched of metallic existed in the lower layer. Some of them were induced by the incompletely isolation by the sonication, while others were induced by the rebundling during the recovery process. Therefore we performed a post sonication after recovery of 1st separated semiconducting SWCNTs to disperse the bundles, and the results depending on the sonication time were shown

in Figure 2.16.

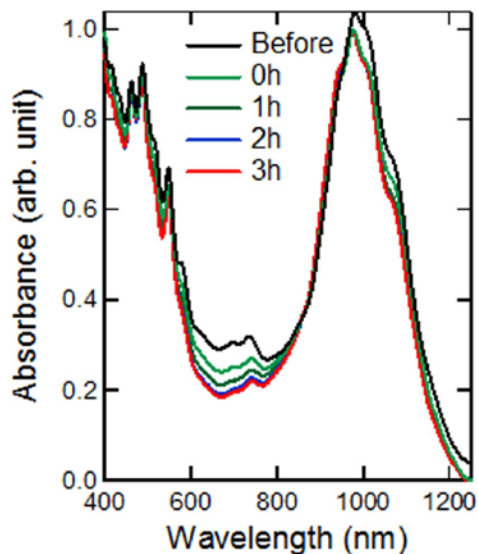


Figure 2.16. The absorption spectra of lower layer after 2nd separation with different post sonication time.

It was seen from the Figure 2.16 that the metallic absorption peak around 750 nm decreased with the increase of sonication time. However, when the time reached as long as 3 hours, the intensity of the peaks did not nearly change. Because the bundles formed during recovery process had weaker interaction between SWCNTs as some surfactants had wrapped around them. The short time sonication was enough to disperse them, while was not enough to disperse those small bundles made by initial sonication. Although a longer time ultracentrifugation helped to remove these bundles, they can't be completely removed, especially for the SWCNTs made by Arc discharge, which has a stronger coulomb interaction than those made by CVD process. It implies that a sufficient dispersion of SWCNTs is the precondition to obtain high purity single species of SWNTs.

Figure 2.17 showed a comparison of the density profile in the centrifuge tube after 1st and 2nd separation. It can be seen in both separation green layer was separated away from the brown layer, which means the metallic enriched SWCNTs had been extracted from the semiconducting ones. We had known from the above discussion that the metallic portions were different in each separation so that we should use different parameter to separate them out. The different dielectric environment will result in different densities of them. It can be seen from the density profile shown in the Figure 2.17b, in which the density of metallic layer was labeled with green marks. The interesting thing is that the density of most pure

semiconducting SWCNTs was almost same in both separations. It suggested that the density of pure semiconducting SWCNTs had less dependence on the dielectric environment than metallic ones, both isolated and bundles ones.

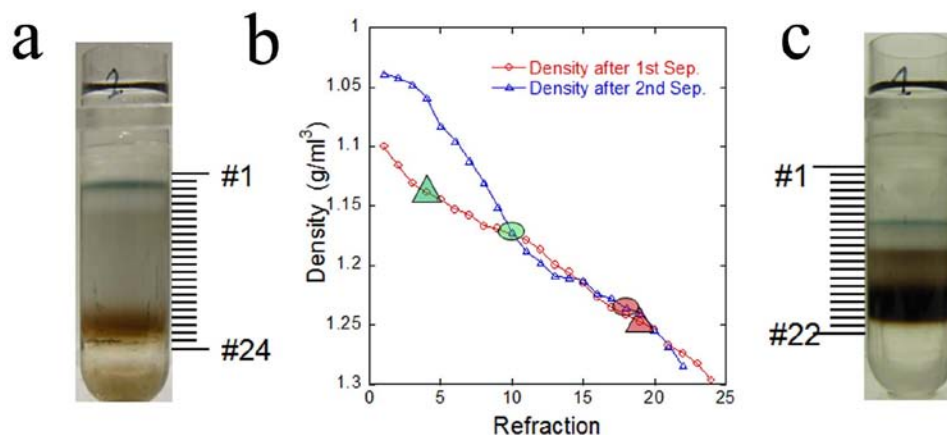


Figure 2.17. The photograph after 1st (a) and 2nd (c) separation. b) the density profile in the centrifuge

2.3.2 Raman spectra of 1st/2nd separation

As described in section 2.2.3, the purity improvement after 2nd separation was also revealed by Raman spectra. Figure 2.18 showed the comparison of Raman spectra of semiconducting SWCNTs after 1st and 2nd separation by measurement with a laser of 488 nm. The absorption spectra of 1st and 2nd separated S-SWCNTs were normalized at 488nm, as shown in Figure 2.18a. From the results shown in Figure 2.18b, a sharp peak was observed at 170 cm⁻¹ for both cases. However, no intensity difference between two spectra was observed, although an obvious difference can be seen from the absorption spectra. It is because the absorption band of metallic

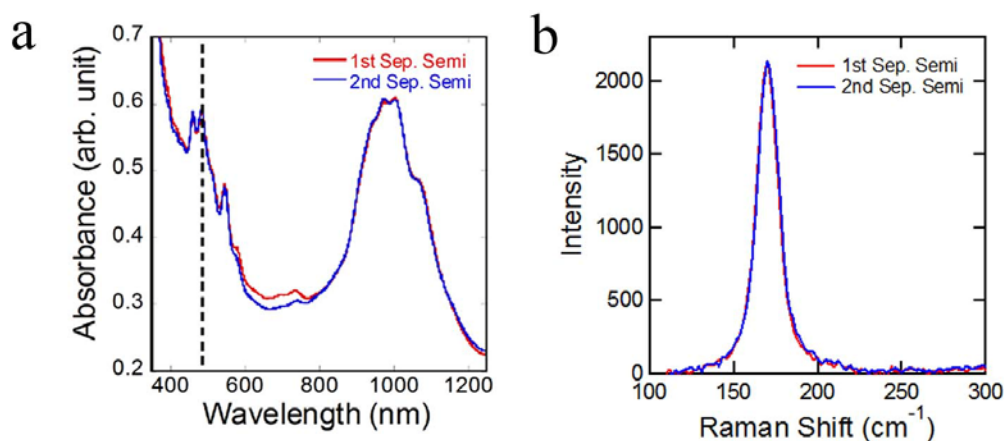


Figure 2.18. (a) Normalized absorption spectra of 1st and 2nd separated semiconducting SWCNTs at 488 nm. (b) The RBM Raman spectra of 1st and 2nd separated semiconducting SWCNTs with a laser of 488 nm.

SWCNTs is around 700 nm, which is away from 488 nm. As the intensity was very weak, the metallic absorption had no contribution to that in 488 nm. Although the optical density was normalized at 488 nm, it reflected only the concentration of semiconducting SWCNTs. Thus the intensity of RBM Raman spectra was same under the laser of 488 nm. The little difference of high purity semiconducting SWCNT can't be distinguished by this way. Therefore, we performed the measurement with a laser of 633 nm, which is in the range of metallic absorption band.

Figure 2.19b showed the RBM Raman spectra with a laser of 633 nm. The absorption spectra were also normalized at 633 nm, as shown in Figure 2.17a. A sharp peak was observed at 170 cm^{-1} for both cases as similar as that with 488 nm laser. It is known the RBM frequency, ω_{RBM} , depends linearly on the reciprocal nanotube diameter d . Since the metallic SWCNTs also has the similar diameter as semiconducting SWCNTs and 633 nm is in the range of metallic absorption band, this peak means the resonance mode induced by metallic SWCNTs. The intensity of this peak reflected the concentration of the metallic SWCNTs in the solution. From the Figure 2.19b, the intensity of this peak for 2nd separated semiconducting SWCNT decreased to 413.2 from 517.28 observed in 1st semiconducting SWCNTs. It means the concentration of metallic SWCNT in the 2nd separated semiconducting SWCNTs decreased, namely the concentration of semiconducting SWCNTs increased. It showed another evidence of purity improvement by iterative separation.

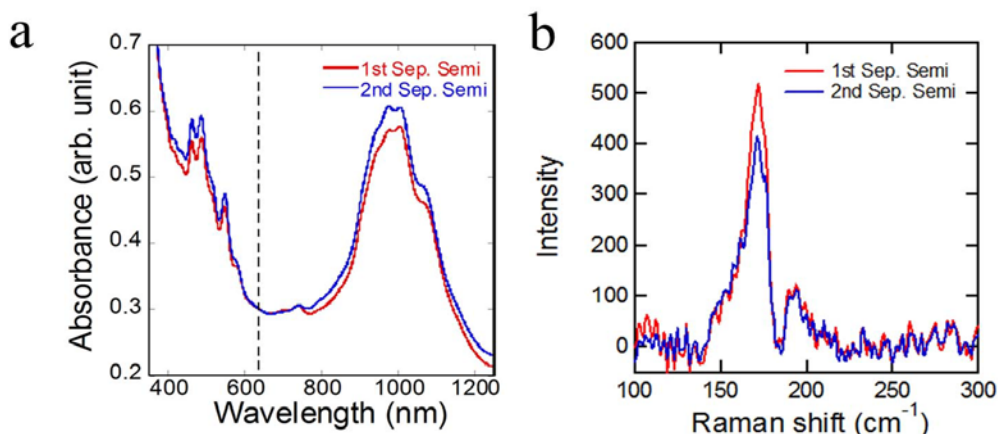


Figure 2.19. (a) Normalized absorption spectra of 1st and 2nd separated semiconducting SWCNTs at 633 nm. (b) The RBM Raman spectra of 1st and 2nd separated semiconducting SWCNTs with a laser of 633 nm.

2.4 I-V characteristic

In this section, we made the thin film transistors with semiconducting SWCNTs obtained by U-DGU and showed semiconducting characteristic which is important for application on electronic devices.

2.4.1 Experimental

Preparation of silicon substrate:

A SiO₂/Si wafer was cutted into small squares with an area of 1 cm². The substrates were cleaned by bath sonication in acetone and isopropyl alcohol (IPA) sequantly, each twice for 3 minutes, followed by dry with Nitrogen flow. Then the substrates were put in a petri dish with dropped several drops of 1% 3-aminopropyltriehoxysilane (APTS) IPA solution around them. The petri dish was put in a 150 °C chamber for 10 minutes to evaporate APTS on the silicon subtrates. After cooling to the room temperature, the substrates were bath sonicated for 1 minutes in IPA to remove the excess APTS. Finally, a thin layer of APTS was covered on the surface of the subtrates and helped to make a uniform SWCNT film.⁷¹

Preparation of semiconducting SWCNTs solution:

During DGU process, iodixanol was used as density gradient medium to make different density in the centrifuge tube. After the separation, the recovered semiconducting SWCNTs had a high density, which meant the solution contained high concentration of iodixanol. Iodixanol has iodine atoms. If iodine remains in the semiconducting SWCNT, the iodine will work as an electron acceptor for the SWCNTs.^{121,122} The remaining iodine will increase the conductivity of the semiconducting SWCNTs and will degrade their semiconducting characteristics. And the high viscosity makes it inconvenient to operate on SWCNTs, such as concentration or deposition on a substrate. It is necessary to remove the iodixanol before the application of SWCNTs.

Usually filtration was used to remove the iodixanol. At first, methanol was added into the solution with iodixanol. The surfactant on the surface of SWCNTs was replaced by methanol and SWCNTs would aggregate into bundles with big aspect not to pass through the membrane. Then the solution was filtrated with membrane by vacuum pumping. As Iodixanol is a

relatively large molecule (molecule weight: 1550), it takes a considerable time to remove it. After filtration, the SWCNTs remained on the membrane were redispersed in methanol, followed by repeated filtration and cleaning with acetone and toluene sequentially. If the amount of SWCNT is large, the SWCNTs can form a thick film on the membrane and pilled off as a bucky paper. The bucky paper was heated in vacuum at 450 °C for 4h to remove the excess solvent and surfactant.

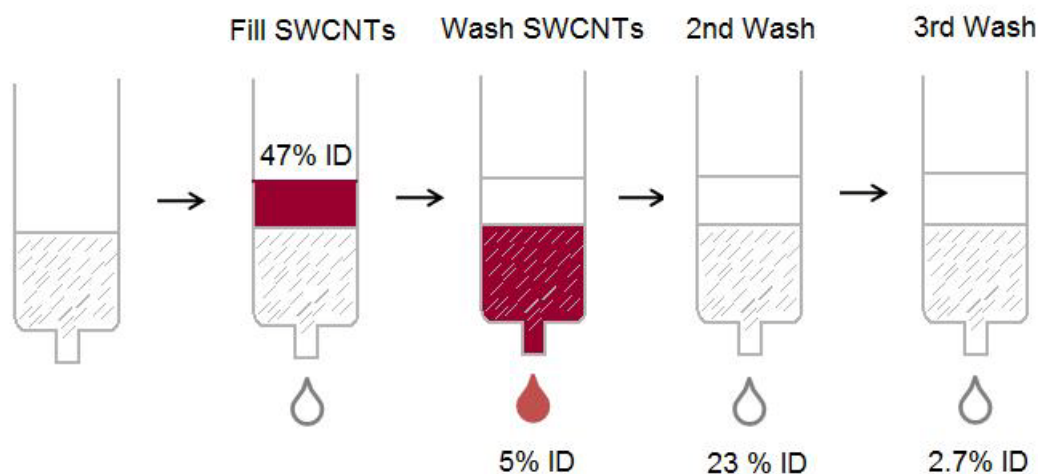


Figure 2.20. The schema of operation procedure of removing iodixanol by gel permeation.

Another method to remove the iodixanol is gel permeation. We used a 30ml syringe as the container. 10ml suphcral-300 gel was filled in the syringe with a gauze was fitted on the bottom to prevent the leak of gel. Then the gel was washed with distilled water and 2% SC solution. Because the gel has a interaction with SWCNTs, which varied with the concentration of surfactant. The high concentration of SC ensures that most of SWCNTs will pass through the gel without being trapped by it. The schema of operation procedures was shown as Figure 2.18. At first, half volume of the gel, namely 5ml recovered 1st separated semiconducting SWCNTs, were injected on the top of gel. The solution contained about 47% iodixanol induced from the refraction. During passing the gel, the speed of the moving of water and ioxinaol is different, therefore when we washed the column with another 5ml 2% SC, the aqueous solution with SWCNT will dropped out prior to the iodixanol. Due to the high concentration of surfactant, most of SWCNTs were recovered and the concentration of iodixanol was about 5%. Then 5 ml 2% SC was added in the column to wash the iodixanol out. The concentration is about 23%. It means that iodixanol can be washed out without blocking the gel. With 3rd wash, the final

solution dropped from the syringe showed a concentration of iodixanol about 2.7%. It means the column remained no iodixanol and could be repeatedly used. The recovered SWCNTs were ultracentrifugated for 2h at 289, 000 g and the deposition was redispersed in surfactant solution for fabrication of SWCNTs film.

Fabrication of thin film transistor

(a) Organic solvent: The bucky paper of semiconducting SWCNTs was dispersed in N-methylpyrrolidone (NMP) for fabrication of SWCNT film with a concentration of 20 $\mu\text{g/mL}$ by sonication for 2h using an ultrasonic homogenizer. The SWCNT dispersion was then centrifuged for 15min at 282,000g. The supernatant was recovered for fabrication of SWCNT films. 50 μl SWCNTs solution dispersed with NMP was dropped on the APTS covered substrate. The solution was kept on the substrate for 5 minutes. The substrate was then rinsed with IPA and dried by blowing with Nitrogen gas. Then, Au (50 nm)/Ti (5 nm) electrodes were deposited on the substrate through a shadow mask using an electron beam evaporator. The channel the width was 200 μm and length was 10 μm for odd rows, as well as 20 μm for even rows, as shown in Figure 2.21b.

(b) Aqueous solution: The solution after removing the iodixanol by gel permeation can be used to fabricate SWCNT film directly. The procedure is almost as same as that with organic solvent except the deposition time is longer. Usually, we kept the solution on the substrate for 2h hours and rinsed it by water.

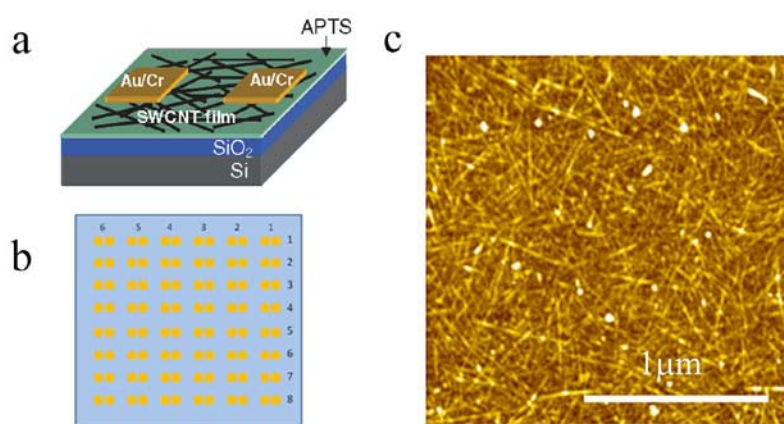


Figure 2.21. Schematic diagram of a back-gated transistor (a) and TFT devices with pairs of source/drain electrodes on substrate (b). (c) AFM image of SWCNTs on SiO₂/Si substrate.

Morphology observation and I-V characterization

The topography of the SWCNT network was characterized by dynamic force mode atomic force microscopy (AFM; SII SPI3800, appendix V). Electrical measurements of the TFTs were performed in air at room temperature using a prober (Nagase Techno-Engineering Grail10, appendix VI) and a semiconductor parameter analyzer (keithley 4200-SCS, appendix VI).

2.4.2 The I-V characteristic of TFT

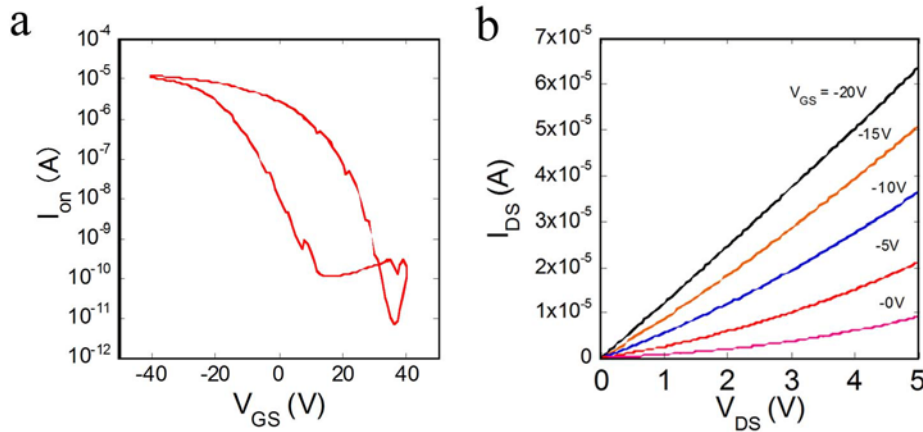


Figure 2.22 (a) Transfer characteristics ($V_{DS} = -1V$) for forward and reverse sweeps of I_{DS} vs V_{GS} . (b) I_{DS} vs V_{DS} characteristics measured at gate voltage of -20 to 0 V.

We made the devices with aqueous solution of 98% semiconducting SWCNTs. Figure 2.22(a) shows typical transfer characteristics of TFTs with drain-source voltage (V_{DS}) = -1 V for forward and reverse sweeps of drain current (I_{DS}) versus gate voltage (V_{GS}). The TFT exhibited p-type behavior. A large hysteresis was observed. The hysteresis probably originates from water molecules absorbed in the vicinity of the electrode or on the nanotubes themselves, which act as charge traps. As reported in previous research, the device had a high on-off ratio up to 10^6 , but the on-current was about 10^{-5} A. The linear-regime mobility extracted from Figure 2.20(b) was $2.29 \text{ cm}^2/(\text{V}\cdot\text{s})$, which was estimated using the standard formula $\mu = (dI_{DS}/dV_{GS})/(\epsilon V_{DS} W/L_{ox}L_{DS})$, where L_{ox} is the SiO_2 thickness, L_{DS} is the channel length, ϵ is the dielectric constant of SiO_2 (3.9), and W is the channel width. A clear I_{DS} - V_{DS} curve was obtained showing no reduction in the on/off ratio with increasing V_{DS} . Comparing with the data obtained from the devices fabricated with semiconducting SWCNTs of 95% purity. Both on-current and mobility were one order higher. It is because the purity is improved so that a high density film can be made on the substrate without short by the pathway of metallic

SWCNT. In the previous research, the on-current was about 10^{-6} A when a high on-off ratio was obtained, and if a large on-current was achieved by increase the density of film, the on-off ratio decreased greatly to 100. For the actual application in the electronic devices, the high-off ratio is more important, thus the high purity semiconducting SWCNT is necessary.

Figure 2.23a shows a histogram of the on/off current ratios for all the TFTs constructed on same substrate. For the large channel length as 20 μm , 17 of 24 devices had high on-off ratio up to $10^5/10^6$. The left 7 pcs of them showed a worse performance with an on-off ratio greatly decreased to $10/10^2$. It was noticed that the worse devices were all at the edge of the substrate, such as sample 28, 48 and 68 (shown in the schema of Figure 2.19b). It is probably due to the nonuniformity of the SWCNTs film formed during the process of SWCNTs deposition. A thicker film might be formed at the edge of substrate and resulted in more bundles of SWCNTs in these devices, and increased the probability of short by metallic SWCNTs. For those devices with channel length of 10 μm , a smaller on-off ratio was observed with comparison to those of 20 μm . Because SWCNTs had an average length over 500 nm, which can be seen from the AFM image, several nanotubes were needed to be jointed to form a pathway between two electrodes. If these nanotubes were metallic SWCNTs, it would be short. The threshold value of metallic nanotubes to set up this pathway is lower when the channel length is shorter. Assuming the density of the SWCNTs was uniform except for the edge area, it should be easier to form a short pathway within a shorter channel by metallic SWCNTs. Therefore, the on-off ratio decreased. Beside this, the decrease of on-off ratio depending on the nonuniformity was also observed. The

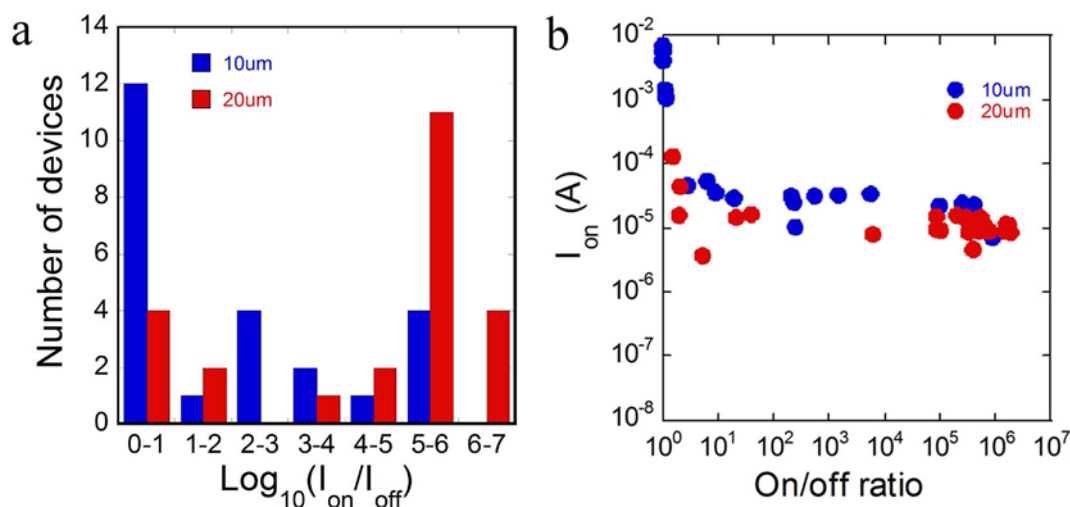


Figure 2.23. (a) Histogram of distribution of $I_{\text{on}}/I_{\text{off}}$ ratios. 24 devices were characterized for 10 μm and 20 μm channel length. (b) On-state current plotted against on/off ratio of devices.

on-current was about 10^{-2} , which was 2 orders larger than that of $20\ \mu\text{m}$.

We compared the I-V characteristics of TFTs fabricated with different deposition time and the result was shown in Figure 2.24. With the increase of deposition time, an increase of on-current was observed, while the on-off ratio decreased simultaneously. This phenomenon was same for both 10 and $20\ \mu\text{m}$ channel length. Because the film density increased with the increase of deposition time, the amount of metallic SWCNTs increased accordingly. It increased the possibility to induce the short and thus decreased the on-off ratio. Meanwhile, the on-current increased because of the increased SWCNTs density.

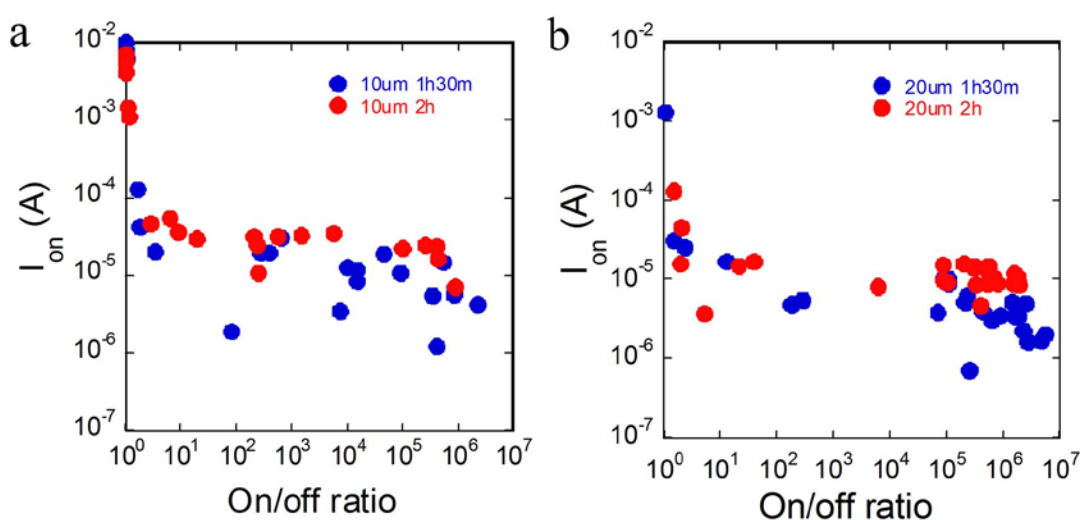


Figure 2.24. On-state current plotted against on/off ratio of devices fabricated by different deposition time with channel length of $10\ \mu\text{m}$ (a) and $20\ \mu\text{m}$ (b).

Except the aqueous solution, the TFT can also be made with SWCNTs solution dispersed in organic solvent, as described above. As the CNT rebundled during the process of making bucky paper, the length of SWCNTs were longer than that made by aqueous solution, evaluated as $1\ \mu\text{m}$ from the AFM image, as shown in Figure 2.25a. Three images showed different densities of SWCNTs film, but were all lower than that made by aqueous solution. It is because the SWCNTs were longer and could make a pathway between electrodes even with fewer nanotubes. The comparison of on-current and on-off ratio of these devices were shown in Figure 2.23b,c. For the devices with channel length of $20\ \mu\text{m}$, they had the on-off ratios about 10^4 and the on-current about $10^{-5} \sim 10^{-6}$. With the increase of deposition time, the density of film increased and the on-off ratio decreased, while the on-current increased conversely. It is similar to the observation on the devices made by aqueous solution. However, comparing with the

devices made by aqueous solution, they had a lower on-off ratio. Because the organic solvent had a worse dispersity of SWCNTs than aqueous surfactant solution, and a plus rebundle effect during the process of making bucky paper, the SWCNTs in the organic solvent had more bundles than that in aqueous solution. It can also be seen from the height profiles of the films. The films made by aqueous solution had a maximum height about 3.8 nm, which is about twice than the diameter of SWCNTs. Considering the overlap of random arrayed nanotubes, the film mostly consisted of individual SWCNTs. However, for the devices made by organic solvent, the average height was about 11.5 nm, which is about eight times than the diameter of SWCNTs. And the film had low density and no much overlap between nanotubes. It means this film mostly consisted of large bundles. It will increase the possibility of short by metallic SWCNTs, because even one metallic SWCNTs was mixed in the bundles, they will failed to show the semiconducting characteristics. Although a longer sonication will increase the dispersity in the organic solvent, it will also increase the defects on the SWCNTs simultaneously.

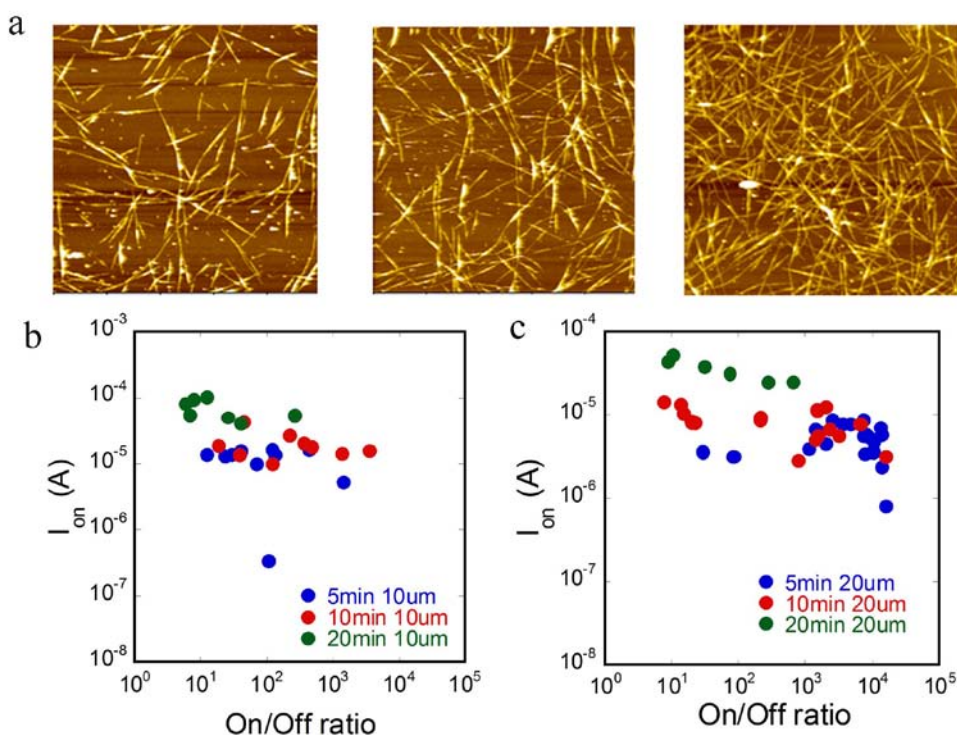


Figure 2.25. (a) AFM image of SWCNTs film made by organic solution (NMP) with different deposition time. From left to right is 5 min, 10 min and 20 min. On-state current plotted against on/off ratio of devices with channel length of 10 μm (a) and 20 μm (b)

2.5 Conclusion

In this chapter, we presented a high-efficiency method to separate the metallic and semiconducting SWCNTs with high purity and large volume, which is called Uniform Density Gradient Ultracentrifugation. The iodixanol moves under the centrifugal force and forms a self-generated density. When the density gradient is optimized to fit the density of metallic and semiconducting SWCNTs, the separation of SWCNTs can be realized without a preset initial density, which usually is linear and step gradient. As the accompanied movement of iodixanol molecule accelerates that of SWCNTs, the U-DGU shows comparable separation ability with S- and L-DGU. And the gentle slope after ultracentrifugation for U-DGU leads to a larger distance between separated metallic and semiconducting SWCNTs, which makes it easier to recover the high purity SWCNTs technically. The important advantage of U-DGU is the large capacity of separation. As the SWCNTs can be filled in the whole centrifuge tube due to uniform density, all the space of centrifuge tube is utilized and more SWCNTs can be separated at once. According to the result to date, 5 times yield had been achieved without degrading the purity of separated SWCNTs. It provides a simple and efficiency way for the large scale separation which opens a pathway to new scientific research in near future such as neutron scattering that requires a large amount of sample.

The application of semiconducting SWCNTs on electronic devices has a strict requirement about the purity of SWCNTs. Although we can obtain the large amount of semiconducting SWCNTs with purity of 98%, higher purity is necessary for better application. With the iterative separation, the purity of semiconducting SWCNTs can be further improved. With other optimizations, such as longer ultracentrifugation time to remove more bundles, it is suggested that the purity can reach 99.9%.

We characterized the semiconducting feature of separated SWCNTs with thin film transistor. With the increased purity, the performance was improved about one order comparing to that reported in previous research. The film made by aqueous solution showed better dispersity than that made by organic solution. The bundles and metallic SWCNTs will decrease the performance of the devices.

3. The application to organic solar cell

3.1 Introduction

Organic photovoltaic devices have attracted much attention since their discovery, due to their potential of creating low cost solar cells in large area and flexible substrates.^{96,97} The current drawback with organic photovoltaic (OPV) cells is the lower efficiency comparing to inorganic PVs. The organic solar cells are known as excitonic solar cells, which are characterized by bound electron-hole pairs that are formed after excitation with light. There are mainly two reasons: one is that the binding energy of exciton in polymer is usually about several hundred meV, which is too high to directly dissociate electron-hole into free charge by the difference of work function of electrodes, as working in inorganic solar cell. Another one is the low carrier mobility of the polymers limits the transfer of the free charge to the electrodes.

Recently research demonstrates that the photovoltaic properties of a conjugated polymer can be drastically enhanced by being blended with another polymer or an organic molecule with different electronic structures and higher electron affinity, which is called heterojunction structure.³⁾ The difference potential between the LUMOs of two semiconductors provides an efficient charge separation, while the separated electron/hole will be transfer to the electrode via a percolation work of the acceptor/donor material. To date the most efficiencies as high as 5% have been produced by blending P3HT with fullerene derivative [6,6]-phenyl-C61-butyric acid methyl ester (PCBM).^{101,102}

Like fullerenes, SWCNTs also are electron conducting materials which are considered as a substitute of PCBM with additional advantages like larger surface area and higher carriers mobilities. Previous researchers have used SWCNTs as electron acceptors in polymeric photovoltaics and shown promising results.¹¹¹⁻¹¹³ However, their efficiency is so far not possible to approach that of other composites, such as those using PCBMs for example. Many recently researches showed a energy transfer occurred between polymer and SWCNTs. It calls into question about whether the SWCNTs are suitable for the electron acceptor in the organic solar cell. For better applications of SWCNTs in organic solar cells, it is necessary to have more understanding about the photoconversion process in the composites.

In this chapter, we investigated the optical properties of P3HT and SWCNT composites and

the photoconversion process was discussed. Using photoluminescence excitation mapping, energy is observed to transfer from the polymer to SWCNTs when the polymer is excited across their minimum energy gaps. Limited by the experiment condition, we used SWCNTs with smaller diameters (0.8 ~ 1.2 nm). Because SWCNTs with smaller diameters have a larger E_{11} energy level from 1000 to 1600 nm, which the emission from E_{11} can be detected with in-house equipment. SWCNTs used in the DGU separation have diameters about 1.4 nm, indicating a E_{11} over 1800 nm, which is out of the measurement range.

3.2 The optical properties of SWCNT-polymer composites

3.2.1 Experimental

SWCNTs synthesized by High-pressure carbon monoxide (Hipco) processing were purchased from Carbon Nanotechnologies Inc. while the polymer, Poly(3-hexylthiophene-2,5-diyl) (P3HT, regioregular) was purchased from Sigma Aldrich. 5mg P3HT with 1mg SWCNTs were dispersed in 20 ml toluene by 1/2 inch tip type ultrasonic homogenizer (Branson, Sonifire 450D, 20% output power) for 24 h. During the sonication, the bottle containing composites solution was immersed in cold water (15 °C) to prevent heating. Then the solution was ultracentrifugated (Hitachi Koki, CP80WX, Appendix I) at 9kg for 5min to remove the large bundles and impurities using a swing rotor (Hitachi Koki, P40ST, Appendix I), followed by a further centrifugation at 284,000 g for 1h to extract the pure P3HT-SWCNT composites from the excessive P3HT solution. Finally the precipitated P3HT-SWCNT composites were collected and re-dispersed in toluene solution. The film samples were prepared by drop-casting the as-collected solution onto spectrosil for raman measurement. The aqueous solution of SWCNTs with 2 wt. % SC was prepared as described in section 2.

Optical absorption spectra were measured using a UV-vis-NIR spectrophotometer (Shimadzu, SolidSpec - 3700DUV, Appendix III). Photoluminescence (PL) spectra were measured by the high sensitive CCD detector with the excitation wavelength of 488nm (Ar⁺ laser). The near-infrared (NIR) PLE mapping were measured with a spectrofluorimeter (Nanolog, HORIBA, Appendix VII) equipped with a liquid nitrogen-cooled InGaAs near-IR alloy detector. The xenon lamp was used as the excitation source. The emission was collected in the back-scattering geometry. Emission in the 1000 ~ 1500 nm range was recorded while the

excitation wavelength was scanned from 500 to 900 nm. The raw data were corrected with instrumental factors. Raman spectra were measured by a single monochromator (Bunko Keiki, M331-TP, Appendix IV) with an edge filter for excitation wavelength of 488nm.

3.2.2 Properties of SWCNT-polymer composites

Figure 3.1 shows the solution absorption spectra of pristine SWCNT, P3HT and P3HT-SWCNT composites. The SWCNTs were dispersed with a 2 wt. % SC aqueous solution, while P3HT and P3HT-SWCNT composites were dissolved in toluene solution. The resolved peaks in the optical transition of SWCNTs aqueous solution identified different SWCNT species due to the well known van Hove singularities in the electronic structure. These peaks were also observed in the P3HT-SWCNTs toluene solution. Because of the low solubility of toluene, small amount of SWCNTs were dispersed but the amplified spectra showed a similar distribution although relative intensity of some peaks was different. It means the P3HT have no selectivity on the SWCNTs like some polymers, such as PFO. However, these peaks had a red shift about 25 nm comparing to those in SC solution calculated from the absorption peaks over 800 nm. This shift is independent of solvent and indicates a significant alteration of the excitonic transition energies caused by interaction between P3HT and SWCNTs. Around 580 nm, a stronger absorption band was observed for the P3HT-SWCNT composites, while was not observed in SWCNTs aqueous solution. It was suggested to be the absorption of P3HT. The

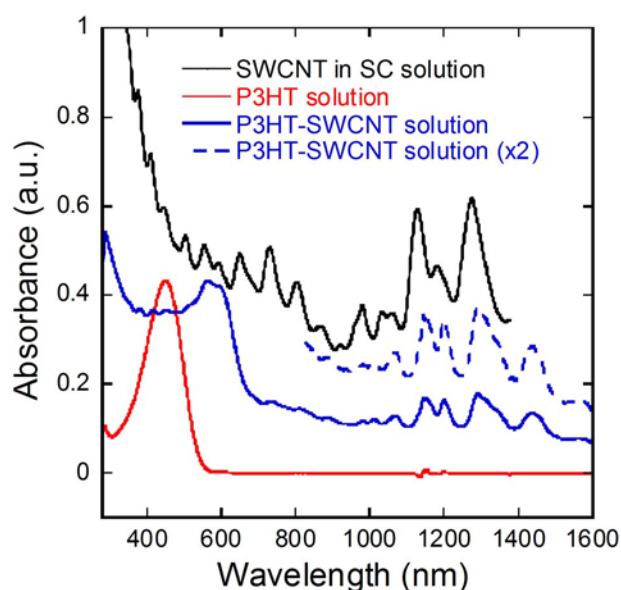


Figure 3.1. Absorption spectra of 2% SC SWCNT aqueous solution, pure P3HT toluene solution and P3HT-SWCNT composites toluene solution.

pure P3HT exhibits an absorption band centered at 450nm, corresponding to a regioregular nature of the P3HT.^{123,124} This peak was greatly decreased after the extraction by centrifugation. It means that mostly free P3HT had been removed. So the absorption band around 580 nm of P3HT-SWCNT composites was contributed to the P3HT adsorbed on the surface of SWCNT. The big red shift (~130 nm) is because of interaction between P3HT and SWCNTs, indicating the formation of well ordered polymer domains.¹²⁵

The Raman spectrum of P3HT-SWCNT composites was shown in Fig. 2. The spectra of pristine SWCNTs and pure P3HT were also taken for comparison. The characteristic peaks of P3HT were all observed.¹²⁶ The band at 1452 cm⁻¹ can be assigned to symmetric C=C stretching deformation. The band at 1378 cm⁻¹ is due to C-C stretching deformations in the aromatic thiophene ring. Two bands at lower wavenumbers (1172 cm⁻¹ and 1204 cm⁻¹) are ascribed to the inter-ring C-C symmetric stretching and C-H bending, respectively. And the peak at 1091 cm⁻¹ can be assigned to the stretching deformation of C-C_{sub} (the carbon in the aromatic ring and the carbon in the side chain). The G and D bands of the SWCNTs were observed as in the pristine one. No obvious shifts were found for these peaks. It suggests that the P3HT in solid state has a similar structure as the P3HT on the surface of SWCNTs. It was noticed that the absorption band of P3HT in composites had two peaks, 556 nm and 602 nm. These peaks is in good agreement with regioregular P3HT as observed in solid state,¹²⁷ suggesting a $\pi - \pi$ stacked structure of P3HT chains in solid state. These results indicate that the backbone of polymer might form a similar $\pi - \pi$ stacked structure with SWCNT as in the solid state.

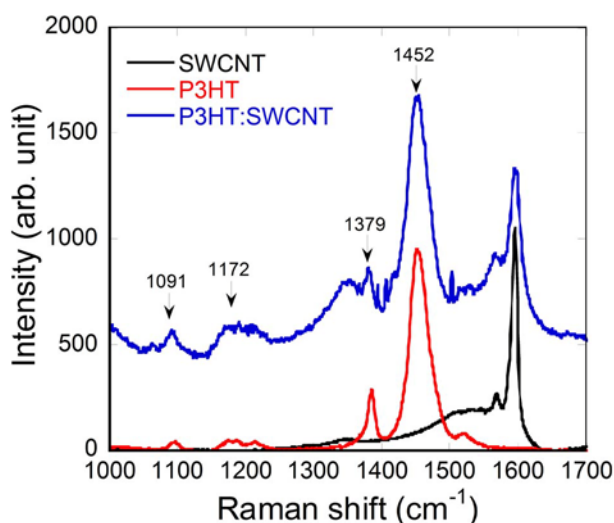


Figure 3.2. Raman spectra of pristine SWCNTs, P3HT, and P3HT-SWCNTs composites.

The photoluminescence (PL) spectra obtained from pure P3HT and P3HT-SWCNTs solution were shown in the Figure 3.3. The P3HT concentration was normalized according to the optical density. The strong emission around 600 nm was observed for pure P3HT solution. If we fit multiple Gaussian peaks with the PL spectrum, three strong peaks at wavelengths of 578 nm, 626 nm and 665 nm were resolved. With the blending of SWCNTs, these peaks became very weak and a great decrease in the intensity (about 96.5%) was observed. According to the Guassian fitting of the spectra (Fig. 3(b)), the peak positions of P3HT-SWCNTs showed slightly red shift (1 ~ 3 nm) comparing to the pure P3HT. As we described above, the structure of P3HT on the surface of SWCNTs is similar to that of solid state P3HT. Thus the emission of the P3HT on the surface of SWCNTs supposed to have identical peaks with that of solid state P3HT. However, the PL peaks of the solid state P3HT have a red shift about 9 ~ 27 nm comparing to the solution P3HT, which is larger than the shift (1 ~ 3 nm) observed in P3HT-SWCNTs. It means that the weak emissions in P3HT-SWCNTs are probably derived from the small quantity P3HT peeled off the surfaces of SWCNTs, while the emissions derived from the P3HT adsorbed on the surface of SWCNTs are completely quenched due to energy/charge transfer.

The further study of the interaction between P3HT and SWCNTs was investigated by PL mapping in lower wavelength range (1000 ~ 1500 nm). The result was shown in Figure 3.4.

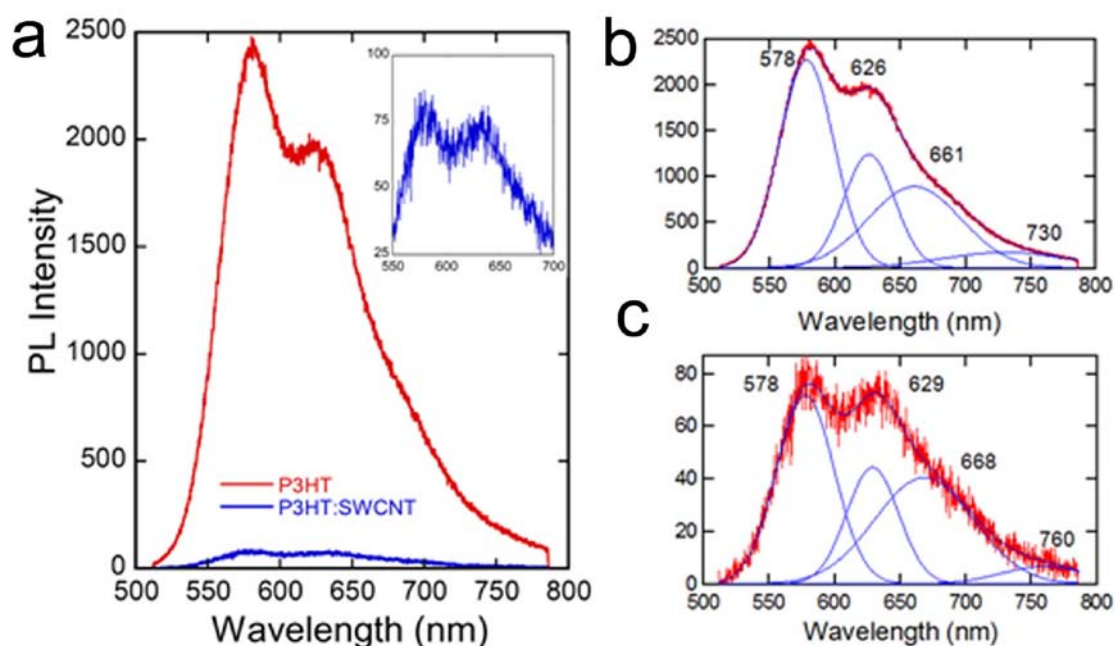


Figure 3.3 (a) PL spectra of P3HT and P3HT-SWCNTs solution (inset is the amplified spectra of P3HT-SWCNTs). (b) Guassian fitting of P3HT solution. (c) Guassian fitting of P3HT-SWCNTs solution.

Figure 3.4(a) presents a standard PLE map of SWCNTs aqueous solution, allowing the contributions of individual nanotube species to be identified. These emissions are resulted from the resonantly enhanced emission from the SWCNTs' primary E_{11} electronic transitions (1000 ~ 1500 nm) when the excitation matches their secondary E_{22} electronic levels (550 ~ 900 nm). The vertical and horizontal values of each spot with strong emission correspond to the E_{11} and E_{22} of different SWCNT species. Although these values have slight shift according to the dielectric environment, they can deduce the specie of each spot by cross inspection of each other. The decided species were labeled on the map. These emissions can also be observed in the PLE map of P3HT-SWCNTs solution as shown in Figure 2.4(b). A red shift (~ 25 nm) is seen for all nanotubes species when compared to the peaks taken using aqueous solution. This shift can be attributed to the reduced energy gap which is induced by the change in the local dielectric environment.¹⁷⁾ Except the emissions which are excited from E_{22} electronic levels, it was seen that strong emissions occurred from all of the nanotube species when excitation wavelengths were in the range 550 ~ 620 nm. The emissions were not observed neither in pure SWCNT nor P3HT solution. The excitation spectral range did not correspond to any electronic transitions in the nanotubes, however, closely match the optical absorbance of the ploymer in the P3HT-SWCNT composite, as shown in Figure 2.1. It suggests the photo-excited P3HT is transferring energy to the SWCNTs, resulting in the creation of an electron-hole pair which then recombines at the nanotube's bandgap.

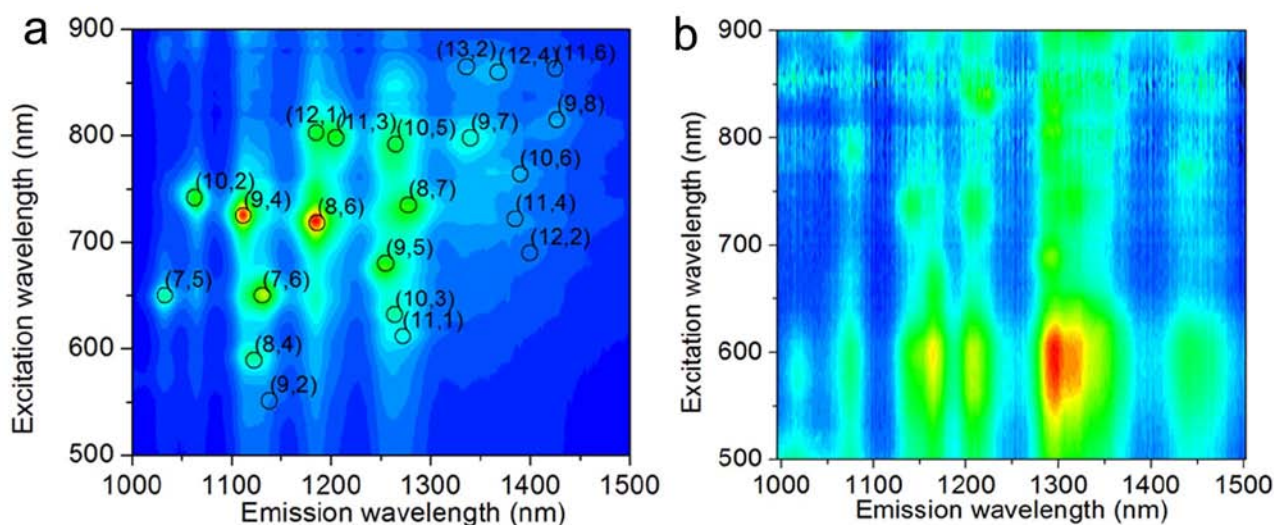


Figure 3.4. Photoluminescence of (a) SWCNTs (2%SC aqueous solution) solution and (b) P3HT:SWCNT toluene solution.

We noticed that the spots having stronger emission gathered in the range 1100 ~ 1200 nm, while the emissions gathering in the longer wavelength were weaker. The stronger emissions contributed to the higher E_{11} level of smaller diameter SWCNTs, such as (7,6), (9,4) and (8,6), which have the diameter less than 0.96 nm. And the weak emissions in 1300 ~1500 nm comes from the lower E_{11} level of larger diameter SWCNTs, such as (9,7), (10,6) and (9,8), which have the diameter larger than 1.1 nm. However, it is contrast to the observation in absorption spectra of SWCNT, in which the absorption band around 1300 nm was stronger than that around 1100 nm. Because the solution included both semiconductor and metal, the existence of metal has no influence to the intensity of absorption band. But the emission just occurred from the semiconducting SWCNTs not from the metallic SWCNTs due to their zero bandgaps. If the semiconducting SWCNTs are bundled with metallic ones, the exciton will recombine in the metal and no emission will be released from semiconductor. Therefore, although there is strong absorption band around 1300 nm, no strong emission is observed. It means the larger diameter SWCNTs are not well dispersed, resulting in many bundles which quench the emissions.

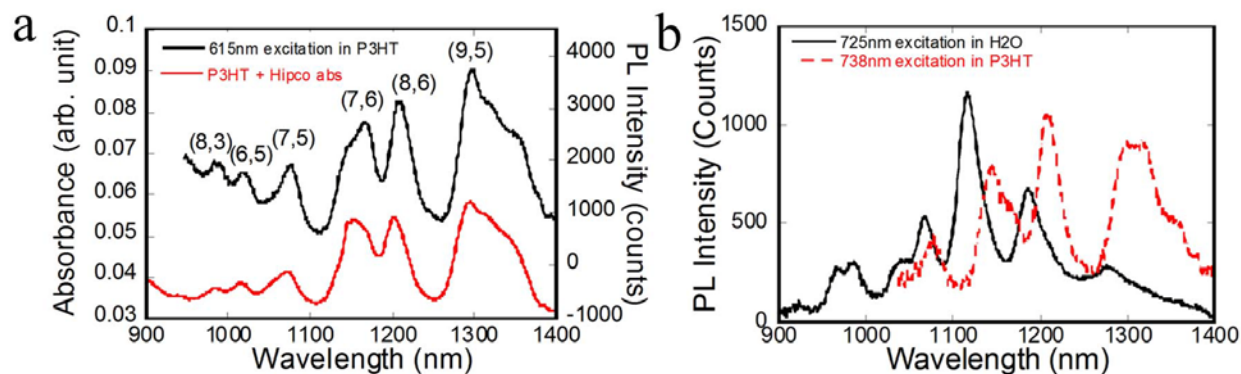


Figure 3.5. (a) Absorption spectrum of P3HT-SWCNT toluene solution and the emission spectrum with excitation wavelength of 615 nm. (b) Emission spectra of SWCNT aqueous solution and P3HT-SWCNT toluene solution with excitation wavelength of 725 nm and 738 nm, respectively.

However, it is different in P3HT-SWCNT solution. For the excitation from E_{22} , such as 725 nm, the emission of SWCNTs aqueous solution, a strong emission around 1115 was observed due to the specie (9,4). The emission over 1200 nm was weaker. In case of P3HT-SWCNT solution, when the composites were excited at 735 nm, not only around 1144 nm but also 1208 nm and 1309 nm had strong emissions, as shown in Figure 3.5b. The shift of wavelength is due to the different dielectric environment. It means that SWCNTs has better dispersibility in P3HT than in SC solution. The semiconducting SWCNTs were isolated into individual ones so

that the emission from them should not be quenched by metallic ones. It is same for the excitation from P3HT absorption band, as shown in Figure 3.5a. There are stronger peaks in longer wavelength range, which is consistent to the distribution in absorption spectrum.

3.2.3 Energy transfer

Such transfer process has been recently observed to operate in covalent oligomer-fullerene dyads in solution¹²⁸ and fullerenes in the solid state.¹²⁹ It is supposed to be induced by the Förster resonance energy transfer (FRET).¹²⁸⁻¹³⁰ It is a mechanism of energy transfer which happens between molecules that have a spectral overlap of emission and absorption. However, we can not know the exactly emission spectra of the P3HT adsorbed on the SWCNTs because the emission are almost quenched due to energy transfer, as described above. We noticed that the absorption of P3HT in composites had a similar absorption band with solid state P3HT, as shown in Figure 3.6a. It suggests that the electronic structure of P3HT should be similar for

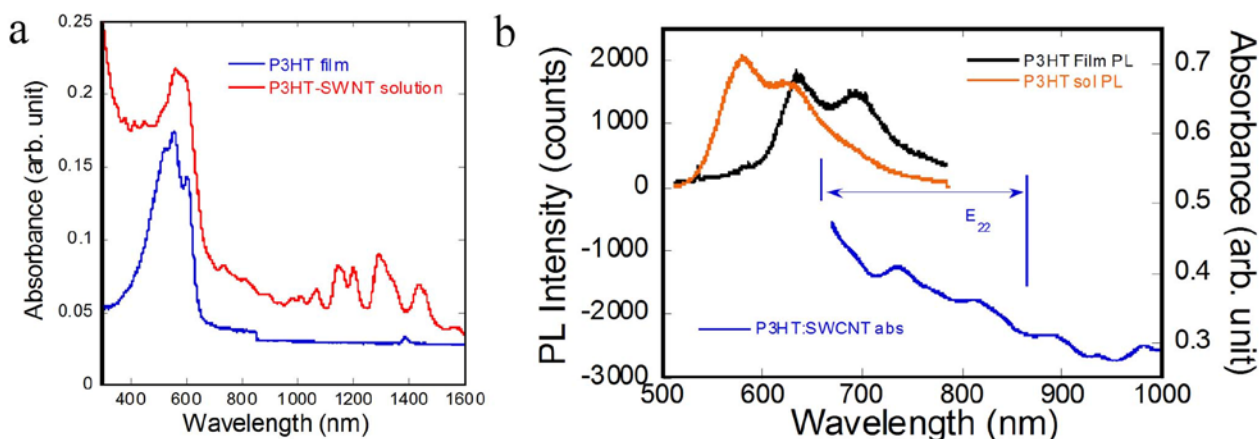


Figure 3.6. (a) Absorption spectra of P3HT film and P3HT-SWCNT solution. (b) Overlapping between photoluminescence of solution and film P3HT and absorption of P3HT-SWCNT solution.

them. Therefore, the photoluminescence of them should have similar emission wavelength. Figure 3.6b shows a comparison of PL of P3HT film and absorption spectra of P3HT-SWCNT composites. Hipco SWCNTs have a wide range of E_{22} absorption (560 nm ~ 800 nm), which overlaps with the strong PL of P3HT film in the range of 650 ~ 800 nm. It implies that the PL of P3HT in the composites also has an overlap with the absorption of SWCNT and makes the transfer possible. However, with the addition of free P3HT to the composite solution, although the emission from free P3HT got stronger, the intensity of emission from SWCNTs did not increase. Because FRET depends on the distance between molecules, the effect will be

weakened if the distance is large. The excess polymer is free in the solution, while the P3HT on the surface of SWCNTs is tightly interacted with SWCNT with an assumed $\pi - \pi$ stacking distance of 3.4 Å. It means the FRET will only occur between the SWCNTs and P3HT wrapped around them.

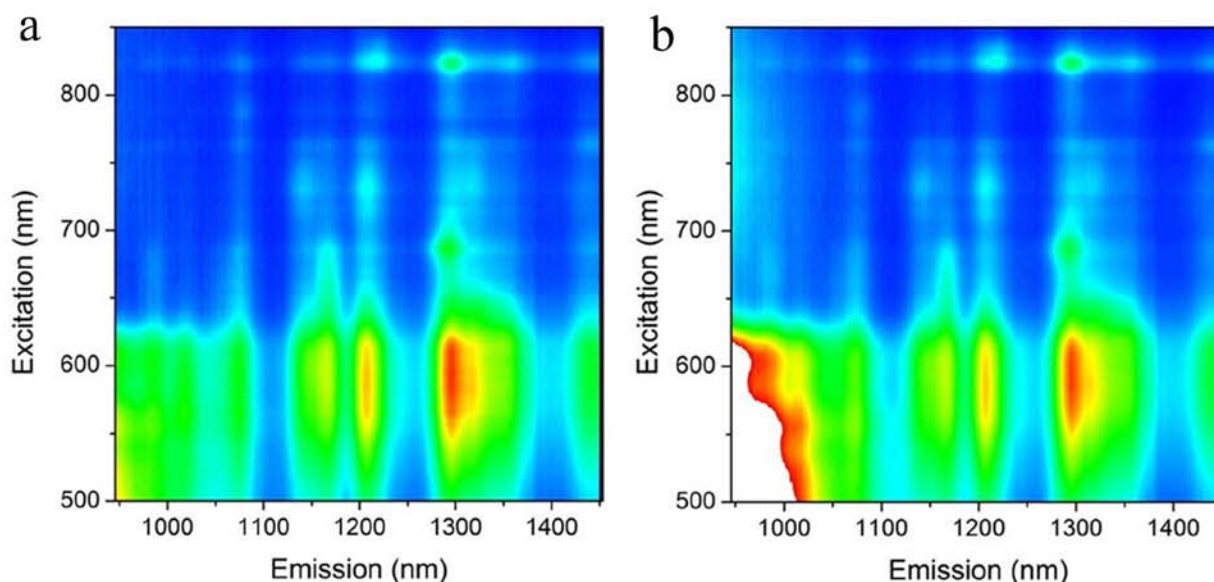


Figure 3.7. PL mapping of P3HT-SWCNT composite without (a) and with (b) excess P3HT.

3.2.4 Energy transfer efficiency

The similar energy transfer can be observed in larger diameter SWCNTs. Ferguson et al reported the energy and charge transfer in composites of P3HT and SWCNTs having an average diameter of ~ 1.35 nm.¹³¹ It means that energy transfer efficiency might be different for different SWCNT species. We performed same experiment on SWCNTs with larger diameter (~ 1.2 nm) to compare the energy transfer rates with those species in Hipco. The result was shown in Figure 3.8. The strong absorption bands were observed in 1300 \sim 1600 nm and 700 \sim 1000 nm, which were contributed to E_{11} and E_{22} energy level of semiconducting SWCNT. A shift about 25 nm was also observed for composites. The PL mapping result was shown in Figure 3.8b. Except the emission for E_{11} level of nanotubes excited from E_{22} level, strong emissions from all nanotube species were observed when the excitation energy matched the absorption band of P3HT, as well as occurred in P3HT:Hipco composites. It means that energy transfer occurs between P3HT and different kinds of SWCNT species.

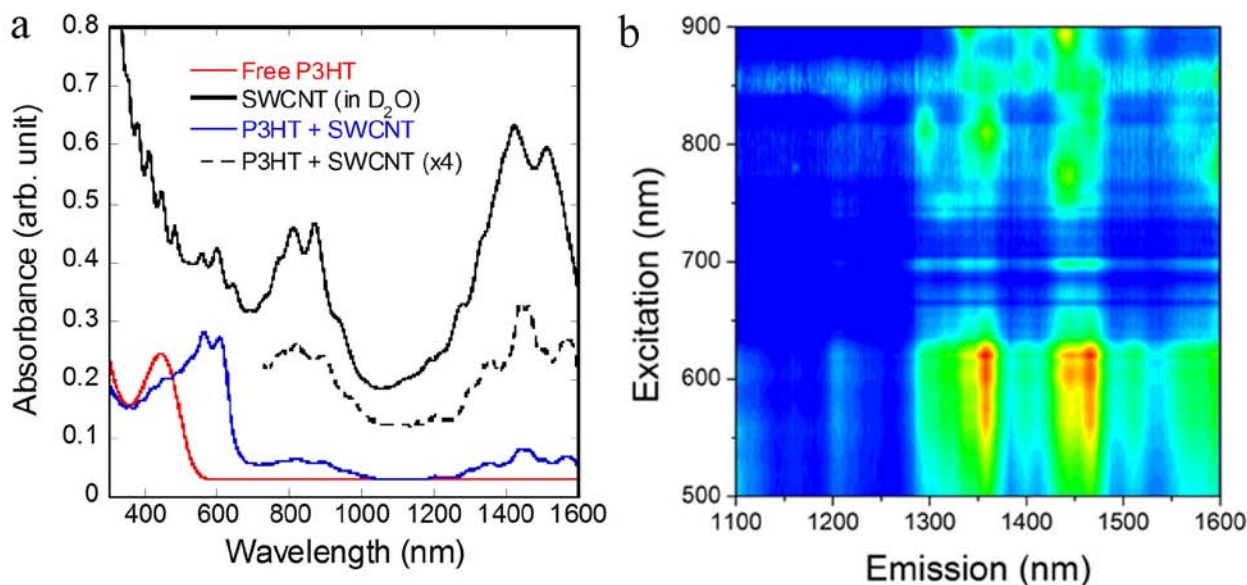


Figure 3.8. (a) Absorption spectra of pure P3HT, SWCNT and P3HT:SWCNT composite solution. (b) PL mapping of P3HT:SWCNT solution. The diameter of SWCNTs are around 1.2 nm.

The energy transfer rate for different SWCNTs species was investigated. These were estimated by comparing the absorption strength of each species to its emission intensity when the exciting light is absorbed by the polymer. However, the amount of polymer attached on all species must be assumed as the same to simplify the estimation. Although it is impossible to calculate the rate quantitatively, the variation in the emission/absorption ratio is still helpful to understand a specie dependency of the energy transfer rate.

Figure 3.9 shows the Gaussian fitting of absorption and PL spectra of the composites of P3HT with two different SWCNTs source. The excitation wavelength is 615 nm for Hipco and 625 nm for LV to make no overlap with any SWCNT resonance. Because many species have close energy level, the broad band in same range was resolved into peaks of different species, according to their resonance emission seen in Figure 3.4b and Figure 3.8b. The relative intensity ratios of resolved peaks of PL and absorption spectra were listed in table 3.1. We choose (8,6) as the base because it appeared in two kinds of source and was not overlapped with other species. For Hipco, in which the diameter is smaller, most of the species showed an energy transfer efficiency larger or equal to (8,6). However, for LV in which the average diameter is larger, most of the species showed an energy transfer efficiency smaller than (8,6). It was assumed that the (8,6) was well dispersed in both cases and had same energy transfer efficiency. It indicates that SWCNTs in LV almost have lower energy transfer efficiency than

that in Hipco, namely SWCNTs having smaller diameter have higher efficiency. An explanation is that smaller diameter SWCNTs usually have higher E22 energy levels, which are closer to the emission of P3HT in composites as shown in Figure 3.6b, thus more excitons can be transferred to SWCNTs from polymer.

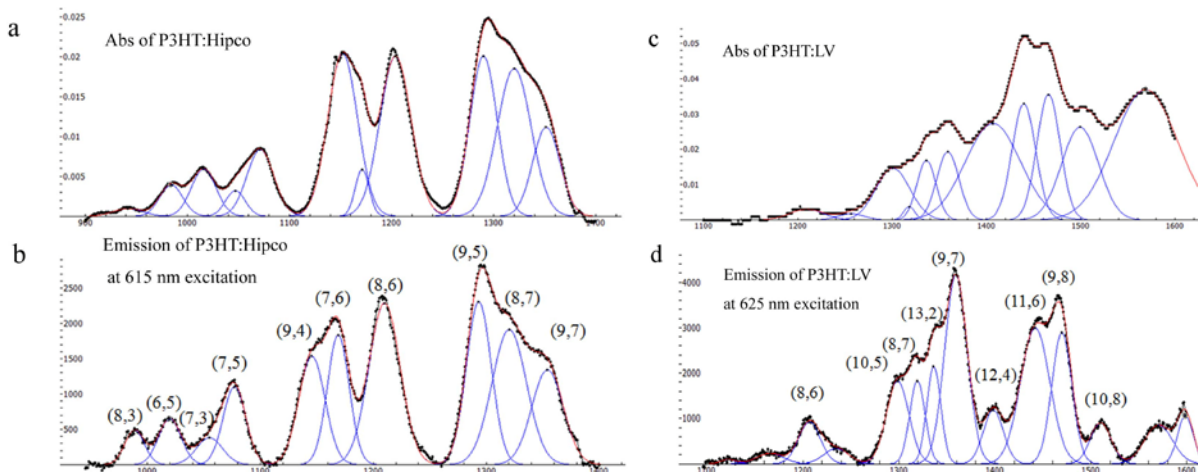


Figure 3.9. Gaussian fitting of absorption (a) and PL with 615 nm excitation (b) of P3HT:Hipco composites. Gaussian fitting of absorption (c) and PL with 625 nm excitation (d) of P3HT:LV composites

Table 3.1. Relative ratio of emission/absorption of different SWCNT species.

	(n,m)	Diameter (nm)	PL (a.u.)	Abs (a.u.)	Relative
Hipco	(9,7)	1.103	1342.34	0.01115	105.55%
	(8,7)	1.032	1911.82	0.01851	90.55%
	(9,5)	0.976	2306.26	0.02006	100.79%
	(8,6)	0.966	2288.12	0.02006	100.00%
	(7,6)	0.895	1836.73	0.00588	273.85%
	(9,4)	0.916	1535.51	0.02038	66.05%
	(7,5)	0.829	1101.72	0.00836	115.54%
	(7,3)	0.706	380.574	0.00322	103.62%
	(6,5)	0.757	649.849	0.0059	96.56%
	(8,3)	0.782	488.503	0.00393	108.97%
LV	(8,6)	0.966	920.636	0.00304	100.00%
	(8,7)	1.032	728	1827.15	158.36%
	(10,5)	1.05	788	1826.1	41.10%
	(9,7)	1.103	793	4163.02	71.26%
	(13,2)	1.12	858	2143.5	41.98%
	(12,4)	1.145	855	1179.42	14.26%
	(9,8)	1.17	809	2891.57	26.86%
	(11,6)	1.186	858	2996.67	30.09%
	(10,8)	1.24	869	907.852	11.42%

3.3 The P3HT:PCBM solar cell with the addition of SWCNTs

As discussed above, a high efficiency energy transfer was observed between excited polymer and SWCNTs. It is different from the conventional concept of heterojunction organic solar cell that the exciton was dissociated into free charges at the interface of acceptor and donor. As most of excitons are transferred and emitted, no free charges generate and no photocurrent flows. Therefore, the role of SWCNTs in organic solar cell should be redesigned to meet their function. Although SWCNTs can not act as the acceptor, they can be the network to transfer free charge in the conventional organic solar cell due to their higher hole transfer mobility. In the following section, solar cells with the addition of SWCNTs into typical P3HT:PCBM structure are fabricated and the properties are investigated.

3.3.1 Experimental

SWCNTs were dispersed in Dichlorobenzene with a concentration of 0.125 mg/mL using a bath sonication for 1h. The Dichlorobenzene has a better dispersity of SWCNTs so that SWCNTs can be easily dispersed with sonication and have a good stability with no aggregation for a long time. 10mg P3HT and 8mg PCBM were dissolved in 1 mL Dichlorobenzene. The solution was stirred for 1 h at 60 °C to make P3HT and PCBM mixing with each other sufficiently. Different ratio of P3HT vs PCBM was reported to result in different morphology of film and influenced the performance the solar cell. In this study, it was not optimized and followed the ratio used in the paper in which the highest efficiency of P3HT:PCBM based solar cell was reported. 10 mg/mL P3HT solution was also prepared with same way.

ITO glass substrate was cut into pieces with 1.8 x 2.0 cm² area. The pieces were first cleaned with deionized water with sonication for 5 minutes with following cleaning with acetone and IPA with sonication for 3 minute twice, subsequently. Then they were dried by Nitrogen flow. The substrates were further cleaned with UV ozone for 30 minutes. The cleaned substrates were used for fabricating the solar cell immediately.

At first, 200 ml 1.3 wt % Poly(3,4-ethylenedioxythiophene)-poly(styrenesulfonate) (PEDOT:PSS) (Sigama Aldrich) were spin-coated onto the substrates under 4000 rpm for 90 seconds. Then the substrates were baked in a 150 °C chamber for 10 minutes in air. This film can modify the contact between active layer and electrodes and increases the hole transfer

mobility. Different volume of SWCNT was added into 75 ml P3HT:PCBM solution to make different concentration of SWCNTs. Then the solution was spin-coated onto the substrate under 1000 rpm for 90 seconds and the substrate was put in a petri dish until they were dried naturally. Limited by the experiment condition, all the operations were carried out in air not a Nitrogen atmosphere. Then the substrates were annealed at 150 °C for 10 minutes in a vacuum of 10^{-4} Pa with a vacuum heater.

After annealing, the substrates were put into a vacuum evaporater for Al electrode evaporation. When the vacuum reached over 10^{-4} Pa, about 75 nm thick Al film was evaporated onto the substrate through a mask having an effective area of 1 cm². The evaporation speed is 0.2 nm/s. Faster evaporation speed will cause the nonuniformity of electrode. It will cause space charge accumulation at the interface of active layer and electrode and result in decrease of fill factor.¹³² After the evaporator cooled down, the substrates were taken out and annealed at 150 °C for 10 minutes in vacuum again. The solar cell of P3HT with different concentration SWCNTs were also prepared with same way.

Then the I-V characteristic was tested with source parameter (keithly 2400) under the incident of halogen lamp, which the power had been calibrated with a standard silicon cell. Although the spectrum of halogen lamp is different from solar simulator, the I-V curve show no difference after calibration, as shown in Figure 3.10. It means the results measured under halogen lamp are reliable.

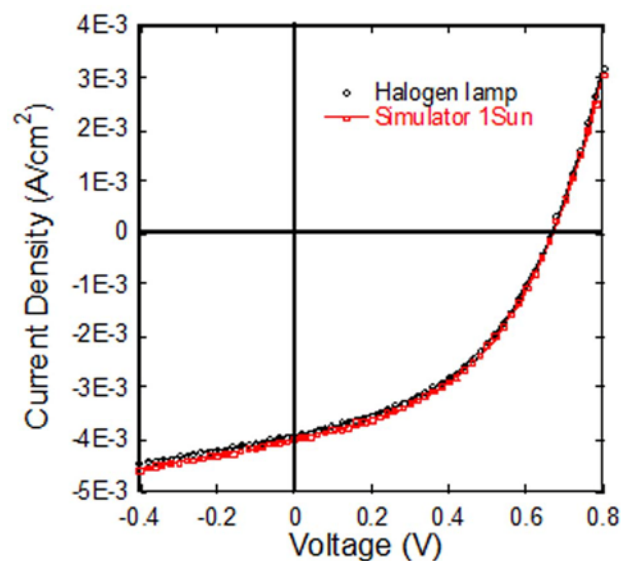


Figure 3.10. *J-V* characteristics of photovoltaic device under calibrated halogen lamp and solar simulator.

3.3.2 The solar cell with the addition of semiconducting SWCNTs

At first, we made the devices in the structure of ITO/PEDOT:PSS/P3HT:PCBM:SWCNT/Al with blending different concentration of semiconducting SWCNTs. Figure 3.11 shows the typical I-V curves of the organic solar cell. The device without additional semiconducting SWCNTs was plotted in black circle. The open voltage (V_{oc}) of the device was 0.67 V and the short circuit (I_{sc}) is 4.46 mA. As the effective area of the cell is 1 cm², the current density (J_{sc}) is calculated as 4.46 mA/cm². The fill factor was calculated as 0.45 and the conversion efficiency is 1.35%. They were lower than the best results reported so far. One reason is that all the operation and transfer of devices were carried out in air atmosphere. It will cause the oxidation of the active layer and degrade the performance of the device. And the parameters, such as P3HT:PCBM ratio, the annealing temperature and time were not optimized. Therefore, the

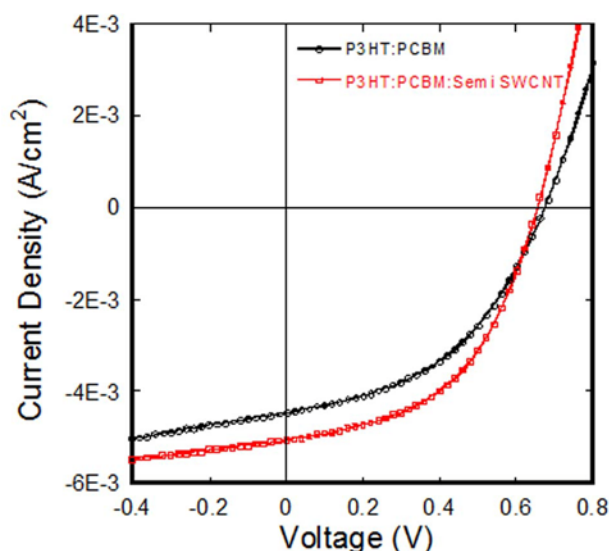


Figure 3.11. Comparison of J - V characteristics of the P3HT:PCBM based photovoltaic cell with (0.0022 wt%) and without additional semiconducting SWCNTs.

efficiency of the device had much space to be improved. However, we made many samples under same conditions and showed similar results. It means this result is reproducible, and reliable for comparison.

The red square plots shows the result with the addition of 0.0022% semiconducting SWCNTs. Although the concentration was very low, SWCNTs had a large aspect ratio and made an obvious effect to the characteristic. The V_{oc} was observed to slightly decrease to 0.65 V, while the J_{sc} increased to 5.06 mA/cm². It is known the V_{oc} of organic solar cell depends on the difference of LUMO of acceptor and HOMO of donor. The introduction of semiconducting

SWCNTs probably increased the Fermi level of P3HT, namely HOMO of polymer and decreased the V_{oc} . But the higher hole transfer mobility of SWCNTs helped to transport hole to anode faster and decreased the possibility of recombination, thus resulted in the increase of J_{sc} . Furthermore, the fill factor was observed to increase to 0.49. It is because of the improved crystallinity of P3HT along SWCNTs. Finally, the photoconversion efficiency increased to 1.63% with 20 % improvement. If the devices were carefully fabricated within Nitrogen atmosphere and optimized condition which led to an assumed efficiency of 5%, the efficiency after addition of semiconducting SWCNTs will be 6%.

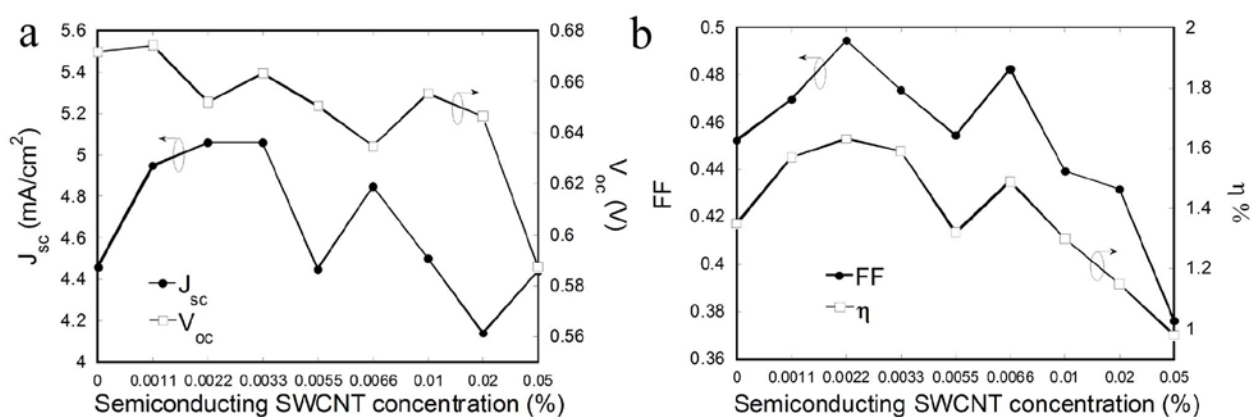


Figure 3.12. The plot of different parameters, (a) J_{sc} and V_{oc} , (b) fill factor and photocovnersion efficiency again the concentration of semiconducting SWCNT.

The devices with different concentration of semiconducting SWCNTs were also measured and the result was shown in Figure 3.12. The trend of V_{oc} and J_{sc} depending on the concentration of semiconducting SWCNT was plotted in Figure 3.14a. It was seen that the V_{oc} kept decreasing with the increase of concentration. For the J_{sc} , at first, a increase was observed when the concentration increased and reached maximum at the concentration of 0.0022 %. Then it decreased as long as the concentration increased. A similar trend was observed for the fill factor, as shown in the Figure 3.12b. A maximum was also obtained at the concentration of 0.0022 %. Base on the equation (4) (in section 1.5), the photoconversion efficiency was calculated to have the maximum as 1.63 % at the concentration of 0.0022 %. Although the efficiency decreased with more semiconducting SWCNTs, it was larger than that of devices without SWCNT till 0.0066 %. Because the SWCNTs dispersion was prepared with quantitative pure semiconducting SWCNTs, the result can be reproduced accurately, unlike other reports which SWCNTs were purified during preparation and the actual concentration of

SWCNT was unknown after purification.

3.3.3 The solar cell with the addition of pristine and metallic SWCNTs

From the result above, we knew that the addition of small amount semiconducting SWCNTs resulted an improvement on the performance of solar cell. However, the influence of the addition of metallic SWCNTs is not yet understood. Although some theoretical calculation indicated the metallic parts have the negative effect on the device, to date no experiment was carried out to show evidences. In this study, we also fabricated the devices with different concentration of metallic and pristine SWCNTs and the properties were investigated. The results were compared in Figure 3.13. For all the devices with SWCNTs, V_{oc} decreased. With the increase of concentration of metallic SWCNTs, the decreased value got larger, from 0.009 of semiconducting-enriched ones to 0.038 of metallic-enriched ones. However, I_{sc} firstly increased

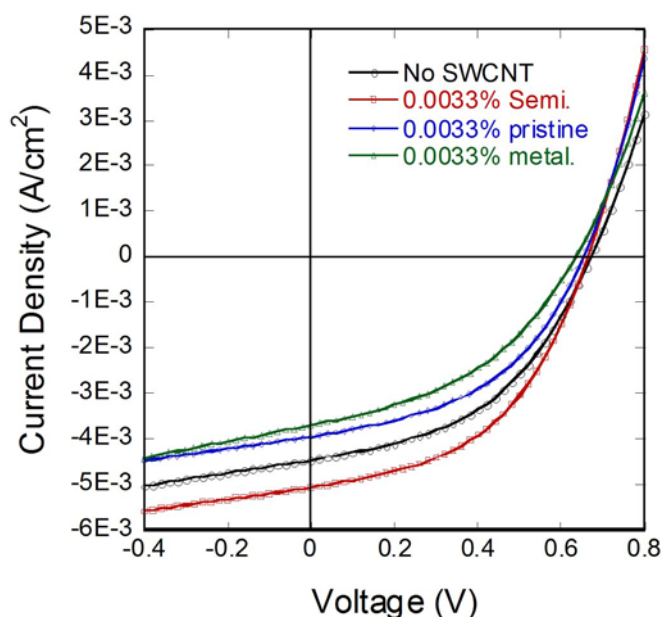


Figure 3.13. J-V characteristics of the P3HT:PCBM based photovoltaic cell with 0.0033 wt% semiconducting, pristine, metallic and no SWCNTs.

with the addition of semiconducting-enriched SWCNTs, and started to decrease when the portion of metallic SWCNTs increased. It is probably due to the increased recombination possibility of hole-electron pair in the metallic SWCNTs. The fill factor also had same trend as I_{sc} , which was shown in the Table 3.2. Finally, the efficiency increased to 1.59 % when the device was blended with semiconducting SWCNT, and turned down to 1.17 % for the pristine one, and further decreased to 0.97 % when SWCNTs was enriched of metal. The efficiencies of

devices depending on the concentration of metallic and pristine SWCNTs were shown in Figure 3.14. The efficiency kept decreasing when the concentration increased. When the concentration of metallic SWCNTs was 0.02%, the efficiency was about 0.01%, which was greatly smaller 1.12% of the device with same concentration of semiconducting SWCNTs. These results provide the evidence of negative influence of metallic SWCNTs, which implies the necessity to extract the metallic portion when SWCNTs are applied to photovoltaic devices.

Table 3.2. Parameters of solar cell with 0.0033% semiconducting, metallic, pristine and without SWCNT.

	Voc (V)	Jsc (mA/cm ²)	FF	η (%)
No SWCNT	0.672	4.46	0.45	1.35
Semiconductor	0.663	5.06	0.47	1.59
Pristine	0.652	3.94	0.45	1.17
Metal	0.634	3.69	0.42	0.97

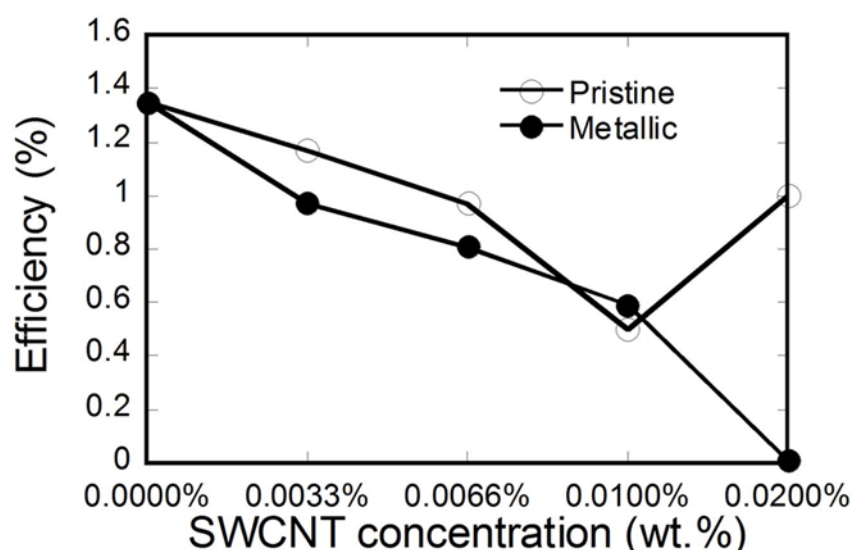


Figure 3.14. Efficiency depending on the concentration of metallic (solid circle) and pristine (open circle) SWCNTs.

3.3.4 The mechanism of the solar cell of P3HT:PCBM:SWCNTs

The proposed energetic charge transfer processes occurring in P3HT:PCBM:SWCNTs based solar cell was presented in Figure 3.15. In the conventional concept of P3HT-fullerene based solar cell, the excitons diffused to the interface of P3HT and PCBM after excitation in P3HT. They were dissociated by the energy difference of LUMOs of two semiconductors, and then the free charges were transferred to the electrodes. The ideal bulk-heterojunction solar cell is defined as a bicontinuous composite of donor and acceptor with maximum interfacial area for

exciton dissociation and a mean domain size commensurate with the exciton diffusion length (5-10 nm). The two components should phase-segregate on a suitable length scale to allow maximum ordering within each phase and thus effective charge transport in continuous pathways to the electrodes so as to minimize the recombination of free charges. Some methods had been reported to improve it, such as solvent choice, concentration ratio of the blend components, solvent evaporation rate, as well as thermal annealing.

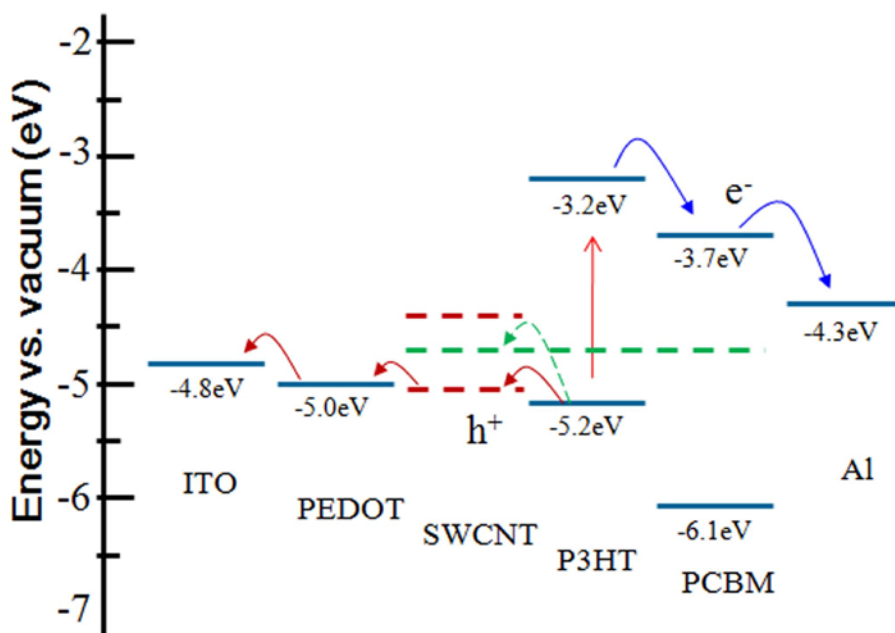


Figure 3.15. Schematic diagram of energy levels of P3HT, PCBM and SWCNT shows the proposed energetic charge-transfer processes occurring in the devices.

The large length/diameter ratio can make SWCNTs forming a network to transport the free charges to electrodes more effectively.¹³⁶ After the dissociation occurred at the interface of P3HT:PCBM, the hole will be transferred from P3HT to SWCNT and then transported to anode through the faster pathway. The low defect surface of SWCNTs and the high mobility decrease the loss during transport and thus higher short-circuit current was observed with the addition of semiconducting SWCNTs (Figure 3.11). It was reported that the V_{oc} of organic solar cells was determined by the difference between the LUMO of acceptor and HOMO of donor. As the Fermi energy of SWCNTs with diameter of 1.4 nm is estimated to be $\sim 5.1\text{ eV}$,¹³⁵ which is a little higher than that of P3HT (Figure 3.15.), V_{oc} will be decreased due to the smaller difference between LUMO of PCBM and HOMO of SWCNTs, as observed in Figure 3.11. However, the metallic SWCNTs will cause the short circuits between P3HT and PCBM which induced the

recombination of hole and electron. Thus the current will decrease, as shown in the Figure 3.13. Because the used semiconducting SWCNT are not 100% pure semiconductors, with the increase of concentration, the portion of metallic parts will increase. Therefore the current decreased opposite to the first increase in low concentration, as seen in Figure 3.12a.

3.4 Conclusion

In this section, we prepared the pure P3HT-SWCNTs composites by ultracentrifugation. A great quench was observed for the photoluminescence of P3HT, while strong emissions from all SWCNT species were observed when the excitation wavelength matched the absorption peak of P3HT in the composites. It implies an energy transfer occurs between the P3HT and SWCNTs. The SWCNT with smaller diameters were found to have higher energy transfer efficiencies than those with larger diameters. These results indicate a different role of SWCNTs in the organic solar cell which was used to be considered as electron acceptor.

Then the solar cells based on the heterojunction structure of P3HT and PCBM with the addition of SWCNTs of different electronic type were fabricated and their characteristics were investigated. With the addition of low concentration of semiconducting SWCNTs, the performance of solar cell was improved about 20%. However, as the purity of semiconducting SWCNTs was not 100%, the performance turned worse at higher concentration. The devices with addition of metallic and pristine SWCNTs showed worse performance even in low concentration. It firstly gives the evidence of negative influence of metallic SWCNTs in the OPVs.

4. Summary

The result of this study can be summarized as the following:

1. A self-generated density gradient was employed for the metal-semiconductor separation of SWCNTs by the DGU method. Spectroscopic analysis of the obtained fractions revealed comparable separation purity to separation with a step-like initial density. SWCNTs could be dispersed in the entire volume of the tube with the U-DGU method, so that a larger amount of SWCNTs than that for S-DGU could be separated without degrading the purity of the semiconductor SWCNTs. With the second separation, the purity of semiconducting SWCNTs can be further improved to fit the need of electronic devices.
2. TFTs were fabricated with the semiconducting SWCNTs separated by DGU. A high on/off ratio of up to 10⁵ was observed in most of the devices on one substrate. It is expected to use a simple solution process to fabricate high performance TFTs.
3. The pure P3HT-SWCNTs composite was prepared by ultracentrifugation and its optical properties were investigated. The great quench of the emission in the polymer demonstrated that energy transfer occurs between semiconducting organic polymers and SWCNTs when the polymer is photo-excited. The strong luminescence from SWCNTs was observed when the excitation energy matches the absorption peaks of P3HT- SWCNTs solution. The results indicate that the energy is transferred from the polymer to the SWCNTs in the composite.
4. SWCNTs were incorporated into P3HT:PCBM photovoltaic devices. The addition of semiconducting SWCNTs led to an increase both in short-circuit current and fill factor, resulting in a 22% improvement of photoconversion efficiency. This improvement is mainly attributed to better charge transport through the SWCNTs.

Reference

- (1) S. Iijima, *J. Cryst. Growth* 50, 675-683, (1980).
- (2) A. Oberlin, M. Endo, and T. Koyama, *Carbon* 14, 133 (1976).
- (3) S. Iijima, *Nature* 354, 56 (1991).
- (4) H. W. Kroto, J. R. Heath, S. C. O'Brien, R. F. Curl, and R. E. Smalley, *Nature* 318, 162-163 (1985).
- (5) S. Iijima, and T. Ichihashi, *Nature* 363, 603 (1993).
- (6) D. S. Bethune, C. H. Kiang, M. S. de Vires, G. Gorman, R. Savoy, J. Vazquez, and R. Beyers, *Nature* 363, 605 (1993).
- (7) M. S. Dresselhaus, G. Dresselhaus, and R. Saito, *Phys. Rev. B* 45, 6234 (1992).
- (8) J. W. Mintmire, B. I. Dunlap, and C. T. White, *Phys. Rev. Lett.* 68, 631-634 (1992).
- (9) N. Hamada, S. Sawada, and A. Oshiyama, *Phys. Rev. Lett.* 68, 1579-1581 (1992).
- (10) J. W. G. Wildöer, L. C. Venema, A.G. Rinzler, R. E. Smalley, and C. Dekker, *Nature* 391, 59-62 (1998).
- (11) T. W. Odom, J. L. Huang, P. Kim, and C. M. Lieber, *Nature* 391, 62-64 (1998).
- (12) A. Thess, R. Lee, P. Nikolaev, H. Dai, P. Petit, J. Robert, C. Xu, Y. H. Lee, S. G. Kim, A. G. Rinzler, D. T. Colbert, G. E. Scuseria, D. Tománek, J. E. Fischer, and R. E. Smalley, *Science* 273, 483-487 (1996).
- (13) M. S. Dresselhaus, G. Dresselhaus, and R. Saito, *Carbon* 33, 883-891 (1995).
- (14) R. Saito, G. Dresselhaus, and M. S. Dresselhaus, *Phys. Rev. B* 61, 2981 (2000).
- (15) H. Kataura, Y. Kumazawa, Y. Maniwa, I. Umezumi, S. Suzuki, Y. Ohtsuka, and Y. Ichiba. *Synth. Metal.* 103, 2555-2558 (1999).
- (16) M. J. O'Connell, S. M. Bachilo, C. B. Huffman, V. C. Moore, M. S. Strano, E. H. Haroz, K. L. Rialon, P. J. Boul, W. H. Noon, C. Kittrell, J. P. Ma, R. H. Hauge, and R. B. Weisman, *Science* 297, 593 (2002).
- (17) Smalley, R. E. M. S. Dresselhaus, and P. C. Eklund, *Adv. Phys.* 49, 705-814 (2000).
- (18) M. S. Dresselhaus, G. Dresselhaus, A. Jorio, A. G. Souza Filho, and R. Saito, *Carbon* 40, 2043-2061 (2002).
- (19) M. A. Pimenta, A. Marucci, S. A. Empedocles, M. G. Bawendi, E. B. Hanlon, A. M. Rao,

- P. C. Eklund, R. E. Smalley, and G. Dresselhaus, *Phys. Rev. B* **58**, R16016 (1998).
- (20) S. D. M. Brown, A. Jorio, P. Corio, M. S. Dresselhaus, G. Dresselhaus, R. Saito, and K. Kneipp, *Phys. Rev. B* **63**, 155414 (2001).
- (21) A. G. Souza Filho, A. Jorio, G. Dresselhaus, M. S. Dresselhaus, R. Saito, A. K. Swan, M. S. Ünlü, B. B Goldberg, J. H. Hafner, C. M. Lieber, and M. A. Pimenta, *Phys. Rev. B* **65**, 035404 (2001).
- (22) M. A. Pimenta, E. B. Hanlon, A. Marucci, P. Corio, S. D. M. Brown, S. A. Empedocles, M. G. Bawendi, G. Dresselhaus, M. S. Dresselhaus, and *Braz. J. Phys.* **30**, 423-427 (2000).
- (23) F. Tuinstra, and J. L. Koenig, *J. Chem. Phys.* **53**, 1126 (1970).
- (24) R. P. Vidano, D. B. Fishbach, L. J. Willis, and T. M. Loehr, *Solid. State. Commun.* **39**, 341 (1981).
- (25) D. D. Bethune, C. H. Kiang, M. DeVries, G. Gorman, R. Savoy, J. Vazquez, and R. Beyers, *Nature* **363**, 605-607 (1993).
- (26) C. Journet, W. K. Maser, P. Bernier, A. Loiseau, M. L. Delachapelle, S. Lefrant, P. Deniard, R. Lee, and J. E. Fischer, *Nature* **388**, 756-758 (1997).
- (27) A. Thess, R. Lee, P. Nikolaev, H. J. Dai, P. Petit, J. Robert, C. H. Xu, Y. H. Lee, S. G. Kim, A. G. Rinzler, D. T. Colbert, G. E. Scuseria, D. Tomanek, J. E. Fischer, and R. E. Smalley, *Science* **273**, 483-487 (1996).
- (28) J. Kong, H. Soh, A. Cassell, C. F. Quate, and H. J. Dai, *Nature* **395**, 878-879 (1998).
- (29) A. Cassell, J. Raymakers, J. Kong, and H. J. Dai, *J. Phys. Chem.* **103**, 6484-6492 (1999).
- (30) H. J. Dai, J. Kong, C. Zhou, N. Franklin, T. Tombler, A. Cassell, S. Fan, M. Chapline, and *J. Phys. Chem.* **103**, 11246-11255 (1999).
- (31) W. Z. Li, S. S. Xie, L. X. Qian, B. H. Chang, B. S. Zou, W. Y. Zhou, R. A. Zhao, and G. Wang, *Science* **274**, 1701-1703 (1996).
- (32) J. Hafner, M. Bronikowski, B. Azamian, P. Nikolaev, D. Colbert, and R. Smalley, *Chem. Phys. Lett.* **296**, 195-202 (1998).
- (33) M. Su, B. Zheng, and J. Liu, *Chem. Phys. Lett.* **322**, 321-326 (2000).
- (34) Y. G. Zhang, A. L. Chang, J. Cao, Q. Wang, W. Kim, Y. M. Li, N. Morris, E. Yenlomez, J. Kong, and H. J. Dai, *Appl. Phys. Lett.* **79**, 3155-3157 (2001).

- (35) S. M. Huang, X. Y. Cai, and J. Liu, *J. Am. Chem. Soc.* 125, 5636 (2003).
- (36) H. P. Liu, D. Takagi, S. Chiashi, and Y. Homma, *Nanotech.* 20, 345604 (2009).
- (37) Y. M. Li, D. Mann, M. Rolandi, W. Kim, A. Ural, S. Hung, and A. Javey, *Nano Lett.* 4, 317 (2004).
- (38) B. Wang, C. H. P. Poa, L. Wei, L.J. Li, Y. H. Yang, and Y. Chen, *J. Am. Chem. Soc.* 129, 9014 (2007).
- (39) D. Ciuparu, Y. Chen, S. Lim, G.L. Haller, and L. Pfefferle, *J. Phys. Chem. B* 108, 503 (2004).
- (40) Y. Chen, D. Ciuparu, S. Lim, Y.H. Yang, G.L. Haller, and L. Pfefferle, *J. Catal.* 226, 351 (2004).
- (41) Y.H. Miyauchi, S.H. Chiashi, Y. Murakami, Y. Hayashida, and S. Maruyama, *Chem. Phys. Lett.* 387, 198 (2004).
- (42) X.L. Li, X.M. Tu, S. Zaric, K. Welsher, W.S. Seo, W. Zhao, and H.J. Dai, *J. Am. Chem. Soc.* 129, 15770 (2007).
- (43) M.C. Hersam, *Nat. Nanotechnol.* 3, 387 (2008)
- (44) M. Endo, K. Takeuchi, S. Igarashi, K. Kobori, M. Shiraishi and H. W. Kroto: *J. Phys. Chem. Solids* 54, 1841 (1993).
- (45) T. Tanaka, H.H. Jin, Y. Miyata, H. Kataura, *Appl. Phys. Express* 1, 114001 (2008).
- (46) T. Tanaka, H. Jin, Y. Miyata, S. Fujii, H. Suga, Y. Naitoh, T. Minari, T. Miyadera, K. Tsukagoshi, H. Kataura, *Nano Lett.* 9, 1497 (2009).
- (47) K. Moshhammer, F. Hennrich, M.M. Kappes, *Nano Res.* 2, 599 (2009).
- (48) M.S. Arnold, S.I. Stupp, M.C. Hersam, *Nano Lett.* 5, 713 (2005).
- (49) S.N. Kim, Z.F. Kuang, J.G. Grote, B.L. Farmer, R.R. Naik, *Nano Lett.* 8, 4415 (2008).
- (50) M. Zheng, A. Jagota, E.D. Semke, B.A. Diner, R.S. Mclean, S.R. Lustig, R.E. Richardson, N.G. Tassi, *Nat. Mater.* 2, 338 (2003).
- (51) M. Zheng, A. Jagota, M.S. Strano, A.P. Santos, P. Barone, S.G. Chou, B.A. Diner, et al., *Science* 302, 1545 (2003).
- (52) M. Zheng, E.D. Semke, *J. Am. Chem. Soc.* 129, 6084 (2007).
- (53) X. Tu, M. Zheng, *Nano Res.* 1, 185 (2008).
- (54) M.C. Hersam, *Nature* 460, 186 (2009).

- (55) X.M. Tu, S. Manohar, A. Jagota, M. Zheng, *Nature* 460, 250 (2009).
- (56) T. Guo, P. Nikolaev, A. Thess, D. T. Colbert and R. E. Smalley: *Chem. Phys. Lett.* 243 (1995) 49.
- (57) M. S. Arnold, A. A. Green, J. F. Hulvat, S. I. Stupp and M. C. Hersam, *Nat. Nanotechnol.* 1 (2006) 60.
- (58) R. Martel, *ACS Nano* 2, 2195 (2008).
- (59) M.S. Arnold, J. Suntivich, S.I. Stupp, M.C. Hersam, *ACS Nano* 2, 2291 (2008).
- (60) A.A. Green, M.C. Hersam, *Nano Lett.* 8, 1417 (2008).
- (61) A.A. Green, M.C. Duch, M.C. Hersam, *Nano Res.* 2, 69 (2009).
- (62) S. Niyogi, C.G. Densmore, S.K. Doorn, *J. Am. Chem. Soc.* 131, 1144 (2009).
- (63) C. Backes, F. Hauke, C.D. Schmidt, A. Hirsch, *Chem. Commun.*, 2643 (2009).
- (64) W.J. Kim, N. Nair, C.Y. Lee, M.S. Strano, *J. Phys. Chem. C* 112, 7326 (2008).
- (65) K. Yanagi, T. Iitsuka, S. Fujii, H. Kataura, *J. Phys. Chem. C* 112, 18889 (2008).
- (66) N. Stiirzl, F. Hennrich, S. Lebedkin, M.M. Kappes, *J. Phys. Chem. C* 113, 14628 (2009).
- (67) J.A. Fagan, M.L. Becker, J. Chun, E.K. Hobbie, *Adv. Mater.* 20, 1609 (2008).
- (68) A.A. Green, M.C. Hersam, *Nat. Nanotechnol.* 4, 64 (2009).
- (69) D.A. Tsyboulski, Y. Hou, N. Fakhri, S. Ghosh, R. Zhang, S.M. Bachilo, M. Pasquali, L. Chen, J. Liu, R.B. Weisman, *Nano Lett.* 9, 3282 (2009).
- (70) H. Liu, Y. Feng, T. Tanaka, Y. Urabe and H. Kataura, *J. Phys. Chem. C* 114, 9270, 2010.
- (71) S. Fujii, T. Tanaka, Y. Miyata, H. Suga, Y. Naitoh, T. Minari, T. Miyadera, K. Tsukagoshi, H. Kataura, *Appl. Phys. Express* 2, 071601 (2009).
- (72) K. Yanagi, Y. Miyata, and H. Kataura, *Appl. Phys. Express* 1, 034003, (2008).
- (73) X.Y. Deng, D. Xiong, H.F. Wang, D.D. Chen, Z. Jiao, H.J. Zhang, M.H. Wu, *Carbon* 47, 1608 (2009).
- (74) X. Sun, S. Zaric, D. Daranciang, K. Welsher, Y. Lu, X. Li, H. Dai, *J. Am. Chem. Soc.* 130, 6551 (2008).
- (75) M.F. Zhang, T. Yamaguchi, S. Iijima, M. Yudasaka, *J. Phys. Chem. C* 113, 11184 (2009).
- (76) X.M. Sun, S.M. Tabakman, W.S. Seo, L. Zhang, G.Y. Zhang, S. Sherlock, L. Bai, H.J. Dai, *Angew. Chem. Int. Ed.* 48, 939 (2009).

- (77) A.A. Green, M.C. Hersam, *Nano Lett.* 9, 4031 (2009).
- (78) M. S. Arnold, S. I. Stupp and M. C. Hersam, *Nano Lett.* 5 (2005) 713.
- (79) Y. Miyata, K. Yanagi, Y. Maniwa and H. Kataura: *J. Phys. Chem. C* 112 (2008) 3591.
- (80) S. Ghosh, S. M. Bachilo and R. B. Weisman: *Nat. Nanotechnol.* 5 (2010) 443.
- (81) J. Graham, T. Ford and D. Rickwood: *Anal. Biochem.* 220 (1994) 367.
- (82) A.A. Green, M.C. Hersam, *Mater. Today* 10, 59 (2007).
- (83) S.J. Tans, A.R.M. Verschueren, C. Dekker, *Nature* 393, 49 (1998).
- (84) R. Martel, T. Schmidt, H. Shea, T. Hertel, Ph. Avouris, *Appl. Phys. Lett.* 73, 2447 (1998).
- (85) E. Snow, J.P. Novak, P.M. Campbell, D. Park, *Appl. Phys. Lett.* 82, 2145 (2003).
- (86) S. Kumar, J.Y. Murthy, M.A. Alam, *Phys. Rev. Lett.* 95, 066802 (2005).
- (87) E. Artukovic, M. Kaempgen, D. S. Hecht, S. Roth, and G. Grüner, *Nano Lett.* 5, 757 (2005).
- (88) T. Takenobu, T. Takahashi, T. Kanbara, K. Tsukagoshi, Y. Aoyagi, and Y. Iwasa, *Appl. Phys. Lett.* 88, 033511 (2006).
- (89) S. J. Kang, C. Kocabas, T. Oze, M. Shim, N. Pimparkar, M. A. Alam, S. V. Rotkin, and J. A. Rogers, *Nat. Nanotechnol.* 2, 230 (2007).
- (90) Q. Cao, H. Kim, N. Pimparkar, J. P. Kulkarni, C. Wang, M. Shim, K. Roy, M. A. Alam, and J. A. Rogers, *Nature*, 454, 495 (2008).
- (91) M. C. LeMieux, M. Roberts, S. Barman, Y. W. Jin, J. M. Kim, and Z. Bao, *Science*, 321, 101 (2008).
- (92) C. W. Lee, C. H. Weng, L. Wei, Y. Chen, M. B. Chan-Park, C. H. Tsai, K. C. Leou, C. H. Patrick Poa, J. Wang, and L. J. Li, *J. Phys. Chem. C* 112, 12089 (2008).
- (93) M. Engel, J. P. Small, M. Steiner, M. Freitag, A. A. Green, M. C. Hersam, and P. Avouris, *ACS Nano* 2, 2445 (2008).
- (94) N. Izard, S. Kazaoui, K. Hata, T. Okazaki, T. Saito, S. Iijima, and N. Minami, *Appl. Phys. Lett.* 92, 243112 (2008).
- (95) P. G. Collins, M. S. Arnold and P. Avouris, *Science*, 292, 706 (2001).
- (96) A. K. Ghosh, and T. Feng *J. Appl. Phys.* 49,5982–5989 (1978).
- (97) T. Moriizumi, and K. Kudo, *Appl. Phys. Lett.* 1981, 38I, 85–86.

- (98) V. Choong, Y. Park, Y. Gao, T. Wehrmeister, K. Müllen, B. R. Hsieh, and C. W. Tang, *Appl. Phys. Lett.* 69, 1492 (1996).
- (99) S. S. Sun, N. S. Sariciftci, Johannes Kepler University of Linz, Austria, *Organic Photovoltaics: Mechanisms, Materials, and Devices*, 2005.
- (100) C. W. Tang, *Appl. Phys. Lett.* 48, 183 (1986).
- (101) W. Ma, C. Yang, X. Gong, K. Lee, A. J. Heeger, *Adv. Funct. Mater.* 15, 1617 (2005).
- (102) G. Li, V. Shrotriya, J. Huang, Y. Yao, T. Moriarty, K. Emery, Y. Yang, *Nat. Mater.* 4, 864 (2005).
- (103) M. Reyes-Reyes, K. Kim, D. L. Carroll, *Appl. Phys. Lett.* 87, 083506 (2005).
- (104) J. Xue, B. P. Rand, S. Uchida, S. R. Forrest, *J. Appl. Phys.* 98, 124903 (2005).
- (105) J. Xue, B. P. Rand, S. Uchida, S. R. Forrest, *Adv. Mater.* 17, 66 (2005).
- (106) J. Xue, S. Uchida, B. P. Rand, S. R. Forrest, *Appl. Phys. Lett.* 84, 3013 (2004).
- (107) N. S. Sariciftci, D. Braun, C. Zhang, V. I. Srdanov, A. J. Heeger, G. Stucky, F. Wudl, *Appl. Phys. Lett.* 62, 585 (1993).
- (108) M. Granstrom, K. Petritsch, A. C. Arias, A. Lux, M. R. Andersson, R. H. Friend, *Nature* 395, 257 (1998).
- (109) J. J. M. Halls, C. A. Walsh, N. C. Greenham, E. A. Marseglia, R. H. Friend, S. C. Moratti, A. B. Holmes, *Nature* 376, 498 (1995).
- (110) G. Yu, A. J. Heeger, *J. Appl. Phys.* 78, 4510 (1995).
- (111) E. Kymakis, and G. A. J. Amaratunga, *Rev. Adv. Mater. Sci.* 10, 300 (2005).
- (112) E. Kymakis, and G. A. J. Amaratunga, *J. Appl. Phys.* 99, 084302 (2006).
- (113) E. Kymakis, E. Koudoumas, I. Franghiadakis and G. A. J. Amaratunga, *J. Phys. D: Appl. Phys.* 39, 1058 (2006).
- (114) C. D. Canestraro, M. C. Scnitzler, A. J. G. Zarbin, M. G. E. da Luz and L. S. Roman, *Appl. Surf. Sci.* 252, 5575 (2006).
- (115) S. Berson, R. Bettignies, S. Bailly, S. Guillerez, and B. Jousset, *Adv. Funct. Mater.* 17, 3363, (2007).
- (116) S. Chaudhary, H. W. Lu, A. M. Müller, C. J. Bardeen, and M. Ozkan, *Nano Lett.* 7, 1973, (2007).
- (117) Y. Miyata, K. Yanagi, Y. Maniwa and H. Kataura, *J. Phys. Chem. C* 112, 13187 (2008).

- (118) D. Nishide, Y. Miyata, K. Yanagi, T. Tanaka and H. Kataura, *Phys. Status Solidi B* 246, 2728 (2009).
- (119) M. S. Dresselhaus, G. Dresselhaus, A. Jorio, A. G. Souza and R. Saito, *Carbon* 40, 2043 (2002).
- (120) Yanagi, K.; Iitsuka, T.; Fujii, S.; Kataura, H. *J. Phys. Chem. C* 112, 18889 (2008).
- (121) A. M. Rao, P. C. Eklund, S. Bandow, A. Thess, R. E. Smalley, *Nature* 388, 257 (1997).
- (122) V. Skákalová, A. B. Kaiser, U. Dettlaff-Weglikowska, K. Hrnčjariková, S. Roth, *J. Phys. Chem. B* 109, 7174 (2005).
- (123) K. Yoshino, and S. Nakajima, *Jpn. J. Appl. Phys.* 26, L2046 (1987).
- (124) P. J. Brown, D. S. Thomas, A. Köhler, and J. S. Wilson: *Phys. Rev. B* 67, 064203 (2003).
- (125) T. Schuettfort, H. J. Snaith, A. Nish, and R. J. Nicholas, *Nanotechnol.* 21, 025201 (2010).
- (126) G. Louarn, M. Trznadel, J. P. Buisson, J. Laska, A. Pron, M. Lapkowschi, and S. Lefrant, *J. Phy. Chem.* 100, 12532 (1996).
- (127) K. Tashino, Y. Minagawa, M. Kobayashi, S. Morita, T. Kawai and K. Yoshino, *Synth. Met.* 55-57, 321 (1993).
- (128) P. A. Van Hal, S. C. J. Meskers, and R. A. J. Janssen, *Appl. Phys. A* 79, 41 (2004).
- (129) Y. X. Liu, M. A. Summers, S. R. Scully, and M. D. McGehee, *J. Appl. Phys.* 99, 093521 (2006).
- (130) B. C. Thompson, and J. M. J. Fréchet, *Angew. Chem. Int. Ed.* 47, 58 (2008).
- (131) A. J. Ferguson, J. L. Blackburn, J. M. Holt, N. Kopidakis, R. C. Tenent, T. M. Barnes, M. J. Herben, and G. Rumbles, *J. Phys. Chem. Lett.* 1, 2406 (2010).
- (132) D. Gupta, S. Mukhopadhyay, and K. S. Narayan, *Solar Energy Materials & Solar Cells*, 94, 1309 (2010).
- (133) L. Qin, X. Zhao, K. Hirahara, Y. Miyamoto, Y. Ando, and S. Iijima, *Nature (London)* 408, 50 (2000).
- (134) N. Wang, Z. K. Tang, G. D. Li, and J. S. Chen, *Nature (London)* 408, 50 (2000).
- (135) B. Shan and K. Cho *Phys. Rev. Lett.* 94, 236602 (2005).
- (136) K. M. Kim, K. W. Lee, A. Moujoud, S. H. Oh, K. Y. Heo, and H. J. Kim, *Jap. J. Appl. Phys.* 49, 11602 (2010).

Abbreviation

APTS:	3-aminopropyltriethoxysilane
BHJ:	Bulk Heterojunction
CVD:	Chemical Vapor Deposition
DGM:	Density Gradient Medium
DGU:	Density Gradient Ultracentrifugation
DOC:	Sodium Deoxycholate
FET:	Field Effect Transistor
FF:	Fill Factor
FRET:	Förster resonance energy transfer
FWHM:	Full Width at Half Maximum
Hipco:	High-pressure carbon monoxide
HOMO:	Highest Occupied Molecular Orbital
HRTEM:	High Resolution Transmission Electron Microscopy
IPA:	Isopropyl Alcohol
L-DGU:	Linear Density Gradient Ultracentrifugation
LUMO:	Lowest Unoccupied Molecular Orbital
MWCNT:	Multi Wall Carbon Nanotube
NIR:	near-infrared
NMP:	N-methylpyrrolidone
OPVs:	Organic Photovoltaic devices
PCBM:	[6,6]-phenyl C ₆₁ butyric acid methyl ester
PEDOT:PSS:	Poly(3,4-ethylenedioxythiophene)-poly(styrenesulfonate)
PL:	Photoluminescence
P3HT:	Poly(3-hexylthiophene)
RBM:	Radial Breathing Mode
SC:	Sodium Cholate
SDS:	Sodium Dodecyl Sulphate
S-DGU:	Step Density Gradient Ultracentrifugation

SWCNT: Single Wall Carbon Nanotube

TFT: Thin film transistor

U-DGU: Uniform Density Gradient Ultracentrifugation

vHS: van Hove singularities

Appendix

Appendix I:

Ultracentrifuges: Hitachi Koki, CS100GX II

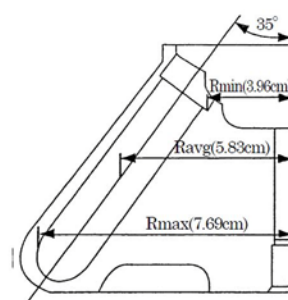


Angle Rotor: Hitachi Koki, S58A



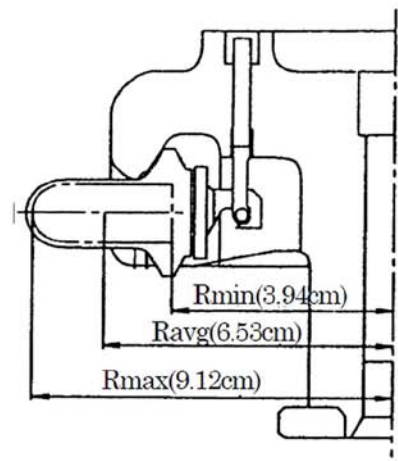
S58A アングルロータ

最高回転速度	58,000rpm
最大遠心加速度	289,000×g
ロータ呼称容量	108ml = 13.5ml × 8
κファクタ	50



回転速度 (rpm)	遠心加速度 (×g)			κ ファクタ
	Rmin (3.96cm)	Ravg (5.83cm)	Rmax (7.69cm)	
10,000	4,430	6,520	8,600	1,681
15,000	9,960	14,700	19,300	747
20,000	17,700	26,100	34,400	420
25,000	27,700	40,700	53,700	269
30,000	39,800	58,700	77,400	187
35,000	54,200	79,800	105,000	137
40,000	70,800	104,000	138,000	105
45,000	89,700	132,000	174,000	83
50,000	111,000	163,000	215,000	67
55,000	134,000	197,000	260,000	56
58,000	149,000	219,000	289,000	50

Swing Rotor: Hitachi Koki, S58A



最高回転速度 52,000rpm
 最大遠心加速度 276,000×g
 ロータ呼称容量 20ml=5.0ml×4
 κファクタ 79

回転速度 (rpm)	遠心加速度 (×g)			κ ファクタ
	Rmin (3.94cm)	Ravg (6.53cm)	Rmax (9.12cm)	
10,000	4,400	7,300	10,200	2,126
15,000	9,910	16,400	23,000	945
20,000	17,600	29,200	40,900	531
25,000	27,500	45,600	63,900	340
30,000	39,600	65,700	92,000	236
35,000	54,000	89,400	125,000	174
40,000	70,500	117,000	163,000	133
45,000	89,200	148,000	207,000	105
50,000	110,000	183,000	255,000	85
52,000	119,000	197,000	276,000	79

Appendix II

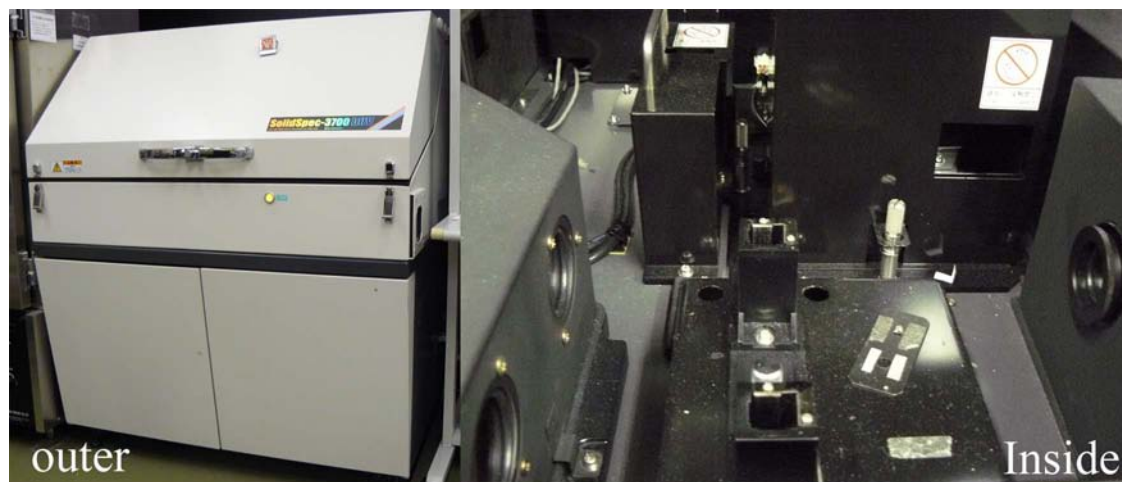
Corona Electric, SH-1000



--- Item ---	--- Specifications ---
Measurement mode	Absorption spectrum measurement* Single / Dual wavelength measurement End point / Kinetic* / Optimal value measurement*
Photometry	Single light path, Upper irradiation Bottom reading
Measurement range	-0.5 to 3.5Abs.
Linearity	±0.5%T or ±0.005Abs (0 to 2.5Abs 492nm)
Reproducibility	CV 1.0 % or less (at Abs is 1.0)
Wavelength range	200 ~ 1000nm in 1nm increments
Measurement direction	Vertical / Horizontal
Microplate Format	6 , 12 , 24 , 48 , 96 , 384 (Flat bottom , Clear) Custom Plate (21mm tall or less) Dimensions of 172 kinds of plate are preset in PC Data processing software.
*Multi point measurement	Selectable.
Dispersion method	Diffraction Grating
Light source	Xenon flash lamp 5W (with Lamp Save function)
Mixing function	Rotation / Linear, 3-step intensity
*Data processing software	Standard accessory SF6 [Win 2000, XP, Mac X (Power PC) supported] Regression model 11 kinds / Cut off 2 kinds / Data analysis 3 kinds / Kinetic 5 kinds Administration software: Instrument operation record, Instrument-PC communication logging
External Port	USB port for PC, D-sub 25-pin female for Optional external printer
Dimension	426(W)×350(D)×193(H) mm
Weight	15kg
Power consumption	AC100V 50/60Hz (200VA)
Accessories	Power cable, Vinyl cover, Fuse, USB cable, Instruction manual
RoHS	EU RoHS compliant
Optional part	Thermal Control: It is selectable within 35°C to 45°C. Cell meas. function (Herma quartz is recommended : Semi-micro black cell #2-475-01) External thermal printer DPU-414-30B-E

Appendix III

Shimadzu, SolidSpec-3700DUV

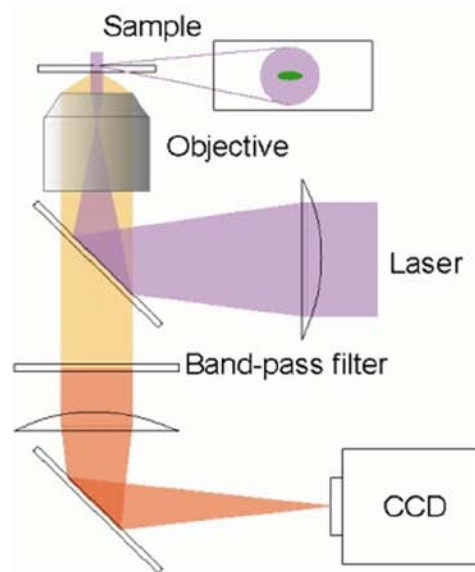
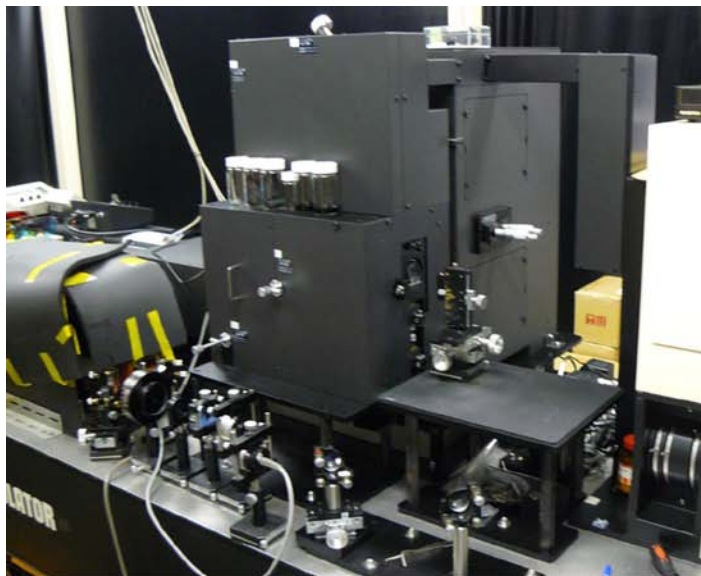


Wavelength range	SolidSpec-3700: 240-2600nm, 190-3300nm(when using Direct Detection Unit DDU) SolidSpec-3700DUV: 175-2600nm, 165-3300nm(when using Direct Detection Unit DDU-DUV) Spectral bandwidth
Spectral bandwidth	UV/VIS: 0.1-8nm (8 steps) NIR: 0.2-32nm (10 steps)
Resolution(*)	0.1nm
Wavelength accuracy(*)	UV/VIS: ± 0.2 nm, NIR: ± 0.8 nm
Wavelength repeatability(*)	UV/VIS: ± 0.08 nm, NIR: ± 0.32 nm
Stray light(*)	Less than 0.00008% (220nm), less than 0.00005% (340nm) Less than 0.0005% (1420nm), less than 0.005%(2365nm)
Noise	Under 0.0002Abs (500nm, SBW 8nm), Under 0.00005Abs (1500nm, SBW 8nm) determined under conditions of RMS value at 0Abs and 1second response. When using Direct Detection Unit DDU/DDU-DUV, Under 0.00005Abs (500nm,SBW 2nm), Under 0.00008Abs(900nm, SBW 2nm), Under 0.00003Abs (1500nm,SBW 2nm) determined under condition of RMS value at 0Abs and 1 second response.
Photometric range	-6 to 6Abs
Photometric system	Double beam, direct ratio measuring system
Dimensions	1000W x 800D x 1200H mm, 170kg

(* Determined with Direct Detection Unit DDU)

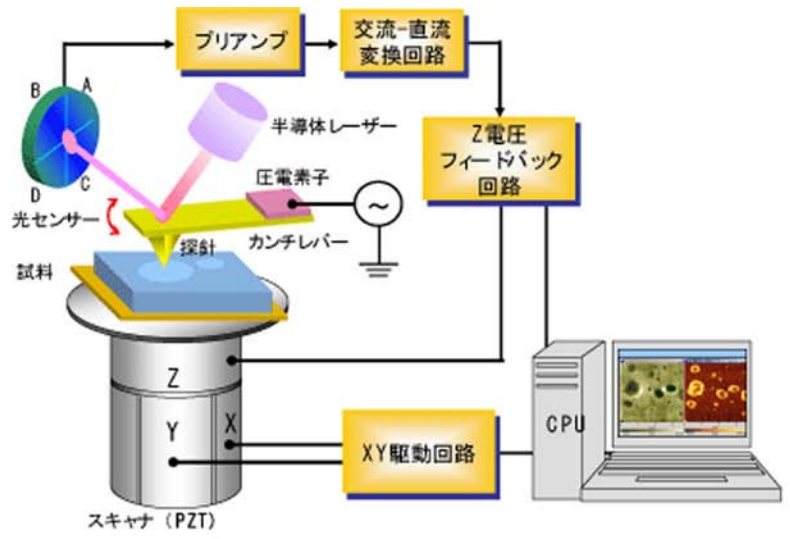
Appendix IV

Raman measurement equipment: Bunko Keiki, M331-TP



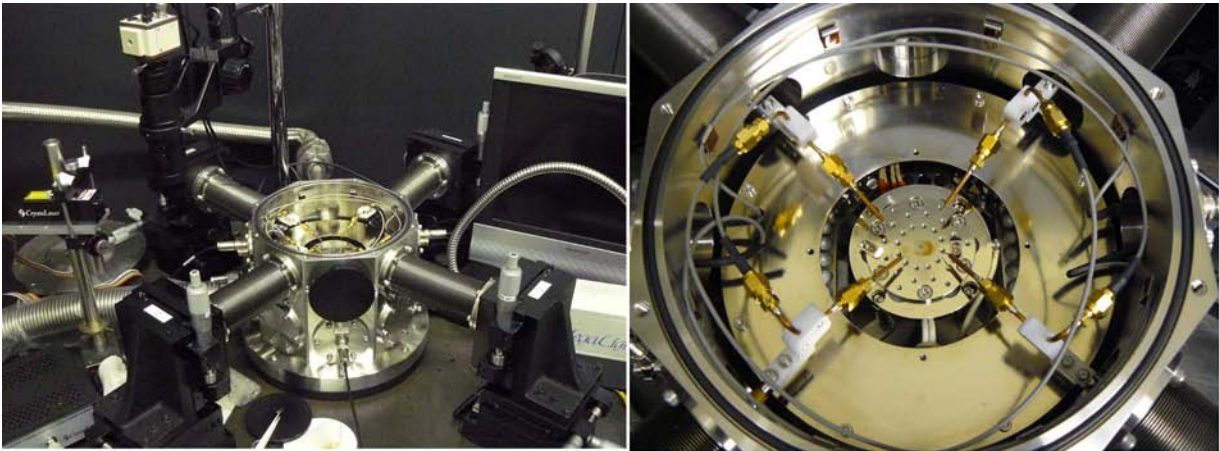
Appendix V

AFM equipment: SII SPI3800



Appendix VI

Probe: Nagase Techno-Engineering Grail10

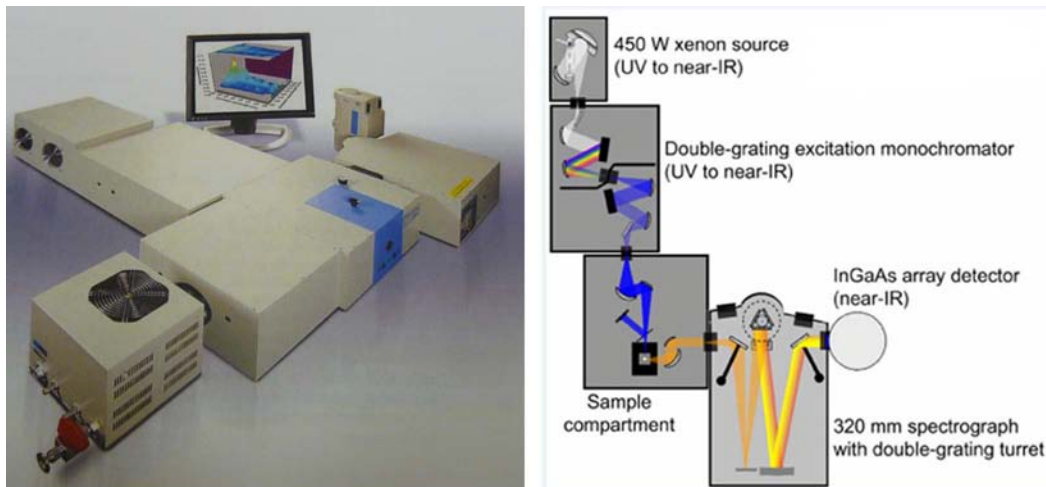


Semiconductor parameter analyzer: keithley 4200-SCS



Appendix VII

Photoluminescence measurement: Horiba, Nanolog



Specifications

- 450 W intense broadband cw xenon lamp for bright excitation from UV to near-IR
- Full excitation-emission matrices in seconds
- Symphony II InGaAs array detectors: 800-1700 nm; 256 x 1,512 x 1, and 1024 x 1 pixel formats as small as 25 μm pitch; noise as low as 650 erms with liquid-nitrogen cooling for best signal-to-noise ratio; optional thermoelectric cooling; extended range option (1.1 - 2.2 μm)
- iHR320 emission spectrograph: focal length = 320 mm; $f/4.1$; dispersion = 2.31 nm/mm; resolution = 0.06 nm (with slit); software-controlled triple-grating turret (all measured with 1200 groove/mm grating)
- Solid-state near-IR detectors, photomultiplier tubes from UV to near-IR, time-correlated single-photon counting lifetime measurement (100 ps to 1 ms, UV to near-IR), phosphorimeter (1 μs to > 10 s, UV to near-IR), and frequency-domain lifetime measurement (10 ps to 10 μs , UV to near-IR) are also available

Acknowledgement

This thesis would not have been possible without the help and support of many people who are gratefully acknowledged here.

First of all, I'm honored to express my deepest gratitude to my supervisors, Prof. Kiyoto Matsuishi and Prof. Hiromichi Kataura, with whose able guidance I could have worked out this thesis. They offered me the great freedom and financial support on my research. They also gave me valuable ideas, suggestions and criticisms with their profound knowledge and rich research experience. Their patience and kindness are greatly appreciated. They always put high priority on our dissertation writing and are willing to discuss with me anytime he is available. I have learnt from him a lot not only about dissertation writing, but also the professional ethics. I'm very much obliged to their efforts of helping me complete the dissertation.

I'm also extremely grateful to my research colleagues in Kataura Laboratory, Dr. Yasumitsu Miyata, Daisuke Nishide, Shunjiro Fujii, Huaping Liu, Yang Huang and other members. My research can not go smoothly without their kind support, praiseworthy tolerance and invaluable suggestions. The discussion with them in the spare time during the research extremely relieved the pressure and inspired me. I cannot make it without their support and encouragement.

What's more, I wish to extend my thanks to the students in Matsuishi Laboratory. They undertook the school affairs to make me focus on my research. The research became more relaxed with their great understanding and support.

Thanks are also due to my friends in University of Tsukuba, who never failed to give me great encouragement and suggestions. Special thanks should go to Mr. Peng Chang and Mrs. Xi Meng. Their friendship made my life in the foreign easier and full of happiness.

At last but not least, I would like to thank my family and my soulmate Miss. Ming Liu for their support all the way of my postgraduate study. Their thoughtfulness and encouragement inspired me throughout the doctoral period and will accompany my whole life.